NASA/TM-1999-209122

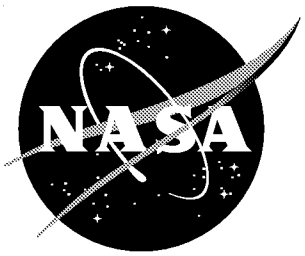

X-33 (Rev-F) Aeroheating Results of Test 6770 in NASA Langley 20-Inch Mach 6 Air Tunnel

Scott A. Berry, Thomas J. Horvath, Matthew K. Kowalkowski and Derek S. Liechty
Langley Research Center, Hampton, Virginia

March 1999

The NASA STI Program Office ... in Profile

Since its founding, NASA has been dedicated to the advancement of aeronautics and space science. The NASA Scientific and Technical Information (STI) Program Office plays a key part in helping NASA maintain this important role.

The NASA STI Program Office is operated by Langley Research Center, the lead center for NASA's scientific and technical information. The NASA STI Program Office provides access to the NASA STI Database, the largest collection of aeronautical and space science STI in the world. The Program Office is also NASA's institutional mechanism for disseminating the results of its research and development activities. These results are published by NASA in the NASA STI Report Series, which includes the following report types:

- TECHNICAL PUBLICATION. Reports of completed research or a major significant phase of research that present the results of NASA programs and include extensive data or theoretical analysis. Includes compilations of significant scientific and technical data and information deemed to be of continuing reference value. NASA counterpart of peer-reviewed formal professional papers, but having less stringent limitations on manuscript length and extent of graphic presentations.

- TECHNICAL MEMORANDUM. Scientific and technical findings that are preliminary or of specialized interest, e.g., quick release reports, working papers, and bibliographies that contain minimal annotation. Does not contain extensive analysis.

- CONTRACTOR REPORT. Scientific and technical findings by NASA-sponsored contractors and grantees.

- CONFERENCE PUBLICATION. Collected papers from scientific and technical conferences, symposia, seminars, or other meetings sponsored or co-sponsored by NASA.

- SPECIAL PUBLICATION. Scientific, technical, or historical information from NASA programs, projects, and missions, often concerned with subjects having substantial public interest.

- TECHNICAL TRANSLATION. English-language translations of foreign scientific and technical material pertinent to NASA's mission.

Specialized services that complement the STI Program Office's diverse offerings include creating custom thesauri, building customized databases, organizing and publishing research results ... even providing videos.

For more information about the NASA STI Program Office, see the following:

- Access the NASA STI Program Home Page at ***http://www.sti.nasa.gov***

- E-mail your question via the Internet to help@sti.nasa.gov

- Fax your question to the NASA STI Help Desk at (301) 621-0134

- Phone the NASA STI Help Desk at (301) 621-0390

- Write to:
  NASA STI Help Desk
  NASA Center for AeroSpace Information
  7121 Standard Drive
  Hanover, MD 21076-1320

NASA/TM-1999-209122

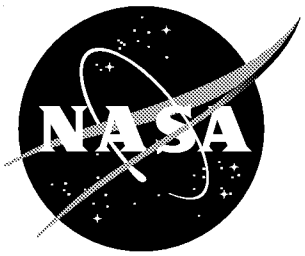

X-33 (Rev-F) Aeroheating Results of Test 6770 in NASA Langley 20-Inch Mach 6 Air Tunnel

Scott A. Berry, Thomas J. Horvath, Matthew K. Kowalkowski and Derek S. Liechty
Langley Research Center, Hampton, Virginia

National Aeronautics and
Space Administration

Langley Research Center
Hampton, Virginia 23681-2199

March 1999

Available from:

NASA Center for AeroSpace Information (CASI)
7121 Standard Drive
Hanover, MD 21076-1320
(301) 621-0390

National Technical Information Service (NTIS)
5285 Port Royal Road
Springfield, VA 22161-2171
(703) 605-6000

Contents

Abstract

Aeroheating characteristics of the X-33 Rev-F configuration have been experimentally examined in the Langley 20-Inch Mach 6 Air Tunnel (Test 6770). Global surface heat transfer distributions, surface streamline patterns, and shock shapes were measured on a 0.013-scale model at Mach 6 in air. Parametric variations include angles-of-attack of 20-deg, 30-deg, and 40-deg; Reynolds numbers based on model length of 0.9 to 4.9 million; and body-flap deflections of 10-deg and 20-deg. The effects of discrete roughness elements on boundary layer transition, which included trip height, size, and location, both on and off the windward centerline, were investigated. This document is intended to serve as a quick release of preliminary data to the X-33 program; analysis is limited to observations of the experimental trends in order to expedite dissemination.

Introduction

The Access to Space Study[1] by NASA recommended the development of a heavy-lift fully reusable launch vehicle (RLV)[2,3] to provide a next-generation launch capability to serve National space transportation needs at greatly reduced cost. This led to the RLV technology program, a cooperative agreement between NASA and industry. The goal of the RLV technology program is to enable significant reductions in the cost of access to space, and to promote the creation and delivery of new space services and other activities that will improve U.S. economic competitiveness. The program implements the National Space Transportation Policy, which is designed to accelerate the development of new launch technologies and concepts to contribute to the continuing commercialization of the national space launch industry. As part of the Single-Stage-To-Orbit (SSTO) RLV program, the X-33 was developed as a technology demonstrator. The X-33 Program will demonstrate the key design and operational aspects of a SSTO RLV rocket system so as to reduce the risk to the private sector in developing such a commercially viable system. The objective of NASA's technology development and demonstration effort, as stated in the National Space Transportation Policy, is to support government and private sector decisions on development of an operational next-generation reusable launch system by the end of this decade. In order to meet its objectives, the X-33 program is an aggressive, focused launch technology development program, with extremely demanding technical objectives and milestones. A Cooperative Agreement is used between NASA and the industry partner, Lockheed Martin Skunkworks, to describe the responsibilities and milestones of both NASA and Lockheed. The X-33 is a lifting body design with symmetric canted fins, twin vertical tails, two body flaps located at the rear of the fuselage, and powered by a linear Aero-spike engine (Ref 4) and is roughly a half-scale prototype of Lockheed's RLV design, the VentureStar. Figure 1 provides a comparison of the X-33 to the VentureStar and the Space Shuttle Orbiter.

As part of the Cooperative Agreement, NASA Langley Research Center (LaRC) has been tasked with providing experimental aeroheating data in support of X-33 aerothermodynamic development and design. Table 1 provides a list of all aeroheating wind tunnel tests that have been completed to date for the X-33 program since the selection of Lockheed's RLV concept (at the end of the Phase I competition in the summer of 1996). Nearly 1000 tunnel runs from nine tests in two facilities have been completed on three X-33 configurations since Aug 1996. The evolution of the X-33 configuration from the onset of Phase II, has necessitated multiple entries into LaRC facilities to investigate the effects of these outer mold line (OML) changes to X-33's aeroheating environment. The OML of the X-33 that was investigated extensively started with the original D-Loft concept, then the F-Loft Revision C (Rev-C), and finally the F-Loft Revision F (Rev-F). These three configurations have been tested in LaRC facilities for not only baseline aeroheating data (i.e. wide range of angles of attack, yaw, Reynolds numbers, body flap deflections, etc.), but also to investigate the effects of surface roughness (both discrete and distributed), and test technique (model scale, blade vs. sting support, etc.). The D-loft configuration emerged from the Phase I downselect and was tested in the early part of Phase II. The Rev-C configuration instituted small modifications to the nose shape (to simplify the construction of the metallic TPS panels) and to the base region (in the vicinity of the engine). The Rev-F has the same forebody shape as Rev-C, but the dihedral of the canted fins was lowered from 37-deg to 20-deg (to improve

pitch-trim characteristics across the speed range) and the size of the body flaps and vertical tails was increased. While other systematic configuration changes have resulted in minor vehicle modifications, these changes were not significant enough to warrant construction of new models and additional wind tunnel testing.

This report presents the preliminary results of wind tunnel test 6770, conducted in the NASA Langley Research Center (LaRC) 20-Inch Mach 6 Air Tunnel during May and June, 1998. The purpose of this test was to investigate the aeroheating characteristics of the X-33 Rev-F configuration and to examine the effect of discrete roughness elements on the windward surface boundary layer along the attachment lines. Test 6770 is one of a series of tests that have been performed to investigate the effect of surface roughness on boundary layer transition. First, the effect of discrete roughness elements on the centerline of the D-Loft forebody was investigated in test 6737. Then during test 6763, the effect of discrete roughness on the centerline of the Rev-F configuration was investigated. While the effect of distributed roughness in the form of a wavy-wall surface (simulating bowed metallic thermal protection system tiles) on Rev-F was investigated in test 6769. These tests provide a systematic investigation of the different boundary layer trip mechanisms for the X-33 flight vehicle. Preliminary trajectory information for the X-33 is presented in Fig. 2 and shows that the flight vehicle will experience a length Reynolds number (Re_L), based on a body length of 63-ft, of roughly 2 to 7 million at a freestream Mach number of 6. These conditions can be simulated in the LaRC 20-Inch Mach 6 Tunnel which has a Re_L range of 0.4 to 6.7 million for a model length of 10-in (thus the model is a 0.0132-scale of the 63-ft long flight vehicle). Test techniques that were utilized during these tests include thermographic phosphors which provide global surface heating images, oil-flow which provide surface streamline information, and schlieren which provide shock system details. Parametrics included in these tests were the effect of angle of attack (α of 20-deg, 30-deg, and 40-deg), unit Reynolds number (Re/ft between 1 and 6 million), body flap deflections (δ_{BF} of 10-deg and 20-deg), and discrete roughness elements (which included height, size, and location). The discrete roughness parametrics were included in these tests to provide information to develop an attachment line roughness transition correlation for the X-33 vehicle. This attachment line correlation would be compared to that which was previously established for the centerline of the X-33 (Ref. 5) and would be used to provide surface roughness tolerances for the flight vehicle and/or guidance for tailoring the flight trajectory.

Nomenclature

M	Mach number
Re	unit Reynolds number (1/ft.)
Re_L	Reynolds number based on body length
α	model angle of attack (deg)
δ_{BF}	body flap deflection (deg)
p	pressure (psi)
T	temperature (degR)
x	longitudinal distance from the nose (in)
y	lateral distance from the centerline (in)
L	reference length of model (10.00 in)
h	heat transfer coefficient (lbm/ft^2-sec), $=q/(H_{aw} - H_w)$ where $H_{aw} = H_{t2}$
h_{F-R}	reference coefficient using Fay-Ridell calculation to stagnation point of a scaled sphere
q	heat transfer rate (BTU/ft^2-sec)
H	enthalpy (BTU/lbm)
k	roughness element height (in)
W	roughness element diagonal width (in)
Subscripts	
∞	freestream static conditions
t1	reservoir conditions

t2	stagnation conditions behind normal shock
aw	adiabatic wall
w	model surface

Test Facility

The present experiment was conducted in the LaRC 20-Inch Mach 6 Air Tunnel (a schematic is provided in Fig. 3). Miller (Ref. 6) provides a detailed description of this hypersonic blowdown facility, which uses heated, dried, and filtered air as the test gas. Typical operating conditions for the tunnel are stagnation pressures ranging from 30 to 500 psia, stagnation temperatures from 760 to 940-degR, and freestream unit Reynolds numbers from 0.5 to 8 million per foot. A two-dimensional, contoured nozzle is used to provide nominal freestream Mach numbers from 5.8 to 6.1. The test section is 20.5 by 20 inches; the nozzle throat is 0.399 by 20.5-inch. A bottom-mounted model injection system can insert models from a sheltered position to the tunnel centerline in less than 0.5-sec. Run times up to 15 minutes are possible with this facility, although for the current heat transfer and flow visualization tests, the model was exposed to the flow for only a few seconds. Flow conditions were determined from the measured reservoir pressure and temperature and the measured pitot pressure at the test section and were compared to a recent unpublished calibration of the facility.

Test Techniques

Surface Heating

The rapid advances in image processing technology which have occurred in recent years have made digital optical measurement techniques practical in the wind tunnel. One such optical acquisition method is two-color relative-intensity phosphor thermography (a diagram is shown in Fig. 4), which is currently being applied to aeroheating tests in the hypersonic wind tunnels of NASA Langley Research Center. Details of the phosphor thermography technique are provided in Refs. 7, 8, and 9, while Refs. 5, 10, 11, and 12 are recent examples of the application of the technique to wind tunnel testing. With this technique, ceramic wind tunnel models are fabricated and coated with phosphors that fluoresce in two regions of the visible spectrum when illuminated with ultraviolet light. The fluorescence intensity is dependent upon the amount of incident ultraviolet light and the local surface temperature of the phosphors. By acquiring fluorescence intensity images with a color video camera of an illuminated phosphor model exposed to flow in a wind tunnel, surface temperature mappings can be calculated on the portions of the model that are in the field of view of the camera. A temperature calibration of the system conducted prior to the study provides the look-up tables that are used to convert the ratio of the green and red intensity images to global temperature mappings. With temperature images acquired at different times in a wind tunnel run, global heat transfer images are computed assuming one-dimensional heat conduction. The primary advantage of this technique is the global resolution of the quantitative heat transfer data. Such data can be used to identify the heating footprint of complex, three-dimensional flow phenomena (e.g., transition fronts, turbulent wedges, boundary layer vortices, etc.) that are extremely difficult to resolve by discrete measurement techniques. Phosphor thermography is routinely used in Langley's hypersonic facilities as quantitative global surface heating information is obtained from models that can be fabricated quickly (a few weeks) and economically (an order of magnitude less than the thin-film technique). Recent comparisons of heat transfer measurements obtained from phosphor thermography to conventional thin-film resistance gauges measurements (Ref. 13) and CFD predictions (Ref. 5, 11, 14, and 15) have shown excellent agreement.

Flow Visualization

Flow visualization techniques, in the form of schlieren and oil-flow, were used to complement the surface heating tests. The LaRC 20-Inch Mach 6 Air Tunnel is equipped with a pulsed white-light, Z-pattern, single-pass schlieren system with a field of view encompassing the entire 20-in test core. Images were recorded on 70-mm film and digitally scanned for incorporation into this report. Surface streamline patterns were obtained using the oil-flow technique. Backup ceramic models were spray-painted black to enhance contrast with the white pigmented oils used to trace streamline movement. A thin basecoat of clear silicon oil was first applied to the surface, and then a mist of

medium-sized pigmented-oil drops was sprayed onto the surface. After the model surface was prepared, the model was injected into the airstream and the development of the surface streamlines was recorded with a conventional video camera. The model was retracted immediately following flow establishment and formation of streamline patterns, and post-run digital photographs were recorded with a Kodak high-resolution camera. The oil-flow images shown in this report are the higher resolution post-run photographs as no significant discrepancies between the post-run and video images were noted.

Model Description

The X-33 Rev-F model dimensions are shown in Fig. 5. A rapid prototyping technique was used to build a resin stereolithography (SLA) model with various, detachable body flaps on both the port and starboard region of the base of the vehicle. The SLA model was then used with the various body flaps as a pattern to cast several ceramic model configurations. Figure 6 is a photograph of 3 Rev-F model configurations that were cast with the various body flap deflections. The designation numbers for these models (shown in bold type) are listed in Table 2, along with the designations for the models used in the other tests listed in Table 1. Typically, two casts of each configuration are made, with the primary ceramic shell (designated in the run log as the –A model) being immediately prepared for testing (backfilled and phosphor coated) and the back-up shell held in reserve, in case of problems with the primary. If necessary, the backup model is prepared for phosphor testing and designated the –B model. Once the phosphor testing is completed, the backup model is spray-coated with a thin black glazing (to seal the surface), final fired in the kiln, and then back-filled for use as the oil-flow and schlieren models (designated as the –O model). For the X-33 program, due to the multiple tunnel entries with the same model configuration, several castings of the same configuration were made. For the current test, models RF10A2-B (δ_{BF} = 10-deg), RF10A3-C and RF10A3-D (δ_{BF} = 20-deg) were used for the heating runs, and models RF10A1-O (δ_{BF} = 0-deg), RF10A3-O and RF10A3-D (δ_{BF} = 20-deg) were used for the flow visualization runs.

In order to obtain accurate heat transfer data using the one-dimensional heat conduction equation, models need to be made of a material with low thermal diffusivity and well-defined, uniform, isotropic thermal properties. Also, the models must be durable for repeated use in the wind tunnel and not deform when thermally cycled. To meet these requirements, a unique, silica ceramic investment slip casting method has been developed and patented (Ref. 16). A hydraulically setting magnesia ceramic was used to backfill the ceramic shell, thus providing strength and support to the sting structure. The models were then coated with a mixture of phosphors suspended in a silica-based colloidal binder. This coating consisted of a 5:1 mixture of lanthanum oxysulfide (La_2O_2S) doped with trivalent europium and zinc cadmium sulfide (ZnCdS) doped with silver and nickel in a proprietary ratio. The coatings typically do not require refurbishment between runs in the wind tunnel and have been measured to be approximately 0.001 inches thick. Figure 7 shows photographs of one of the models installed in the 20-inch Mach 6 Air Tunnel. The final step in the fabrication process is to apply fiducial marks along the body to assist in determining spatial locations accurately. The fiducial marks used for the present study are shown in a sketch in Fig. 8 and the non-dimensional locations are listed in Table 3.

The roughness elements used in this study were similar to the method used in Refs. 5 and 10, which were fabricated to simulate a raised Thermal Protection System (TPS) tile and were cut from 0.0025-inch thick Kapton tape. Variations on the roughness heights (k) were obtained by stacking multiple layers of Kapton tape (k = 0.0025, 0.0050, and 0.0075-inch). Roughness elements fabricated from Kapton tape were easily applied to the various locations of interest on the model without adversely affecting the phosphor coating. Kapton tape was chosen through a trial and error process based on the ease of fabrication and application of the roughness elements, as well as the durability of the material (and adhesive) to heat and shear stress loading. The simulated tile roughness elements were placed directly over the various fiducial marks, which were previously located on the model. Presented in Fig. 9 is a sketch of a typical trip showing dimensions and orientation.

Test Conditions

The LaRC 20-Inch Mach 6 Air Tunnel provides a freestream unit Reynolds number variation of 0.5 to 8.0 million per foot. For a 0.0132-scale model, this corresponds to a length Reynolds number of approximately 0.41 to 6.7 million. For the baseline data, the model angle of attack (α) was varied from 20-deg to 40-deg in 10-deg increments and the sideslip was maintained at zero for all the runs presented herein. Flow conditions, including run-

to-run repeatability, are presented in Table 4. For each model configuration, the unit Reynolds number was varied between 1 and 5 million to obtain the smooth baseline data for comparison to the tripped data. For the transition testing, the tunnel stagnation pressure and temperature were systematically varied over a series of runs with the roughness element firmly applied to the location of interest in order to determine the incipient, critical, and effective Reynolds numbers (using the vernacular coined by Bertin[17]). The maximum Reynolds number that still maintained laminar flow behind the trip identifies the incipient value, the Reynolds number where significant non-laminar flow first appears downstream of the roughness element identifies the critical value, and the minimum Reynolds number where the transition front is fixed at the roughness element identifies the effective value.

Data Reduction

Heating rates were calculated from the global surface temperature measurements using one-dimensional semi-infinite solid heat-conduction equations, as discussed in detail in Refs. 8 and 9. Based on considerations presented in Ref. 9, phosphor system measurement error is believed to be better than ±8%, with overall experimental uncertainty of ±15%. Heating distributions are presented in terms of the ratio of heat-transfer coefficients $h/h_{F\text{-}R}$, where $h_{F\text{-}R}$ corresponds to the stagnation-point heating to a sphere with radius 0.629-in (the nose radius of the Rev-F configuration scaled to the model size) and was calculated based on the theory of Fay and Ridell[18]. Repeatability of the centerline heat transfer distributions was found to be generally better than ±4%.

Results

This report is intended to be a data-release of preliminary experimental results for review by the X-33 program and as such detailed analysis and comparison to computational predictions are not included. The discussion of results that follow is limited to a list of observations based on examinations of the images included in the appendices. Where appropriate, example images from the appendices are listed in order to assist the reader with interpretation of the listed observation. These examples should not be viewed as the only examples that correspond to a given trend. The discussion below has been separated by test technique into separate observation lists based on the surface heating data and the flow visualization results. Within each test technique heading, the list of observations has been arranged under sub-headings that relate to different locations on the model such as the forebody, wings or body flaps, etc. Presented in Fig. 10 is a sketch of the X-33 windward surface detailing the various nomenclature and flow features that will be referred to in the subsequent discussions.

Surface Heating

The phosphor thermography data was acquired in May and June of 1998, during Test 6770. The run log, which lists the parametrics that were investigated during 153 aeroheating runs, is presented in Table 5 and the resulting global heating images are shown in chronological order by run number in Appendix A. All the images were acquired with the camera perpendicular to the model. The primary purpose of this wind tunnel entry was to acquire roughness transition data along the windward attachment lines. Therefore, most of the run matrix was set-up to investigate the effect of trips. A few baseline (no trip) cases were run to provide data that could be compared to previous wind tunnel entries in order to check data quality and repeatability. General observations that can be made based on these baseline-heating images are listed below and followed by a list of trends associated with the boundary layer roughness elements. The $h/h_{F\text{-}R}$ color-bar scale of 0 to 2.0 was selected for all the heating images as this scale provided the best sensitivity to observe the trip effectiveness.

Windward Fuselage

1. As α increases from 20 to 40-deg, heating to the windward forebody increases, most notably on the outboard chine region in the vicinity of the attachment lines. (For example, at a unit Reynolds number of $1x10^6$/ft, see Run # 25 for α = 20-deg, Run # 19 for α = 30-deg, and Run # 24 for α = 40-deg.)

2. As Re increases, the heating ratio $h/h_{F\text{-}R}$ remains relatively constant over the windward forebody until the onset of boundary layer transition occurs. (For example, for α = 30-deg and an increasing Reynolds number, see Runs # 14, 12, and 13)

Windward Canted Fin

1. As α increases from 20 to 40-deg, heating to the windward canted-fin increases, most notably along the leading edge region. (For example, at a unit Reynolds number of $2x10^6$/ft, see Run # 26 for α = 20-deg, Run # 18 for α = 30-deg, and Run # 23 for α = 40-deg.)

2. As Re increases, the heating ratio $h/h_{F\text{-}R}$ remains relatively constant over the windward canted-fin until the onset of boundary layer transition occurs. Transition onset tends to occur in the vicinity of the leading edge, either as a result of attachment-line contamination of non-laminar flow from the fuselage or the bow shock interaction. (For example, for α = 40-deg and an increasing Reynolds number, see Runs # 24, 23, 22, and 21)

Windward Body Flap

1. As α increases from 20 to 40-deg, heating to the deflected body flap increases and the nature of the heating pattern on the flap changes. (For example, at a unit Reynolds number of $1x10^6$/ft and body flap deflection of 20-deg, see Run # 25 for α = 20-deg, Run # 19 for α = 30-deg, and Run # 24 for α = 40-deg.) At the higher angles of attack, a second peak is observed in the heating image that is angled roughly 60-deg to the centerline and is followed by a rapid decrease in heating. This disturbance is also observed in the oil-flow results (to be discussed later) and is likely the result of an interaction of the bow shock with the shock emanating from the deflected body flap.

11. As Re increases, the heating ratio $h/h_{F\text{-}R}$ over the deflected body flap continuously changes which is an indication that the boundary layer on the flap is non-laminar. (For example, for α = 20-deg, δ_{BF} = 20-deg, and an increasing Reynolds number, see Runs # 25, 26, 27, and 28)

Windward Trips

The primary goal of this wind tunnel entry was to obtain roughness transition data along the attachment lines of the X-33 vehicle. Initially, the tripping test matrix was set-up to utilize only one side of the model, with the other side held "in reserve" in case surface defects developed due to repeated placement and retrieval of the roughness elements. Runs 29 through 40 were completed with the trips applied to the port side only. Unfortunately, the trips were not adhering to the model surface as well as with prior experience. Inspection of the trips after each run revealed corners occasionally sticking up and a few cases where the trip was missing (lost during the run). These runs would have to be repeated with new trips to ensure the damaged or missing trip did not corrupt the results. The cases that were repeated for these reasons are identified in the "Notes" section of the run log shown in Table 5. The original roughness element was 0.05 by 0.05-in, which based on prior experience was the smallest trip that could be accurately and consistently manufactured. (Based on the model scale, this corresponds to a 3.8 by 3.8-in protuberance on the surface of the flight-scale X-33.) To improve the adhesion of the trip to the model surface, the decision was made to double the width of the square trips. Runs 41 through 44 compared these two trip widths on the port and starboard sides, but unfortunately the smaller size continued to cause problems. Thus, the 0.10-in width was selected for subsequent testing due to the improved adhesion. On a prior investigation into discrete roughness effects on transition, a systematic variation of the trip width (from 0.05 to 0.10, 0.20, and 0.40) did not strongly influence the Reynolds number where the onset of transition occurred (Ref 19). Also, at this time an attempt was made to consolidate the test matrix as much as possible by placing trips 0.0025-in high (1 layer of Kapton) on the port side and 0.0050-in (2 layers high) on the starboard (effectively doubling the amount of information per run). This approach was utilized for Runs 45 through 59. While the trip adhesion was improved with wider trips, the problem of corners lifting up during the run was not eliminated, as several runs had to be repeated. Finally, the decision was made to place the same size trip on both the port and starboard sides to provide redundancy. If symmetric results were obtained on any given run, the results were considered good pending a visual inspection of the trips. If asymmetric results were observed, the offending trip was replaced and the run was repeated. Additionally, an identical trip was placed on the corresponding centerline x/L location to provide a qualitative comparison of the sensitivity to tripping between the two locations. This approach was utilized for the remainder of the test matrix. The only additional deviation from this matrix was to replace the original model with an identical version. This was done to determine if the original model had some unknown contaminant on the surface that was interfering with the adhesiveness of the trips. This model change was performed prior to Run 64 (and only provided

marginal relief from this problem) and required additional runs to establish a new baseline and to repeat a few trip cases from the original model. General observations that can be made based on the boundary-layer transition images are:

1. When effective, the roughness elements along the attachment line affected a larger area of the windward surface than roughness elements placed on centerline. (Run 72 is just one example.)

2. The attachment line trips give the appearance of being more effective than the corresponding trip on centerline for a given Reynolds number. This may be misleading, as a comparison of the calculated boundary layer thickness along the centerline and attachment line should reveal the centerline to be thicker and thus require a larger trip height to force transition. (See Run 119 for example.)

3. Tripping along the attachment line had a direct effect on size of the separated region in front of and the heating levels on the deflected body flap, while tripping in other regions of the forebody did not. An effective attachment line trip reduced the size of (or eliminated) the separation region and reduced the reattachment heating on the flap. (For example, see Runs 57 or 132.)

11. In general, the trips that were redundantly placed on port, starboard, and centerline revealed, when effective, very symmetric results, which would suggest the fiducial marks were accurately placed and the model orientation was with minimal yaw. (For example, for α = 20-deg see Run 153, for α = 30-deg see Run 58, and for α = 40-deg see Run 109.) However, for the trip station closest to the nose, the turbulent wedge behind the port trip had a tendency to asymmetrically curve towards the centerline, most likely due to a slight inboard misalignment of the port fiducial marks at Station 3. (For example, for α = 20-deg see Run 150, for α = 30-deg see Run 89, and for α = 40-deg see Run 129.)

5. For the one case where an effective trip was purposefully placed off (in this case outside) the appropriate attachment line fiducial mark, the resulting turbulent wedge was quickly swept away from the windward forebody. (For example, see Runs 90, 91, and 92.)

6. Given an effective attachment line trip, which provided turbulent flow in front of the deflected body flap, the location of the trip along the attachment line had little effect on body flap heating levels for a given Reynolds number. (Compare Runs # 109, 124, and 130.)

Flow Visualization

The flow visualization tests were performed in May and June of 1998 during Test 6770. The run log, which shows the flow visualization portion of the run matrix, is presented in Table 6. Schlieren and oil-flow surface visualization images are shown in chronological order in Appendices B and C, respectively. General observations of flow phenomenon that can be made based on these images (along with representative runs indicated in parenthesis) are listed below. Where appropriate, qualitative comparisons are made to the heating images that were presented in Appendix A. Note that during the oil-flow runs, the starboard wing had broken off near the wing-root region during Run 170. As this was the only model available for oil-flows, the remainder of the test matrix was completed with this model. No significant differences between the port and starboard streamlines were noted.

Windward Fuselage

Streamline Directions

11. At the lowest angle of attack, α = 20-deg, the surface streamlines on the windward surface of the forebody are directed in towards the centerline (see Run 165 of Appendix C). This inflow of streamlines produces a thickening of the boundary layer on the centerline, which results in a lower surface-shear that is clearly evident in the lack of oil flow movement (see Run 168). At the highest incidence angle, α = 40-deg, the windward surface streamlines are no longer directed towards the centerline of the model (see Run 4) and appear to spread slightly as the streamline moves aft. This outflow of the streamlines away from the centerline would have the reverse effect of thinning the boundary layer.

2. The attachment lines along the forebody chines, as inferred from the oil-flows, moved inboard with increasing angle of attack (see Runs 168, 174, and 172) and corresponded with the appropriate fiducial mark

locations that identified the predicted inviscid attachment line locations.

11. For all angles of attack tested, α = 20, 30, and 40-deg, a change in unit Reynolds number from 1 to $4x10^6$/ft had little effect on the direction of the surface streamlines or the attachment lines. For example, at α = 40-deg, the degree of outflow and location of the attachment lines is essentially unchanged (see Runs 171, 169, 172, and 170).

Bow Shock

11. Inflections in the bow shock shape due to non-continuous curvature of the body windward surface (the body transitions from a spherical nosecap through a conical transition section to a flat region) are evident at all angles of attack. However, at α = 30 and 40-deg, an additional inflection in the bow shock shape about mid-way back on the body is evident, perhaps due to an over-expansion and recompression of the forebody flow (for example, compare Runs 175 and 183 to Run 184 of Appendix B).

Windward Canted Fin

Streamline Directions

1. For the angles of attack investigated here, the surface streamlines of the windward canted fin flow from the leading edge to the trailing edge with a slight bias away from the fin-root area towards the fin-tip. By increasing the angle of attack from 20 to 40-deg, the degree to which the streamlines flow outboard on the canted fin increases (see Runs 2, 5, and 4).

2. The separated flow found upstream of a deflected body flap did not strongly influence the canted fin windward streamline patterns (compare Runs 166 and 167 to Run 7). An early X-33 configuration (prior to the Phase II downselect) had experimental evidence of significant spillage of the separated flow in front of the deflected body flap onto the canted fin windward surface.

Shock Interactions

1. Planform schlierens were not performed during this test, which would have provided direct evidence of the shock interaction patterns on the canted fin leading edge. Evidence of a shock interaction pattern on the windward leading edge of the canted fin is thus inferred from the localized streamline inflections at α = 20, 30, and 40-deg (see Runs 2, 5, and 4 of Appendix B). Although it is difficult to determine the interaction location accurately from these results alone, the complexity of the surface flow is revealed. At α = 20 and 30-deg (see Runs 2 and 5), striation patterns suggestive of crossflow vortices appear just inboard of the interaction near the fin/body juncture. As incidence angle is increased, the windward disturbances on the fin appear to weaken. Similar evidence of the weakening of the shock interaction pattern on the windward surface as the angle of attack is increased is also observed in the heating patterns on the canted fin (see Runs 28, 15, and 21 of Appendix A).

Windward Body Flap

Streamline Directions

11. The inboard movement of the attachment lines with increasing angle of attack was identified on the body flap as well as the body chine. In fact, at α = 20-deg the attachment line is aligned with the outer edge of the undeflected body flap (see Runs 6, 5, and 3). For a 20-deg deflected control surface at α = 20-deg (see Runs 166 and 179), it appears that the attachment line, which is still aligned with the outboard flap edge at the hingeline, washes back onto the control surface. The heating images (see Runs 25-28, Appendix A) appear to substantiate this observation, and show a curved region of low surface heating on the outboard section of the body flap that was especially evident at lower Reynolds numbers.

2. The separated region found upstream of a deflected body flap was affected by the location of the forebody attachment line. The inboard movement of the attachment line, associated with an increase in angle of attack, reduced the size of the separation area immediately upwind of the hingeline at low Reynolds number (see Runs 181, 180, and 179).

3. Deflecting the body flaps produces a region of separated flow (see Runs 4 and 170, Appendix C), the size of which is influenced by Reynolds number and the state of the boundary layer. For angles of attack of 20, 30, and 40-deg with a fixed body flap deflection of 20-deg, a separation exists upstream of the flap hinge line for a unit Reynolds number of $1x10^6$/ft (see Runs 166, 176, and 171, Appendix C). This flow separation bubble becomes larger as angle of attack is decreased. This conclusion can also be inferred from schlieren images: as the thin white region (interpreted as the boundary layer) becomes noticeably thicker just in front of the hingeline of the deflected flap. This thickened region becomes even thicker as angle of attack is decreased from 40 to 20-deg (see Runs 182 and 176).

11. As unit Reynolds number is increased to $4x10^6$/ft at α = 30 and 40-deg, the separation from a deflected flap is reduced in size (see Runs 175 and 170). For α = 20-deg, as unit Reynolds number is increased to $4x10^6$/ft (see Run 165), the boundary layer remains attached and the separation is eliminated, indicating that the boundary layer upstream of the deflected body flap is non-laminar at a unit Reynolds number of $4x10^6$/ft. The expected trend of decreasing boundary layer thickness with increasing Reynolds number (from 1 to $4x10^6$/ft) is observed in the schlieren images (see Runs 182 and 184 for α = 20-deg)

5. For a laminar flow upstream of a deflected body flap, an increase in angle of attack produced a larger region aft of the hinge line that was influenced by the separation (see Runs 179, 180, and 181). The subsequent flow reattachment on the body flap was nearly parallel to the hinge line. The recirculation of separated flow upstream of the reattachment point on the body flap was highly three-dimensional with a strong curvature of the streamlines away from the body flap centerline. The spatial point on the flap that defines the inboard or outboard flow spillage direction appeared to move inboard on the flap surface with an increase in angle of attack, perhaps in relation to the forebody attachment line. As stated before, the separated region in front of the deflected body flap did not appear to spill over or influence the surface streamlines associated with the nearby windside canted fins (see Runs 166, 167, and 171).

11. Expansion of the flow around the body flap edges is indicated by the local streamline curvature found in this vicinity (see Run 181). The outboard streamline curvature is most pronounced at α = 40-deg and is indicative of a stronger lateral pressure gradient associated with the higher angle of attack.

Shock Interactions

1. The interaction of the bow shock with the compression shock originating from the deflected body flap is observed at all angles of attack. However, the details of the interaction in the vicinity of the flaps are difficult to filter out of the integrated schlieren image. (A focused schlieren system might have been able to provide a clearer picture of the interaction.) The α = 40-deg case with a body flap deflection of 20-deg (see Run 183 of Appendix B) is one which is particularly difficult to interpret without additional information, either from a focusing schlieren system or CFD.

2. A 20-deg deflected body flap at angles of attack of 30 and 40-deg produced a disturbance in the flap streamline pattern (see Runs 180 and 181) which was not strongly effected by Reynolds number (see Runs 175 and 171). This disturbance is likely the result of an interaction of the bow shock with the shock emanating from the deflected body flap. From the corresponding heating images (see Runs 16 and 25 of Appendix A), the disturbance is characterized by high localized heating peak that is angled roughly 60-deg to the centerline and is followed by a rapid decrease in heating.

Conclusions

An experimental investigation of the aeroheating characteristics for the X-33 Rev-F configuration has been conducted in the LaRC 20-Inch Mach 6 Tunnel. Phosphor thermography was used to provide global heating images of the windward surface for a variety of angles-of-attack, Reynolds numbers, and body flap deflections. Additionally, the effect of discrete roughness elements was investigated, which included trip location, height, width, and orientation parametrics. The aeroheating results were complemented with schlieren and oil-flow images that provided shock-shape and surface streamline information. This report is intended to be a "quick-release" of the experimental data for review by the X-33 program, thus, analysis is limited to observations of experimental results.

Acknowledgment

The following individuals were instrumental in the processes that were required to accomplish this experimental work: Mark Cagle of ETTD/MISB for model design; Mike Powers and Mark Griffith of FD/CMFSS for model construction; Ed Covington and Tom Burns of FD/QAIB for model surface inspection and verification; Grace Gleason, Rhonda Manis, and Johnny Ellis of FSSD/ASS, and Bert Senter of CSC for facility technical support; Glen Bittner of CSC and Ron Merski of AGDD/AB for test technique support, and H. Harris Hamilton, II provided the attachment line fiducial mark locations.

References

1.Bekey, I., Powell, R., and Austin. R., "NASA Studies Access to Space," *Aerospace America*, May 1994, pp. 38-43.

2.Cook, S. A., "X-33 Reusable Launch Vehicle Structural Technologies," AIAA Paper 97-10873, Nov. 1996.

3.Freeman Jr., D. C., Talay, T. A., and Austin, R. E., "Reusable Launch Vehicle Technology Program," AIAA Paper IAF 96-V.4.01, Oct. 1996.

4.Baumgartner, R. I., and Elvin, J. D., "Lifting Body – An Innovative RLV Concept," AIAA Paper 95-3531, Sept. 1995.

5.Thompson. R. A., Hamilton, H. H., Berry, S. A., and Horvath, T. J., "Hypersonic Boundary Layer Transition for X-33 Phase II Vehicle," AIAA Paper 98-0867, January 1998.

6.Miller, C. G., "Langley Hypersonic Aerodynamic/Aerothermodynamic Testing Capabilities - Present and Future," AIAA Paper 90-1376, June 1990.

7.Buck, G. M., "Automated Thermal Mapping Techniques Using Chromatic Image Analysis," NASA TM 101554, April 1989.

8.Buck, G. M., "Surface Temperature/Heat Transfer Measurement Using A Quantitative Phosphor Thermography System," AIAA Paper 91-0064, Jan. 1991.

9.Merski, N. R., "Reduction and Analysis of Phosphor Thermography Data With the IHEAT Software Package," AIAA Paper 98-0712, Jan. 1998.

10.Berry, S. A., Bouslog, S. A., Brauckmann, G. J., and Caram, J. M., "Shuttle Orbiter Experimental Boundary-Layer Transition Results with Isolated Roughness," *Journal of Spacecraft and Rockets*, Vol. 35, No. 3, 1998, pp. 241-248.

11.Berry, S. A., Horvath, T. J., DiFulvio, M., Glass, C., and Merski, N. R., "X-34 Experimental Aeroheating at Mach 6 and 10," AIAA Paper 98-0881, January 1998.

12.Horvath, T. J., Rhode, M. N., and Buck, G. M., "Aerothermodynamic Measurements on a Proposed Assured Crew Return Vehicle (ACRV) Lifting Body Configuration at Mach 6 and 10 in Air," AIAA Paper 90-1744, June 1990.

13.Micol, J. R., "Aerothermodynamic Measurement and Prediction for a Modified Orbiter at Mach 6 and 10 in Air," *Journal of Spacecraft and Rockets*, Vol. 32, No. 5, 1995, pp. 737-748.

14.Loomis, M. P., Venkatapathy, E., Davies, C. B., Campbell, C. H., Berry, S. A., Horvath, T. J., and Merski, N. R., "Aerothermal CFD Validation and Prediction for the X-38 Program," AIAA Paper 97-2484, June 1997.

15.Hamilton, H., Berry, S., Horvath, T., and Weilmuenster, J., "Computational/ Experimental Aeroheating Predictions for X-33 Phase II Vehicle," AIAA Paper 98-0869, January 1998.

16.Buck, G. M. and Vasquez, P., "An Investment Ceramic Slip-Casting Technique for Net-Form, Precision, Detailed Casting of Ceramic Models," U. S. Patent 5,266,252, November 30, 1993.

17.Bertin, J. J., Hayden, T. E., and Goodrich, W. D., "Shuttle Boundary-Layer Transition Due to Distributed Roughness and Surface Cooling," *Journal of Spacecraft and Rockets*, Vol. 19, No. 5, 1982, pp. 389-396.

18.Fay, J. A., and Ridell, F. R., "Theory of Stagnation Point Heat Transfer in Dissociated Air," *Journal of Aeronautical Sciences*, Vol. 25, No. 2, 1958.

19. Berry, S. A., Horvath, T. J., Roback, V. E., and Williams, G. B., "Results of Aerothermodynamic and Boundary-Layer Transition Testing of 0.0362-Scale X-38 (Rev. 3.1) Vehicle in NASA Langley 20-Inch Mach 6 Tunnel," NASA TM-112857, September 1997.

Table 1: X-33 Phase II Aeroheating Tests in NASA LaRC AB Tunnels

Year	Tunnel	Test	Occupancy Dates	Runs	Description
1996	20" M6	6731	Aug 28 - Sept	1-46	D-loft Forebody Baseline
1996	M6 CF4	114	Oct 17 - Nov 6	1-43	Yaw Dispersions
1996	20" M6	6737	Dec 6 - Dec 20	1-174	D-loft Forebody Transition
1997	20" M6	6751	June 23 - June 30	1-52	Generic Bowed Panel Models
1997	20" M6	6751	July 15 - July 17	52-56	Generic Bowed Panel Models
1997	20" M6	6753	July 17 - July 22	1-22	Rev C (37-deg Dihedral) Baseline
1997	20" M6	6753	Aug 12 - Aug 20	22-50	Rev C (37-deg Dihedral) Baseline
1997	20" M6	6751	Aug 27 - Aug 29	56-99	Generic Bowed Panel Models
1997	20" M6	6751	Sept 22 - Sept 24	100-115	Generic Bowed Panel Models
1997	20" M6	6763	Dec 30 - Jan 6	1-29	Rev F (20-deg Dihedral) Baseline
1998	20" M6	6763	Jan 15 - Jan 22	30-68	Rev F (20-deg Dihedral) Baseline
1998	20" M6	6763	Feb 17 - Mar 4	69-203	Rev F Discrete Roughness
1998	20" M6	6769	Apr 3 - Apr 17	1-123	Rev F Bowed Panels I
1998	**20" M6**	**6770**	**May 22 - Jun 24**	**1-185**	**Rev F Attach-Line Roughness**
1998	20" M6	6777	Aug 5 - Aug 12	1-40	Rev F Blade vs. sting

Table 2: X-33 Phase II Model Designation List

Designation	Description	scale	Nose rad	δ_{BF}	Panel array	Panel height
DL10-X	D-Loft 10" Forebody	0.0194	1.056	n/a	n/a	n/a
DL09-X	D-Loft 9" Forebody	0.0175	0.950	n/a	n/a	n/a
FL10-X	F-Loft 10" Forebody	0.0194	1.056	n/a	n/a	n/a
FL07-X	F-Loft 7" Forebody	0.0132	0.629	n/a	n/a	n/a
RC10A1-X	F-Loft Rev-C 10" (37-deg Dihedral)	0.0132	0.629	0-deg	n/a	n/a
RC10A2-X	F-Loft Rev-C 10" (37-deg Dihedral)	0.0132	0.629	10-deg	n/a	n/a
RC10A3-X	F-Loft Rev-C 10" (37-deg Dihedral)	0.0132	0.629	20-deg	n/a	n/a
RF10A1-X	**F-Loft Rev-F 10"** (20-deg Dihedral)	**0.0132**	**0.629**	**0-deg**	**n/a**	**n/a**
RF10A2-X	**F-Loft Rev-F 10"** (20-deg Dihedral)	**0.0132**	**0.629**	**10-deg**	**n/a**	**n/a**
RF10A3-X	**F-Loft Rev-F 10"** (20-deg Dihedral)	**0.0132**	**0.629**	**20-deg**	**n/a**	**n/a**
RF10B1-X	F-Loft Rev-F 10" (20-deg Dihedral)	0.0132	0.629	20-deg	Centerline	0.002
RF10B2-X	F-Loft Rev-F 10" (20-deg Dihedral)	0.0132	0.629	20-deg	Centerline	0.004
RF10B3-X	F-Loft Rev-F 10" (20-deg Dihedral)	0.0132	0.629	20-deg	Centerline	0.006
RF10C1-X	F-Loft Rev-F 10" (20-deg Dihedral)	0.0132	0.629	20-deg	Chine	0.002
RF10C2-X	F-Loft Rev-F 10" (20-deg Dihedral)	0.0132	0.629	20-deg	Chine	0.004
RF10C3-X	F-Loft Rev-F 10" (20-deg Dihedral)	0.0132	0.629	20-deg	Chine	0.006
RF10D1-X	F-Loft Rev-F 10" (20-deg Dihedral)	0.0132	0.629	20-deg	Both	0.002
RF10D2-X	F-Loft Rev-F 10" (20-deg Dihedral)	0.0132	0.629	20-deg	Both	0.004
RF10D3-X	F-Loft Rev-F 10" (20-deg Dihedral)	0.0132	0.629	20-deg	Both	0.006
RF10E1-X	F-Loft Rev-F 10" (20-deg Dihedral)	0.0132	0.629	20-deg	Front Row	0.002
RF10E2-X	F-Loft Rev-F 10" (20-deg Dihedral)	0.0132	0.629	20-deg	Front Row	0.004
RF10E3-X	F-Loft Rev-F 10" (20-deg Dihedral)	0.0132	0.629	20-deg	Front Row	0.006
RF06A3S-X	F-Loft Rev-F 6.47" w/ sting mount	0.0085	0.405	20-deg	n/a	n/a
RF06A3B-X	F-Loft Rev-F 6.47" w/ blade mount	0.0085	0.405	20-deg	n/a	n/a
RG05A1-X	F-Loft Rev-G 5.3" w/ blade mount	0.0070	0.333	0-deg	n/a	n/a
RG05A2-X	F-Loft Rev-G 5.3" w/ blade mount	0.0070	0.333	10-deg	n/a	n/a
RG05A3-X	F-Loft Rev-G 5.3" w/ blade mount	0.0070	0.333	20-deg	n/a	n/a

Key: -X refers to casting sequence where -A designates the primary model, -B the secondary, -C the third, etc. and -O refers to the oil-flow model.

Table 3: Windward Trip locations and fiducial marks.

Fiducial	x/L	y/L	Notes
CL1	0.0523	0	
CL2	0.0981	0	
CL3	0.1963	0	
AL3-40	0.1963	±0.0563	*P/S*
AL3-30	0.1963	±0.0712	*P/S*
AL3-20	0.1963	±0.0852	*P/S*
CL4	0.3271	0	
AL4-40	0.3271	±0.1011	*P/S*
AL4-30	0.3271	±0.1211	*P/S*
AL4-20	0.3271	±0.1377	*P/S*
CL5	0.4514	0	
FM5	0.4514	±0.1038	*P/S*
AL5-40	0.4514	±0.1446	*P/S*
AL5-40W	0.4514	±0.1554	*P/S, Wing*
AL5-30	0.4514	±0.1663	*P/S*
AL5-30W	0.4514	±0.1743	*P/S, Wing*
AL5-20	0.4514	±0.1823	*P/S*
AL5-20W	0.4514	±0.1903	*P/S, Wing*
CL6	0.6000	0	
AL6-40	0.6000	±0.1983	*P/S*
AL6-30	0.6000	±0.2203	*P/S*
AL6-20	0.6000	±0.2357	*P/S*
CL-Tail	0.9366	0	

Key to Notes: *P/S* indicates that marks were placed on both port and starboard side of centerline, *Wing* identifies attachment line locations that were selected to influence the wing leading edge.

Table 4: Nominal flow conditions and run-to-run repeatability for 20-Inch Mach 6 Tunnel.

$Re_\infty(x10^6/ft)$	M_∞	P_{t1} (psi)	T_{t1} (-degR)	H_{t1}(BTU/lbm)	P_{t2}(psi)
1.08 ± 2.65%	6.00 ± 0.48%	59.63 ± 1.65%	883.21 ± 0.92%	212.46 ± 0.94%	1.76 ± 2.93%
1.54 ± 2.99%	5.98 ± 0.22%	84.59 ± 2.43%	888.18 ± 0.77%	213.68 ± 0.79%	2.55 ± 2.63%
1.81 ± 1.67%	5.99 ± 0.17%	99.56 ± 1.66%	885.74 ± 0.37%	213.08 ± 0.38%	2.97 ± 1.53%
2.15 ± 1.38%	5.99 ± 0.13%	124.18 ± 1.02%	911.39 ± 0.54%	219.41 ± 0.56%	3.70 ± 1.26%
3.09 ± 1.32%	6.00 ± 0.17%	179.11 ± 0.88%	912.22 ± 0.52%	219.61 ± 0.53%	5.32 ± 1.07%
4.27 ± 2.30%	6.00 ± 0.22%	249.19 ± 1.57%	914.73 ± 0.66%	220.23 ± 0.68%	7.36 ± 1.63%
4.97 ± 1.51%	6.01 ± 0.12%	298.75 ± 0.95%	930.35 ± 0.81%	224.09 ± 0.83%	8.79 ± 1.09%
5.90	6.02	363.44	942.04	226.98	10.62

Table 5: Run log for aeroheating portion of Test 6770 conducted in LaRC 20-Inch Mach 6 Tunnel.

RUN	DATE	MODEL	α	Re/ft	P_0	T_0	Trip		NOTES
	(1998)		deg	x10^6/ft	psi	R	Height	Location	
ESTABLISH BASELINE SMOOTH DATA AT α = 20-deg, 30-deg, and 40-deg									
11	5/27	RF10A2-B	30	4.25	245.79	914.84			Start with old model to establish credibility. Does data repeat when compared to previous test?
12	5/28	RF10A2-B	30	4.22	246.95	913.99			
13	5/28	RF10A2-B	30	5.90	360.84	937.15			
14	5/28	RF10A2-B	30	2.15	124.39	909.93			
15	5/29	RF10A3-C	30	4.33	251.77	912.88			Starting with new model
16	5/29	RF10A3-C	30	4.34	251.72	910.77			
17	5/29	RF10A3-C	30	3.11	180.08	912.76			
18	5/29	RF10A3-C	30	2.15	124.51	911.18			
19	5/29	RF10A3-C	30	1.07	59.02	881.75			
20	5/29	RF10A3-C	40	4.23	248.93	918.56			Surface defect, rub down and repeat
21	6/1	RF10A3-C	40	4.26	249.84	914.54			
22	6/1	RF10A3-C	40	3.09	178.52	907.90			
23	6/1	RF10A3-C	40	2.14	123.92	910.65			
24	6/1	RF10A3-C	40	1.09	59.79	881.95			
25	6/1	RF10A3-C	20	1.10	60.38	882.92			
26	6/1	RF10A3-C	20	2.15	124.58	912.23			
27	6/1	RF10A3-C	20	3.06	178.62	914.60			
28	6/1	RF10A3-C	20	4.29	250.61	913.87			
DISCRETE ROUGHNESS ON PORT SIDE ONLY @ α = 30-deg									
29	6/1	RF10A3-C	30	2.17	125.05	912.17	0.0025	AL6-30-P	
30	6/2	RF10A3-C	30	3.06	177.88	914.64	0.0025	AL6-30-P	Lost trip during Run, replace and repeat
31	6/2	RF10A3-C	30	3.13	179.76	906.53	0.0025	AL6-30-P	Lost trip during Run, replace and repeat
32	6/2	RF10A3-C	30	2.17	124.83	909.06	0.0025	AL6-30-P	
33	6/2	RF10A3-C	30	3.09	178.52	910.19	0.0025	AL6-30-P	
34	6/2	RF10A3-C	30	4.23	248.86	918.44	0.0025	AL6-30-P	
35	6/2	RF10A3-C	30	4.93	298.12	933.17	0.0025	AL6-30-P	Lost Trip After Run
36	6/2	RF10A3-C	30	1.07	59.47	885.37	0.005	AL6-30-P	
37	6/2	RF10A3-C	30	2.16	125.15	913.18	0.005	AL6-30-P	
38	6/2	RF10A3-C	30	1.56	85.87	887.29	0.005	AL6-30-P	
39	6/2	RF10A3-C	30	1.82	100.18	886.77	0.005	AL6-30-P	
40	6/2	RF10A3-C	30	3.11	179.93	911.70	0.005	AL6-30-P	
COMPARISON OF ORIGINAL W=0.05-IN ON PORT TO W=0.10-IN WIDE TRIPS ON STARBOARD									
41	6/3	RF10A3-C	30	3.08	178.67	913.30	0.0025	AL5-30	Lost W=0.05-in trip, replace and repeat
42	6/3	RF10A3-C	30	3.08	179.64	915.93	0.0025	AL5-30	
43	6/3	RF10A3-C	30	4.15	247.00	923.11	0.0025	AL5-30	W=0.05-in trip sticking up after run
44	6/3	RF10A3-C	30	4.96	298.27	930.85	0.0025	AL5-30	W=0.05-in trip sticking up after run
CONTINUE WITH 0.1-IN WIDE TRIPS ONLY, WITH 0.0025-IN HIGH ON PORT AND 0.0050-IN ON STARBOARD									
45	6/3	RF10A3-C	30	1.50	82.95	888.55	BOTH	AL6-30	
46	6/3	RF10A3-C	30	1.78	98.43	887.37	BOTH	AL6-30	
47	6/3	RF10A3-C	30	2.15	124.01	912.01	BOTH	AL6-30	
48	6/3	RF10A3-C	30	3.06	177.86	913.18	BOTH	AL6-30	
49	6/3	RF10A3-C	30	4.29	249.08	911.52	BOTH	AL6-30	**BAD RUN**, TPS crashed during run
50	6/3	RF10A3-C	30	4.25	248.34	915.67	BOTH	AL6-30	
51	6/3	RF10A3-C	30	4.97	299.93	932.16	BOTH	AL6-30	Port trip sticking up after run
52	6/4	RF10A3-C	30	1.09	59.05	878.33	BOTH	AL5-30	

53	6/4	RF10A3-C	30	2.15	124.44	913.28	BOTH	AL5-30	
54	6/4	RF10A3-C	30	3.09	179.56	914.21	BOTH	AL5-30	Port trip corner up, replace & repeat
55	6/4	RF10A3-C	30	3.06	177.93	913.40	BOTH	AL5-30	Port trip corner up, replace & repeat
56	6/4	RF10A3-C	30	3.09	179.14	912.65	BOTH	AL5-30	Port trip corner up, replace & repeat
57	6/4	RF10A3-C	30	3.11	179.76	911.60	BOTH	AL5-30	
58	6/4	RF10A3-C	30	4.26	248.58	914.39	BOTH	AL5-30	
59	6/4	RF10A3-C	30	4.94	298.00	932.67	BOTH	AL5-30	
NEW APPROACH: REDUNDANT TRIPS ON PORT AND STARBOARD WITH ADDITIONAL CL TRIP OF SAME HEIGHT									
60	6/4	RF10A3-C	30	3.09	179.09	912.70	0.0025	AL4-30	CL trip corner sticking up after run
61	6/4	RF10A3-C	30	3.07	178.40	915.38	0.0025	AL4-30	CL trip corner sticking up after run
62	6/4	RF10A3-C	30	4.22	246.19	916.01	0.0025	AL4-30	Lost STBD trip, replace & repeat
63	6/5	RF10A3-C	30	4.16	244.08	918.62	0.0025	AL4-30	Decided to change out model
NEW MODEL BASELINE @ α = 30-deg									
64	6/5	RF10A3-D	30	1.08	59.59	883.29			
65	6/5	RF10A3-D	30	2.15	124.24	911.74			
66	6/5	RF10A3-D	30	3.07	178.67	915.32			
67	6/5	RF10A3-D	30	4.28	249.28	913.99			Surface defect, rub down and repeat
68	6/5	RF10A3-D	30	4.26	248.39	913.97			
TRIPPING ON NEW MODEL @ α = 30-deg									
69	6/5	RF10A3-D	30	3.08	178.65	912.43	0.0025	AL4-30	
70	6/8	RF10A3-D	30	4.28	250.34	913.20	0.0025	AL4-30	Asymmetric, visual looked OK
71	6/8	RF10A3-D	30	4.27	248.91	911.00	0.0025	AL4-30	
72	6/8	RF10A3-D	30	4.96	300.28	932.52	0.0025	AL4-30	
73	6/8	RF10A3-D	30	1.09	59.52	882.56	0.005	AL4-30	
74	6/8	RF10A3-D	30	2.14	123.87	911.52	0.005	AL4-30	
75	6/8	RF10A3-D	30	1.52	83.72	887.15	0.005	AL4-30	
76	6/8	RF10A3-D	30	1.81	99.89	885.17	0.005	AL4-30	
77	6/8	RF10A3-D	30	3.07	179.19	914.51	0.005	AL4-30	
78	6/8	RF10A3-D	30	3.10	179.64	910.90	0.0025	AL3-30	
79	6/8	RF10A3-D	30	4.30	249.87	912.15	0.0025	AL3-30	
80	6/8	RF10A3-D	30	4.94	298.47	933.27	0.0025	AL3-30	Port trip corner up, replace & repeat
81	6/8	RF10A3-D	30	4.28	250.41	916.60	0.0025	AL3-30	Port trip corner up, replace & repeat
82	6/8	RF10A3-D	30	4.28	249.37	914.07	0.0025	AL3-30	
83	6/8	RF10A3-D	30	1.51	83.23	888.29	0.005	AL3-30	
84	6/9	RF10A3-D	30				0.005	AL3-30	**BAD RUN**, DAS did not trigger
85	6/9	RF10A3-D	30	1.80	99.15	885.88	0.005	AL3-30	P/S trips, corner up, replace & repeat
86	6/9	RF10A3-D	30	1.82	100.65	886.44	0.005	AL3-30	Port trip corner up, replace & repeat
87	6/9	RF10A3-D	30	1.81	99.05	882.80	0.005	AL3-30	
88	6/9	RF10A3-D	30	2.16	124.36	908.19	0.005	AL3-30	
89	6/9	RF10A3-D	30	3.09	179.61	912.82	0.005	AL3-30	
TRIPPING ON NEW MODEL @ AOA=40-deg									
90	6/10	RF10A3-D	40	1.53	84.81	889.22	0.005	**AL3-30**	Note previous trip left on outboard fiducial
91	6/10	RF10A3-D	40	2.16	124.19	908.75	0.005	**AL3-30**	
92	6/10	RF10A3-D	40	3.08	178.30	911.08	0.005	**AL3-30**	
93	6/10	RF10A3-D	40	3.10	180.01	913.69	0.0025	AL6-40	
94	6/10	RF10A3-D	40	4.30	251.11	915.57	0.0025	AL6-40	
95	6/10	RF10A3-D	40	2.15	124.14	910.29	0.0025	AL6-40	
96	6/10	RF10A3-D	40	5.00	301.17	932.02	0.0025	AL6-40	

97	6/10	RF10A3-D	40	1.09	59.81	888.16	0.005	AL6-40	
98	6/10	RF10A3-D	40	1.51	83.99	893.77	0.005	AL6-40	
99	6/10	RF10A3-D	40	2.13	123.05	911.70	0.005	AL6-40	
100	6/10	RF10A3-D	40	2.13	123.92	914.33	0.0025	AL5-40	
101	6/10	RF10A3-D	40	3.07	177.36	911.28	0.0025	AL5-40	STBD trip corner up, replace & repeat
102	6/10	RF10A3-D	40	3.11	178.60	908.83	0.0025	AL5-40	
103	6/10	RF10A3-D	40	4.20	245.89	917.30	0.0025	AL5-40	
104	6/10	RF10A3-D	40	4.93	296.72	930.75	0.0025	AL5-40	
105	6/10	RF10A3-D	40	1.07	59.77	890.79	0.005	AL5-40	
106	6/10	RF10A3-D	40	1.56	85.47	887.44	0.005	AL5-40	
107	6/11	RF10A3-D	40				0.005	AL5-40	**BAD RUN**, DAS did not trigger
108	6/11	RF10A3-D	40	2.13	123.52	913.38	0.005	AL5-40	
109	6/11	RF10A3-D	40	3.08	177.98	909.86	0.005	AL5-40	
110	6/11	RF10A3-D	40				0.0025	AL4-40	**BAD RUN**, DAS did not trigger
111	6/11	RF10A3-D	40	2.17	125.13	911.87	0.0025	AL4-40	
112	6/11	RF10A3-D	40	3.11	178.97	909.02	0.0025	AL4-40	STBD trip corner up, replace & repeat
113	6/12	RF10A3-D	40	3.13	180.80	910.03	0.0025	AL4-40	
114	6/12	RF10A3-D	40	4.32	250.93	911.58	0.0025	AL4-40	P/CL trips, corner up, replace & repeat
115	6/12	RF10A3-D	40	4.28	249.82	913.04	0.0025	AL4-40	P/CL trips, corner up, replace & repeat
116	6/12	RF10A3-D	40	4.32	250.19	910.59	0.0025	AL4-40	Port trip, corner up, replace & repeat
117	6/12	RF10A3-D	40	4.28	250.78	916.94	0.0025	AL4-40	Port trip, corner up, replace & repeat
118	6/12	RF10A3-D	40	4.40	253.16	908.06	0.0025	AL4-40	Still asymmetric, visual looked OK
119	6/12	RF10A3-D	40	4.96	296.62	927.13	0.0025	AL4-40	
120	6/12	RF10A3-D	40	1.52	83.89	891.56	0.005	AL4-40	Port trip, corner up, replace & repeat
121	6/12	RF10A3-D	40	1.54	84.56	886.55	0.005	AL4-40	Port trip, corner up, replace & repeat
122	6/12	RF10A3-D	40	1.55	84.07	882.06	0.005	AL4-40	Still asymmetric, visual looked OK
123	6/12	RF10A3-D	40	2.14	123.12	910.77	0.005	AL4-40	
124	6/15	RF10A3-D	40	3.05	178.92	915.38	0.005	AL4-40	
125	6/15	RF10A3-D	40	4.29	250.19	912.49	0.005	AL4-40	
126	6/15	RF10A3-D	40	1.11	60.61	875.24	0.005	AL3-40	
127	6/15	RF10A3-D	40	2.15	123.92	911.50	0.005	AL3-40	Replaced both trips based on visual
128	6/15	RF10A3-D	40	1.53	85.43	894.09	0.005	AL3-40	
129	6/15	RF10A3-D	40	2.11	123.30	918.32	0.005	AL3-40	Asymmetric, visual looked OK
130	6/15	RF10A3-D	40	3.08	179.14	915.46	0.005	AL3-40	
131	6/15	RF10A3-D	40	2.17	125.60	911.93	0.005	AL3-40	Still asymmetric, visual looked OK
132	6/15	RF10A3-D	40	2.17	123.79	904.79	0.0025	AL3-40	
133	6/15	RF10A3-D	40	3.09	179.12	912.01	0.0025	AL3-40	P/CL trips, corner up, replace & repeat
134	6/15	RF10A3-D	40	3.08	178.60	913.61	0.0025	AL3-40	Port trip, corner up, replace & repeat
135	6/15	RF10A3-D	40	3.13	179.29	907.60	0.0025	AL3-40	Visual looked OK, remove Port & repeat
136	6/15	RF10A3-D	40	4.21	246.73	917.83	0.0025	AL3-40	Port still tripped, rub down surface defect
137	6/16	RF10A3-D	40	5.90	366.03	946.93	0.0025	AL3-40	
NEW MODEL BASELINE @ α = 20-deg and 40-deg									
138	6/16	RF10A3-D	40	1.06	59.10	885.13			
139	6/16	RF10A3-D	40	2.14	123.84	912.39			
140	6/16	RF10A3-D	40	4.23	248.56	918.11			
141	6/16	RF10A3-D	40	3.09	179.19	911.74	0.0025	AL3-40	

142	6/17	RF10A3-D	40	4.31	251.25	913.34	0.0025	AL3-40	Asymmetric, visual looked OK
143	6/17	RF10A3-D	40	4.94	299.76	934.73	0.0025	AL3-40	Asymmetric, visual looked OK
144	6/17	RF10A3-D	20	3.12	180.21	909.52	0.0025	**AL3-40**	Note previous trip left on inboard fiducial
145	6/17	RF10A3-D	20	4.28	250.26	915.89	0.0025	**AL3-40**	
146	6/17	RF10A3-D	20	5.04	298.05	921.06	0.0025	**AL3-40**	
TRIPPING ON NEW MODEL @ AOA=20-deg									
147	6/17	RF10A3-D	20	2.14	123.62	911.83	0.005	AL3-20	
148	6/17	RF10A3-D	20	3.12	179.64	910.35	0.005	AL3-20	Room lights left on during run, repeat
149	6/17	RF10A3-D	20	3.09	179.22	915.18	0.005	AL3-20	Asymmetric, visual looked OK
150	6/17	RF10A3-D	20	4.26	250.49	919.04	0.005	AL3-20	
151	6/17	RF10A3-D	20				0.005	AL3-20	**BAD RUN**, model inj. during startup
152	6/17	RF10A3-D	20				0.005	AL3-20	**BAD RUN**, lost heater before run
153	6/17	RF10A3-D	20	5.04	300.32	926.28	0.005	AL3-20	
154	6/17	RF10A3-D	20	3.09	178.77	910.86	0.005	AL3-20	Removed Port trip and repeated R149
155	6/18	RF10A3-D	20	3.10	179.91	912.74	0.0025	AL6-20	STBD trip corner up, replace & repeat
156	6/18	RF10A3-D	20	3.10	179.34	911.28	0.0025	AL6-20	
157	6/18	RF10A3-D	20	4.26	248.16	913.50	0.0025	AL6-20	
158	6/18	RF10A3-D	20	4.96	298.05	927.94	0.0025	AL6-20	
159	6/19	RF10A3-D	20	1.56	85.90	885.74	0.005	AL6-20	
160	6/19	RF10A3-D	20	2.15	123.74	907.54	0.005	AL6-20	
161	6/19	RF10A3-D	20	3.10	180.87	914.84	0.005	AL6-20	
162	6/19	RF10A3-D	20	1.08	59.47	882.99	0.0075	AL6-20	
163	6/19	RF10A3-D	20	1.57	85.75	884.60	0.0075	AL6-20	
164	6/19	RF10A3-D	20	2.16	124.76	912.98	0.0075	AL6-20	

Key to Notes: TPS refers to the Thermographic Phosphor System, DAS refers to the wind tunnel flow conditions Data Acquisition System

Table 6: Run log for flow visualization portion of Test 6770 conducted in the LaRC 20-Inch Mach 6 Tunnel.

RUN	DATE	MODEL	_	Re/ft	Po	To	Oil Viscosity		NOTES
	(1998)		deg	x10^6/ft	psi	R	Base Coat	Dots	
DETERMINATION OF CHINE ATTACHMENT LINES @ Re/ft=4x10^6 BF= 0 deg									
1	5/22	RF10A1-O	30	4.24	247.5	920.1	200B	200D	
2	5/22	RF10A1-O	20	4.37	250.3	909.3	200B	200D	
3	5/22	RF10A1-O	40	4	250	450	200B	200D	
4	5/25	RF10A1-O	40	4.31	249.6	914.8	thin base	200D	Thin Base Allowed Paint to Blister
5	5/25	RF10A1-O	30	4.32	250.5	915.9	thin base	200D	
6	5/25	RF10A1-O	20	4.34	250.3	913.1	thin base	200D	
7	5/25	RF10A1-O	20	2.18	123.9	915.1	200B	200D	
8	5/25	RF10A1-O	30	2.21	124.5	909.3	200B	200D	
9	5/25	RF10A1-O	40	2.19	124.8	915.3	200B	200D	Dot Density Decreased
10	5/25	RF10A1-O	30	2.21	124.5	909.9	200B	200D	Dot Density Decreased
GENERAL FLOW FEATURES WITH BODY FLAP = 20 deg									
165	6/22	RF10A3-O	20	4.29	250.8	912.1	200B	200D	
166	6/22	RF10A3-O	20	1.02	60.23	882.3	200B	200D	
167	6/22	RF10A3-O	20	2.14	124.8	910.1	200B	200D	
168	6/22	RF10A3-O	20	3.12	179.8	907.4	200B	200D	
179	6/23	RF10A3-O	20	2	125	450	200B	200D	Body Flaps Only
173	6/22	RF10A3-O	30	2.21	125.2	913.7	200B	200D	
174	6/23	RF10A3-O	30	3.12	178.9	912.9	200B	200D	
175	6/23	RF10A3-O	30	4.35	250.7	912.8	200B	200D	
176	6/23	RF10A3-O	30	1.13	59.17	880.8	50B	200D, 50D	
177	6/23	RF10A3-O	30	2	125	450	200B	200D	Body Flaps Only
180	6/23	RF10A3-O	30	1	60	425	200B	200D, 50D	Body Flaps Only
169	6/22	RF10A3-O	40	2.2	124	909.1	200B	200D	M-Probe removed, too close to BF
170	6/22	RF10A3-O	40	4.33	247.4	908.3	200B	200D	
171	6/22	RF10A3-O	40	1.14	59.77	884.5	200B	200D	
172	6/22	RF10A3-O	40	3	180	450	200B	200D	
178	6/23	RF10A3-O	40	2	125	450	200B	200D	Body Flaps Only
181	6/23	RF10A3-O	40	1	60	450			Body Flaps Only
SCHLIEREN ONLY									
182	6/24	RF10A3-D	20,40	1,2	60	425			
183	6/24	RF10A3-D	40	2,3,4	125,180 ,250	450			Wing broke
184	6/24	RF10A3-D	20	3,4	180,250	450			

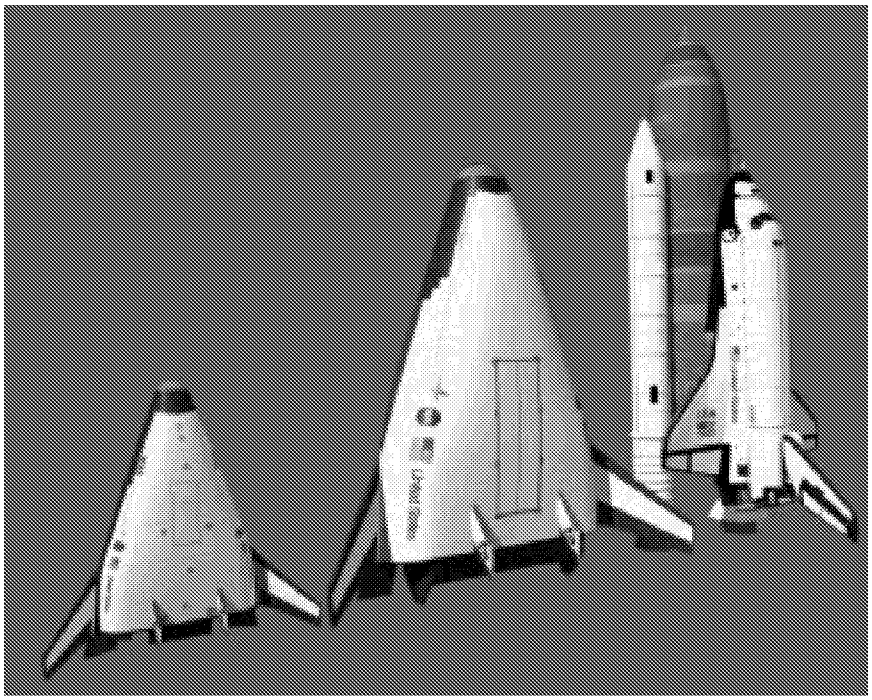

Figure 1. Comparison of X-33 to proposed RLV and the Space Shuttle.

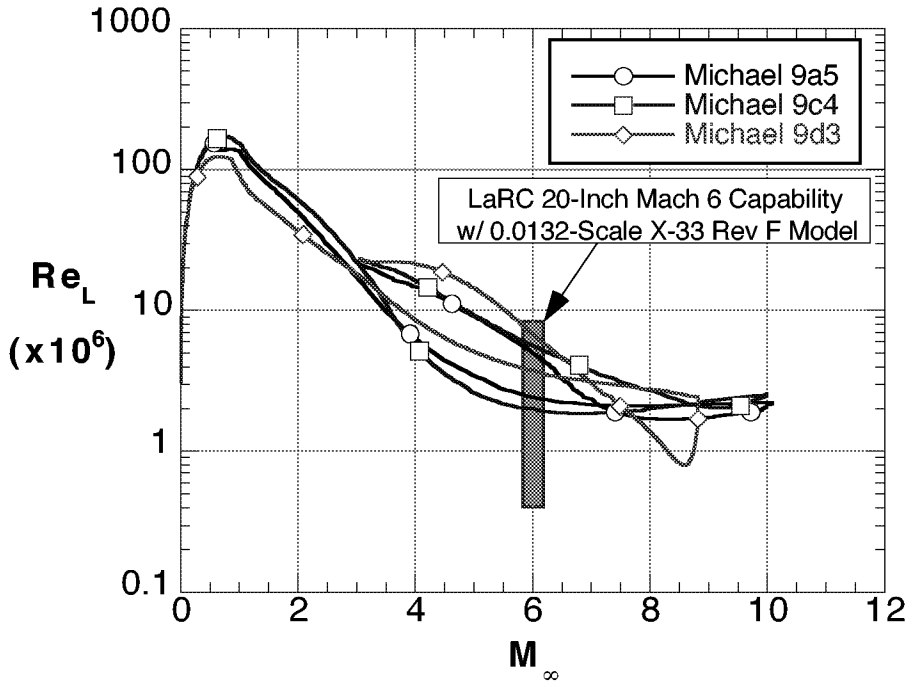

Figure 2. Preliminary X-33 trajectory

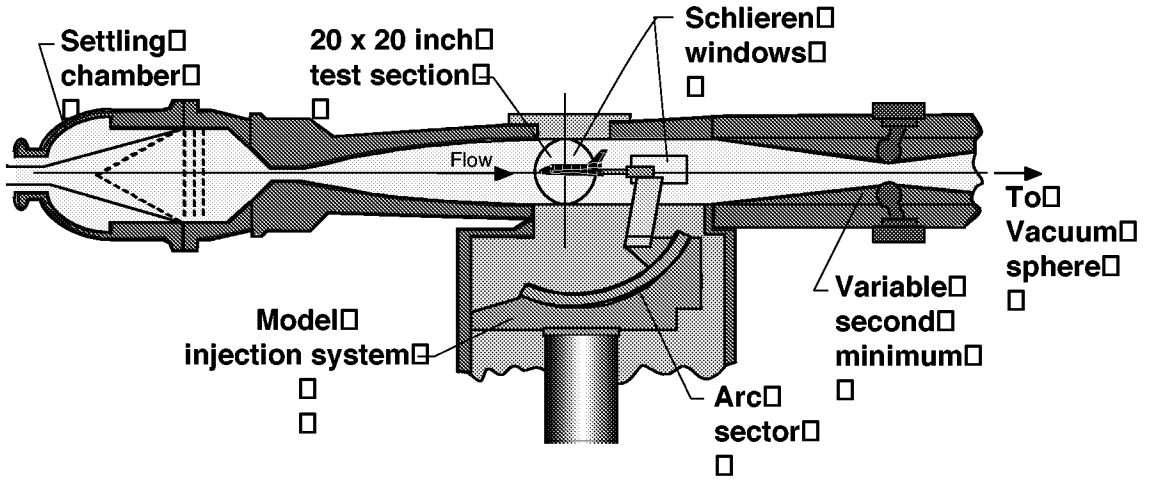

Nominal Mach number:	6.0	Total pressure (psia):	30 to 475
Reynolds number (x 10^6/ft):	0.5 to 8	Total temperature (°R):	810 to 1018
Dynamic pressure (psf):	69 to 1264	Run time (minutes):	1 to 15

Figure 3. Schematic of NASA Langley 20-Inch Mach 6 Tunnel.

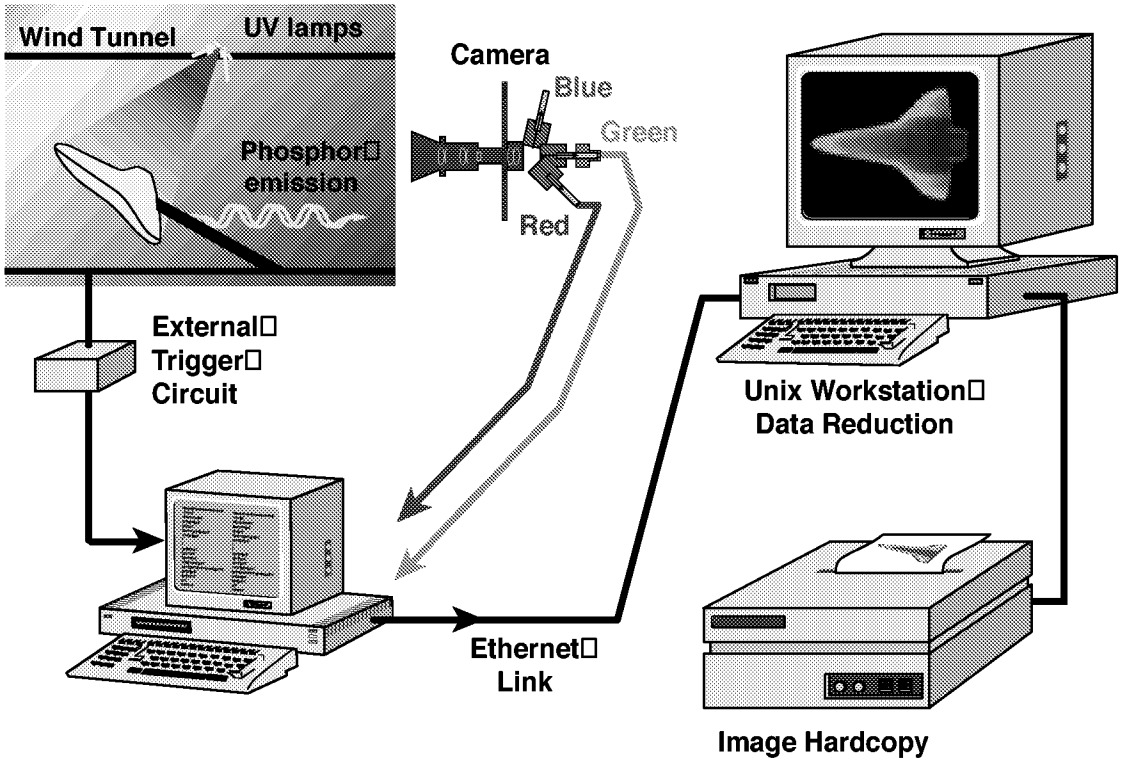

Figure 4. Schematic of phosphor thermography system.

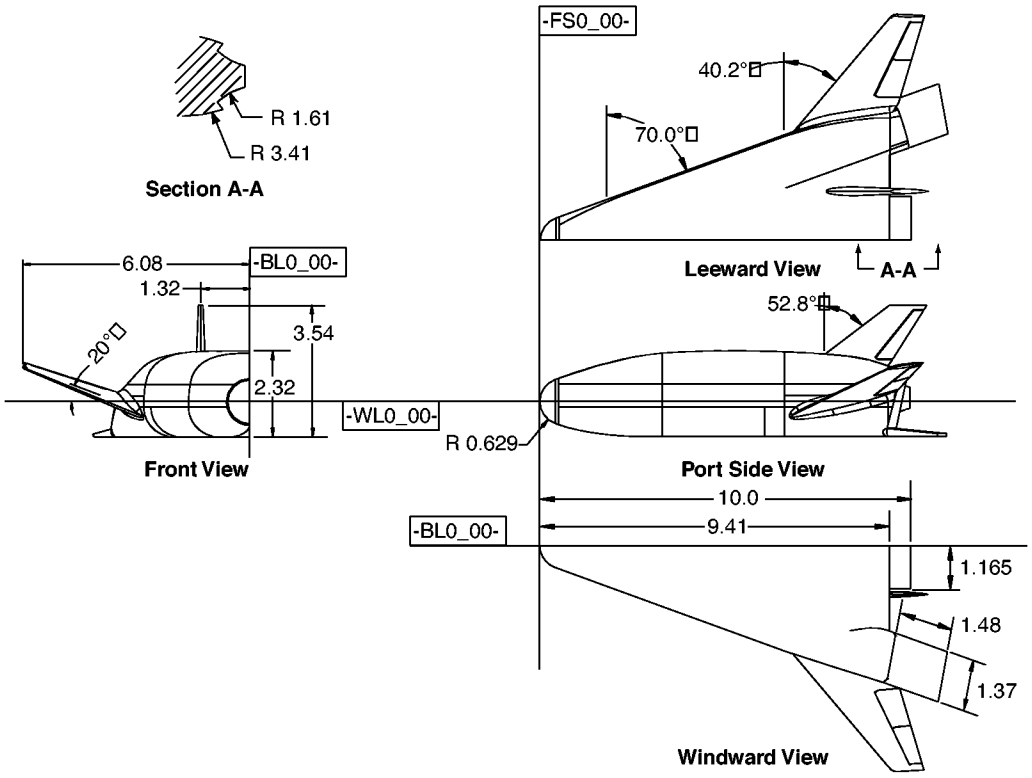

Figure 5. X-33 F-Loft Rev F model dimensions.

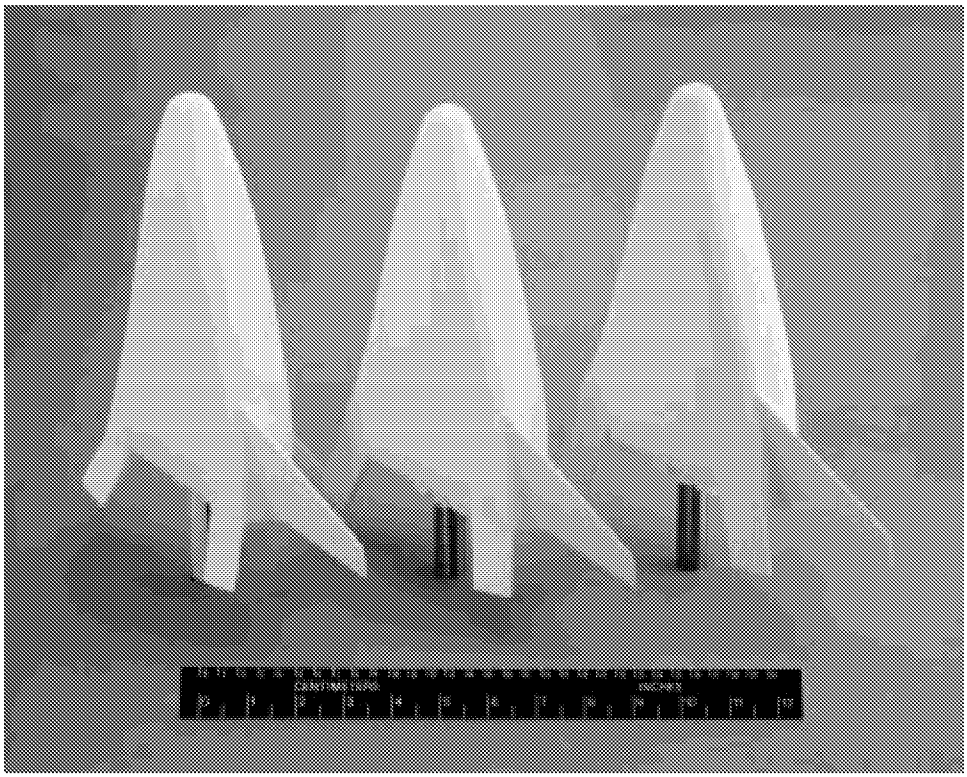

Figure 6. Photograph of 0.0132-scale F-Loft Rev F X-33 models with 3 flap deflections.

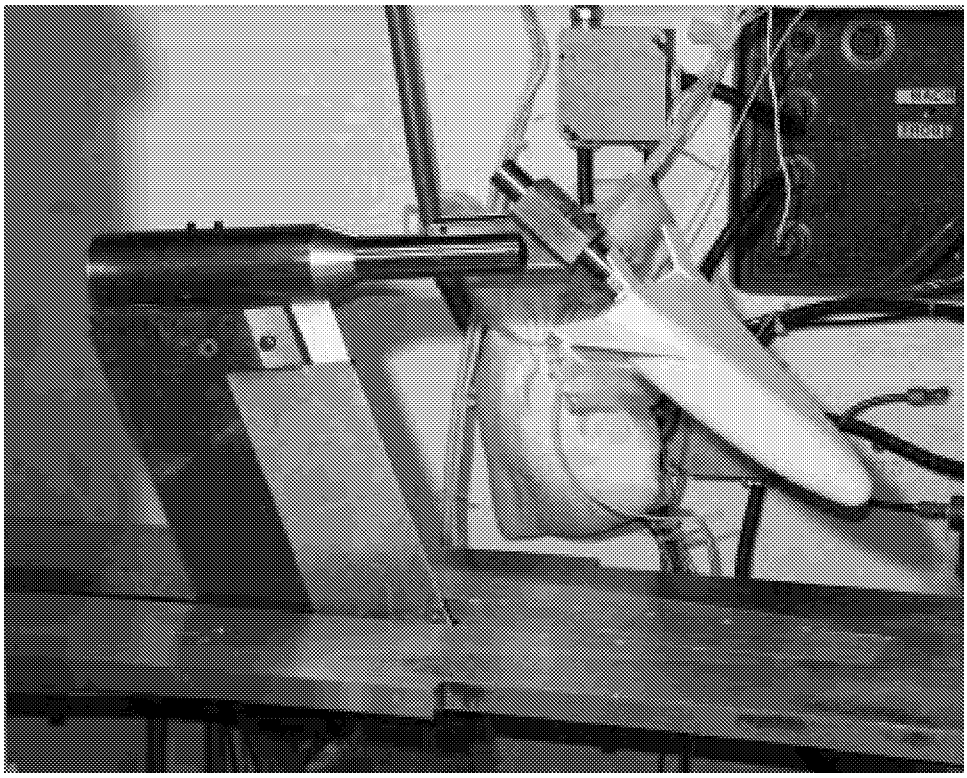

Figure 7. Photograph of model installed in the 20-Inch Mach 6 Tunnel (shown in the retracted position).

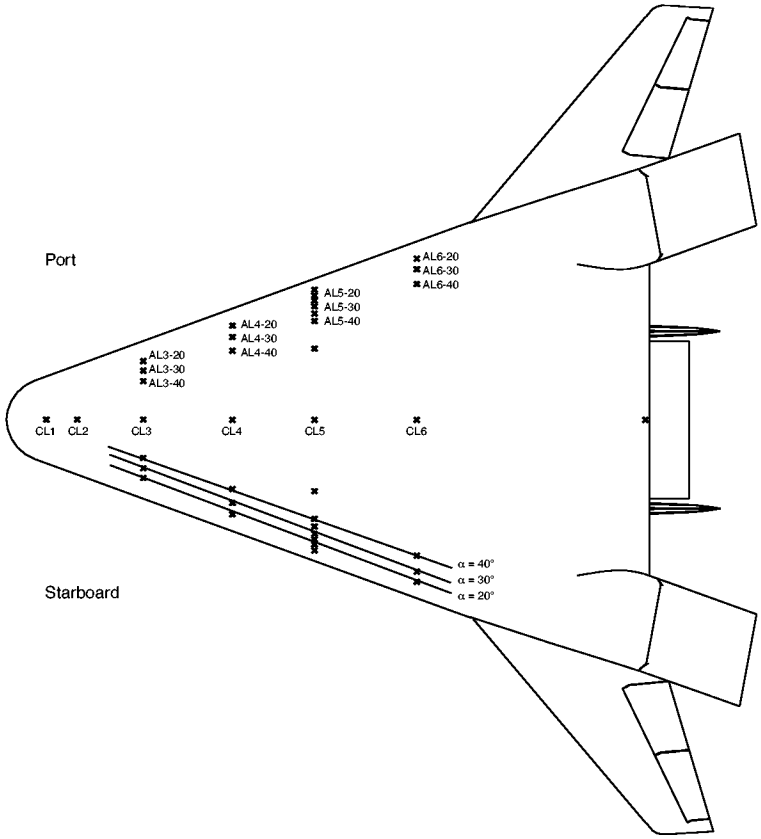

Figure 8. Sketch of trip locations and fiducial marks.

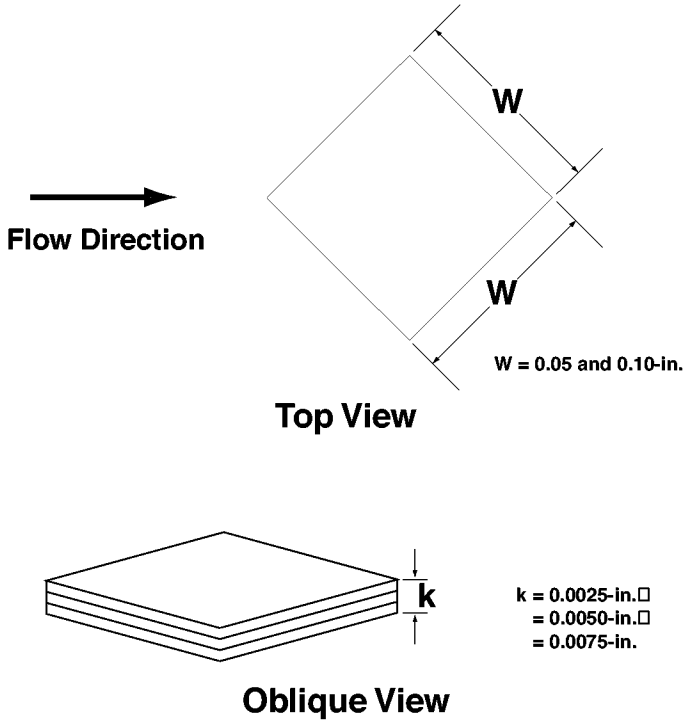

Figure 9. Sketch of trips showing orientation, width, and height.

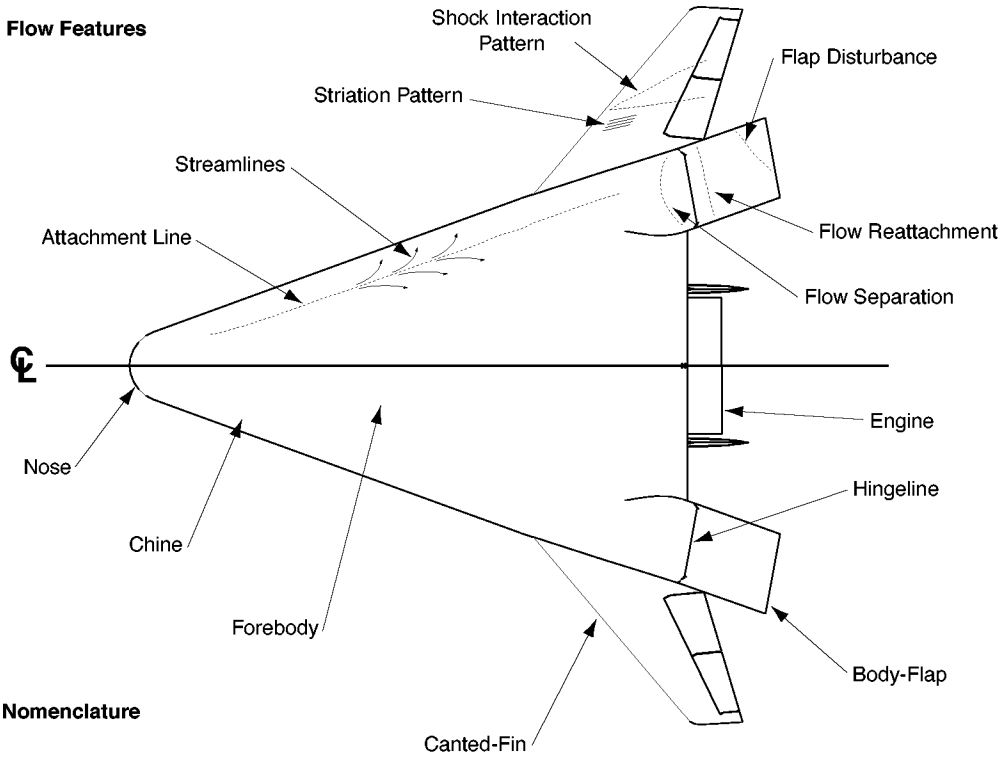

Figure 10. Sketch of X-33 windward nomenclature and flow features.

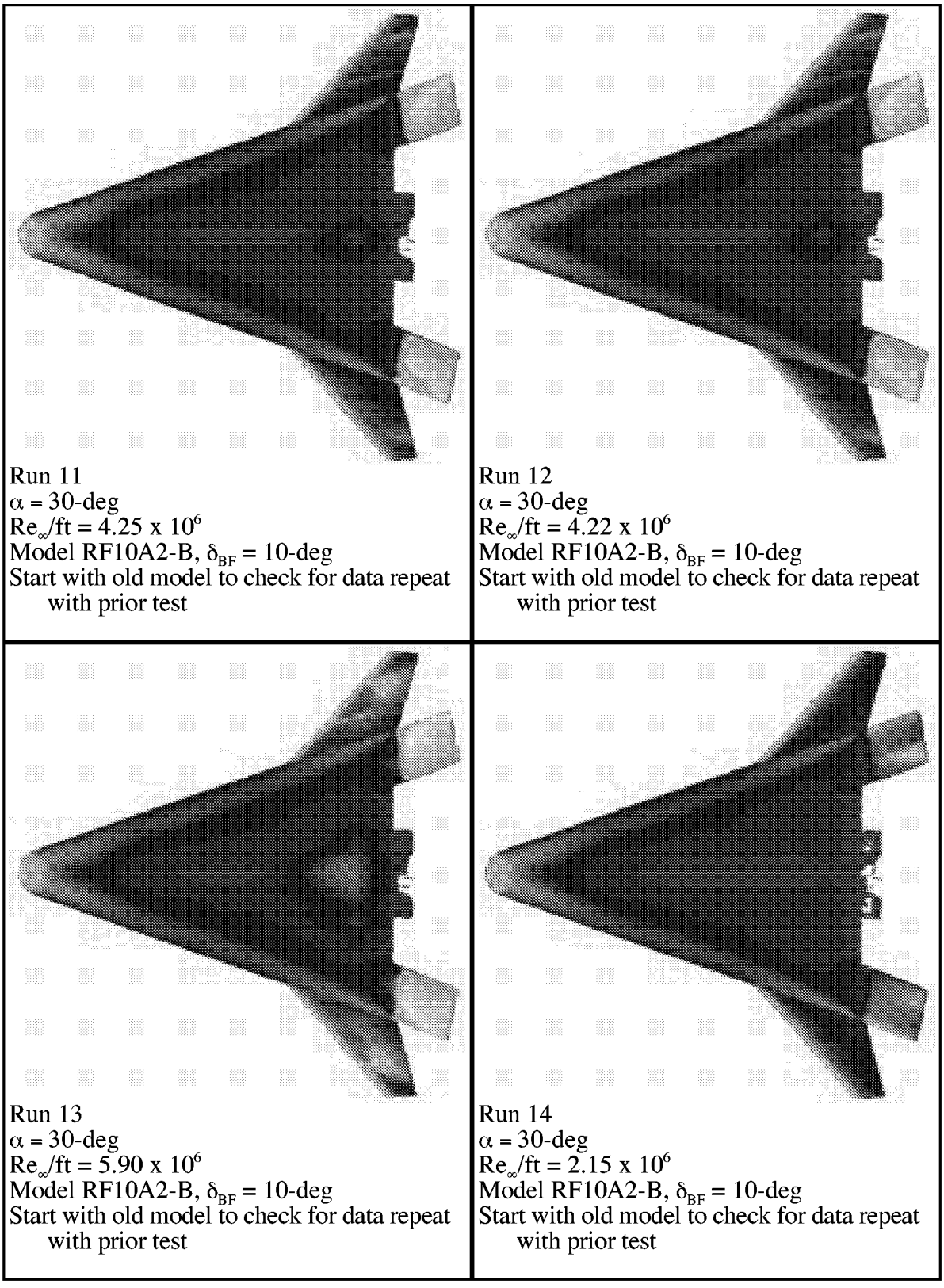

Run 11
α = 30-deg
Re_∞/ft = 4.25 x 10^6
Model RF10A2-B, δ_{BF} = 10-deg
Start with old model to check for data repeat with prior test

Run 12
α = 30-deg
Re_∞/ft = 4.22 x 10^6
Model RF10A2-B, δ_{BF} = 10-deg
Start with old model to check for data repeat with prior test

Run 13
α = 30-deg
Re_∞/ft = 5.90 x 10^6
Model RF10A2-B, δ_{BF} = 10-deg
Start with old model to check for data repeat with prior test

Run 14
α = 30-deg
Re_∞/ft = 2.15 x 10^6
Model RF10A2-B, δ_{BF} = 10-deg
Start with old model to check for data repeat with prior test

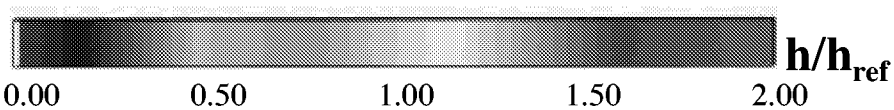

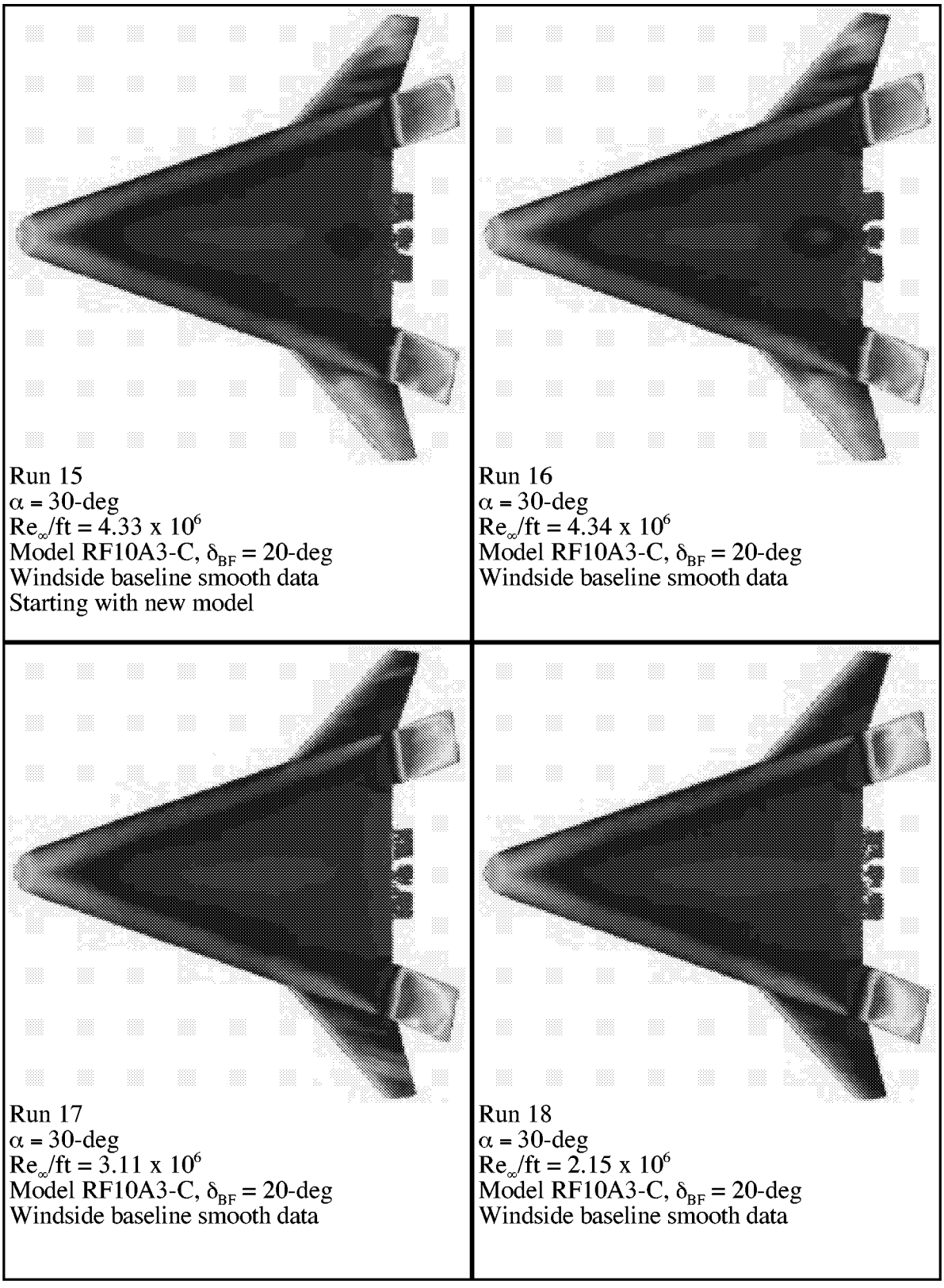

Run 15
α = 30-deg
Re_∞/ft = 4.33 x 10^6
Model RF10A3-C, δ_{BF} = 20-deg
Windside baseline smooth data
Starting with new model

Run 16
α = 30-deg
Re_∞/ft = 4.34 x 10^6
Model RF10A3-C, δ_{BF} = 20-deg
Windside baseline smooth data

Run 17
α = 30-deg
Re_∞/ft = 3.11 x 10^6
Model RF10A3-C, δ_{BF} = 20-deg
Windside baseline smooth data

Run 18
α = 30-deg
Re_∞/ft = 2.15 x 10^6
Model RF10A3-C, δ_{BF} = 20-deg
Windside baseline smooth data

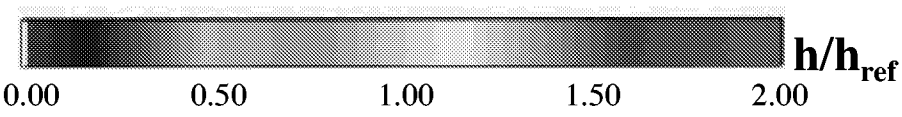

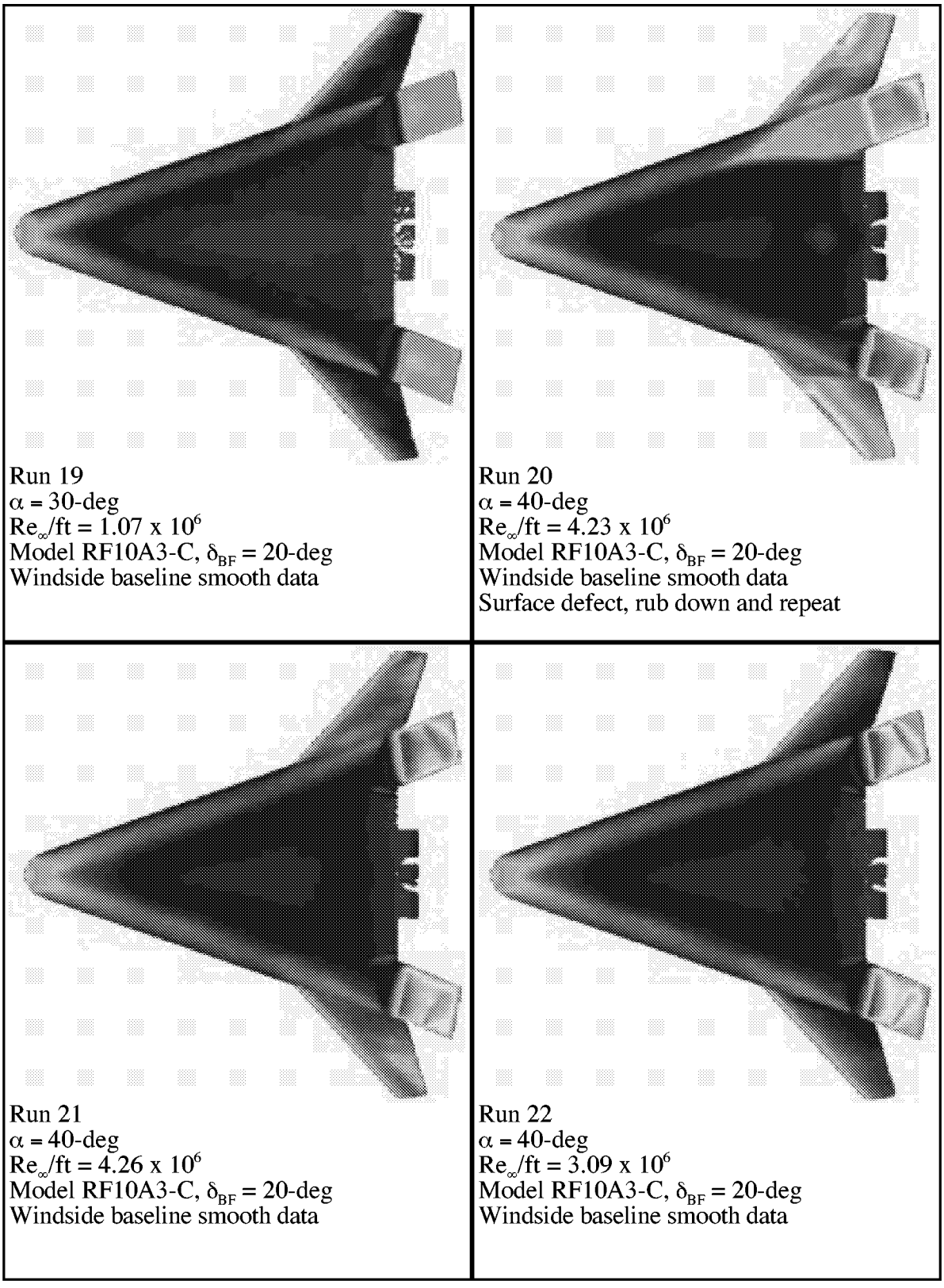

Run 19
α = 30-deg
Re_∞/ft = 1.07 x 10^6
Model RF10A3-C, δ_{BF} = 20-deg
Windside baseline smooth data

Run 20
α = 40-deg
Re_∞/ft = 4.23 x 10^6
Model RF10A3-C, δ_{BF} = 20-deg
Windside baseline smooth data
Surface defect, rub down and repeat

Run 21
α = 40-deg
Re_∞/ft = 4.26 x 10^6
Model RF10A3-C, δ_{BF} = 20-deg
Windside baseline smooth data

Run 22
α = 40-deg
Re_∞/ft = 3.09 x 10^6
Model RF10A3-C, δ_{BF} = 20-deg
Windside baseline smooth data

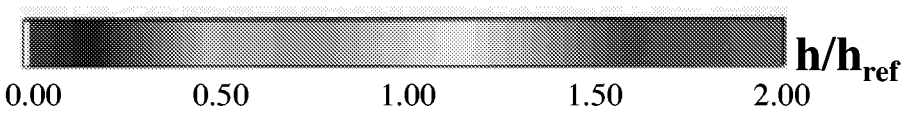

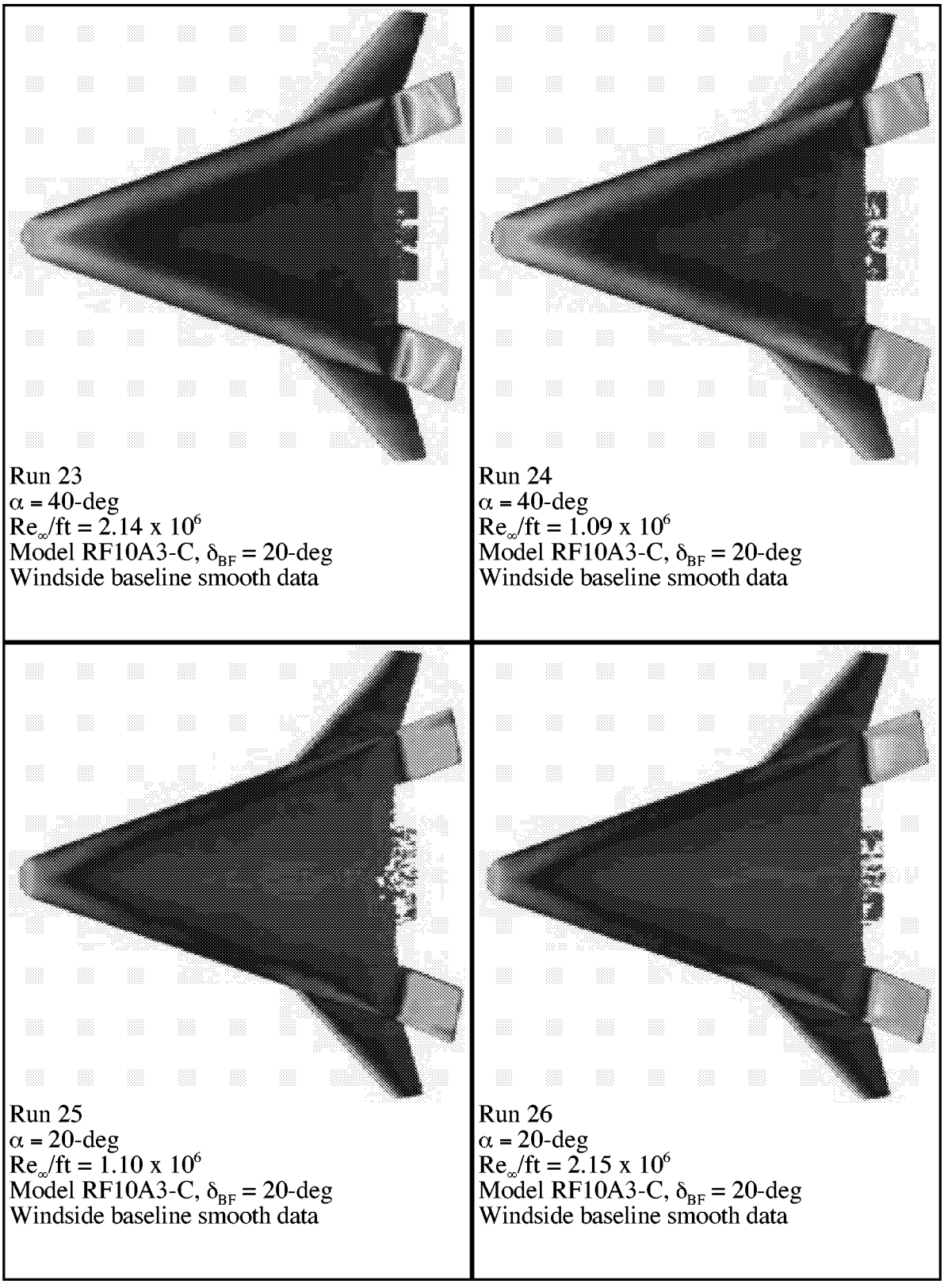

Run 23
α = 40-deg
Re_∞/ft = 2.14 x 10^6
Model RF10A3-C, δ_{BF} = 20-deg
Windside baseline smooth data

Run 24
α = 40-deg
Re_∞/ft = 1.09 x 10^6
Model RF10A3-C, δ_{BF} = 20-deg
Windside baseline smooth data

Run 25
α = 20-deg
Re_∞/ft = 1.10 x 10^6
Model RF10A3-C, δ_{BF} = 20-deg
Windside baseline smooth data

Run 26
α = 20-deg
Re_∞/ft = 2.15 x 10^6
Model RF10A3-C, δ_{BF} = 20-deg
Windside baseline smooth data

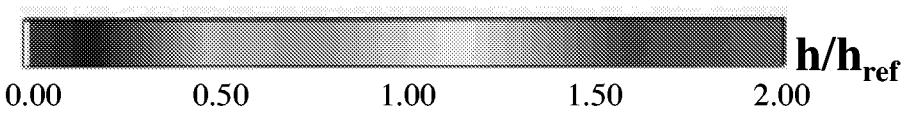

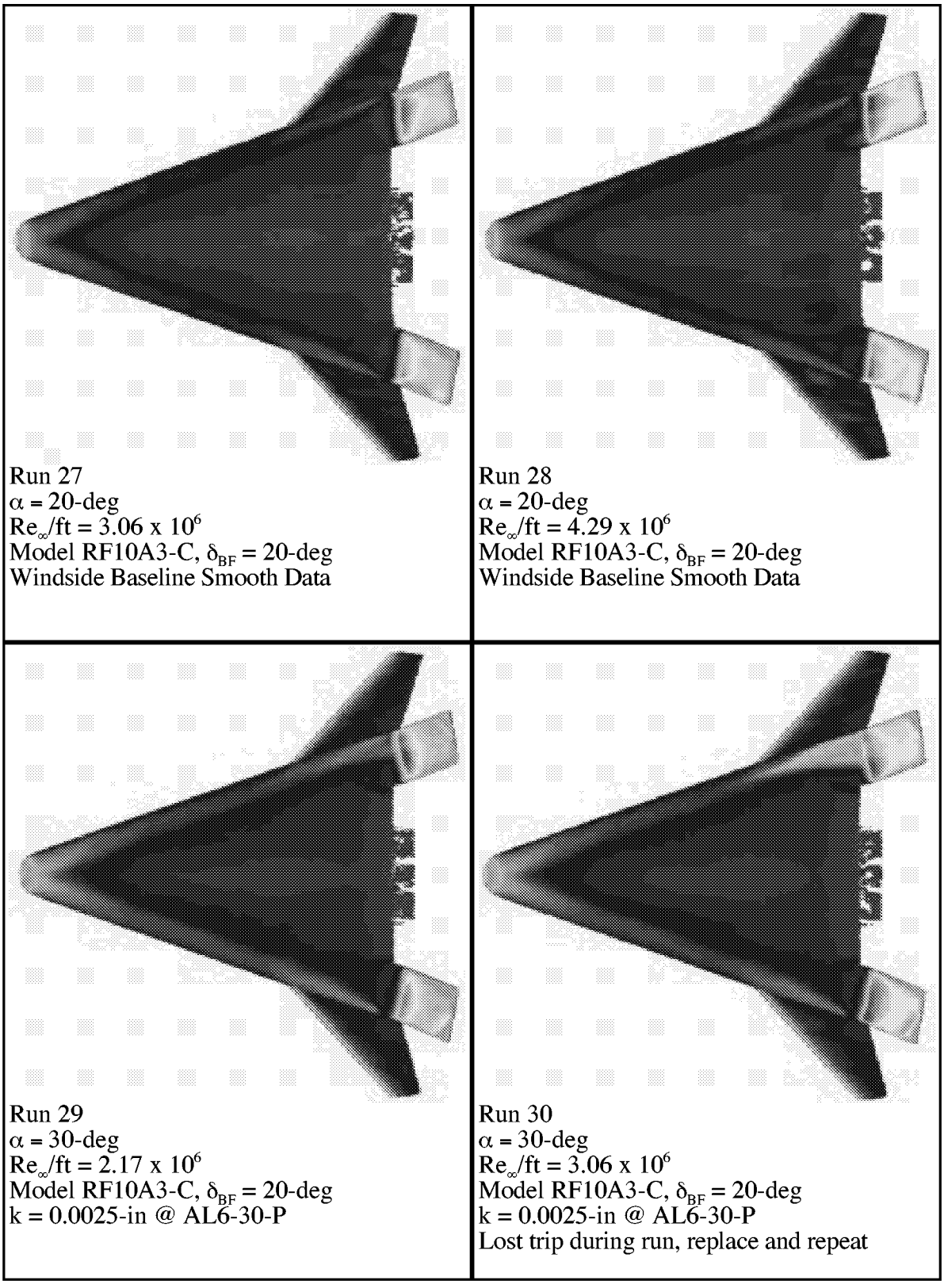

Run 27
α = 20-deg
Re_∞/ft = 3.06 x 10^6
Model RF10A3-C, δ_{BF} = 20-deg
Windside Baseline Smooth Data

Run 28
α = 20-deg
Re_∞/ft = 4.29 x 10^6
Model RF10A3-C, δ_{BF} = 20-deg
Windside Baseline Smooth Data

Run 29
α = 30-deg
Re_∞/ft = 2.17 x 10^6
Model RF10A3-C, δ_{BF} = 20-deg
k = 0.0025-in @ AL6-30-P

Run 30
α = 30-deg
Re_∞/ft = 3.06 x 10^6
Model RF10A3-C, δ_{BF} = 20-deg
k = 0.0025-in @ AL6-30-P
Lost trip during run, replace and repeat

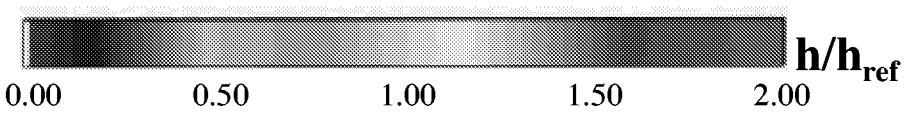

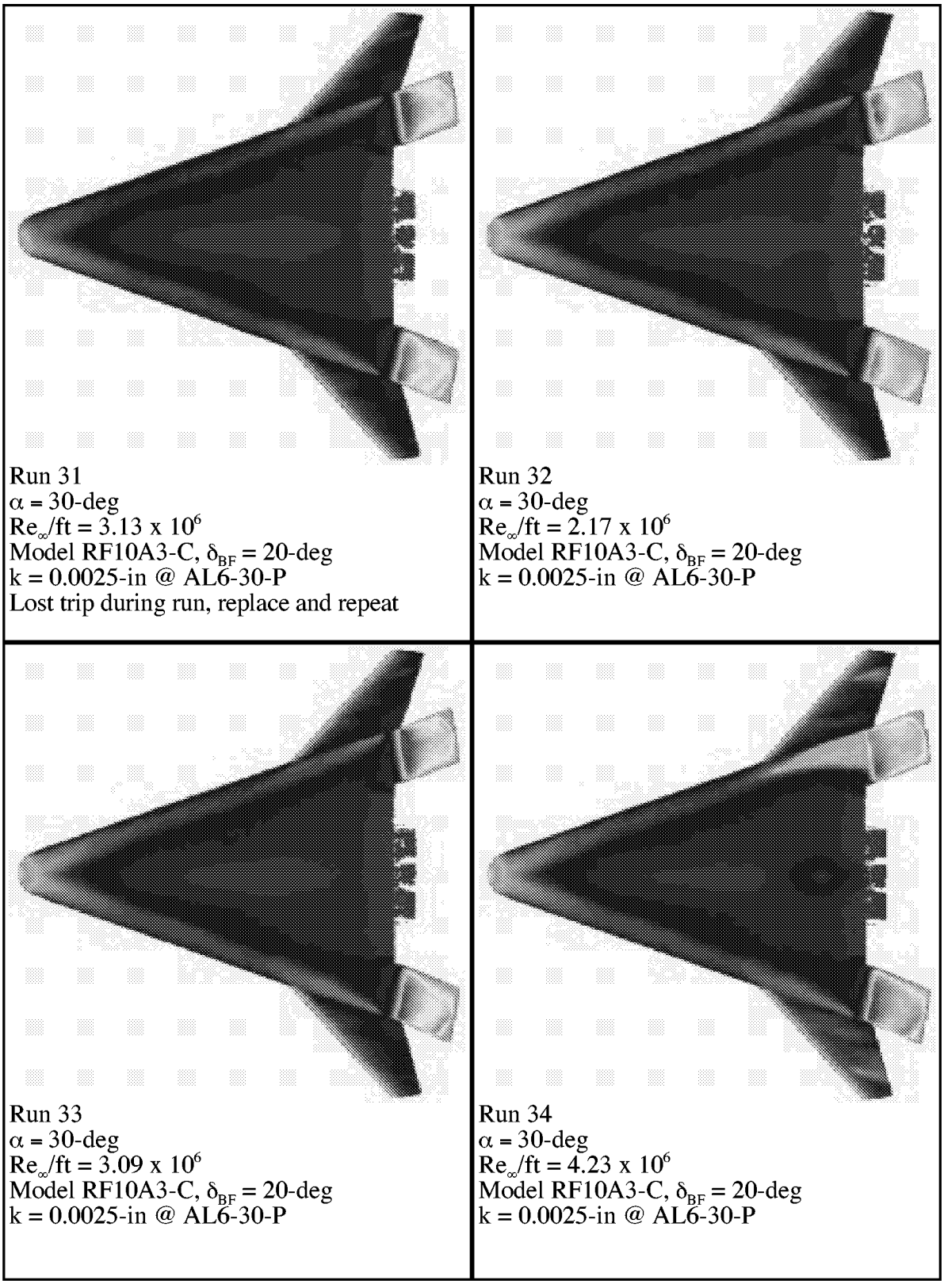

Run 31
α = 30-deg
Re_∞/ft = 3.13 x 10^6
Model RF10A3-C, δ_{BF} = 20-deg
k = 0.0025-in @ AL6-30-P
Lost trip during run, replace and repeat

Run 32
α = 30-deg
Re_∞/ft = 2.17 x 10^6
Model RF10A3-C, δ_{BF} = 20-deg
k = 0.0025-in @ AL6-30-P

Run 33
α = 30-deg
Re_∞/ft = 3.09 x 10^6
Model RF10A3-C, δ_{BF} = 20-deg
k = 0.0025-in @ AL6-30-P

Run 34
α = 30-deg
Re_∞/ft = 4.23 x 10^6
Model RF10A3-C, δ_{BF} = 20-deg
k = 0.0025-in @ AL6-30-P

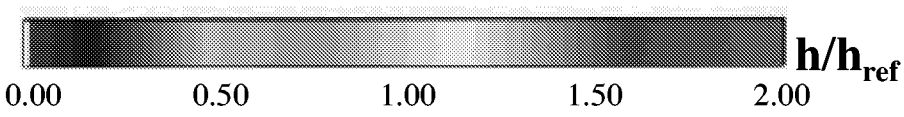

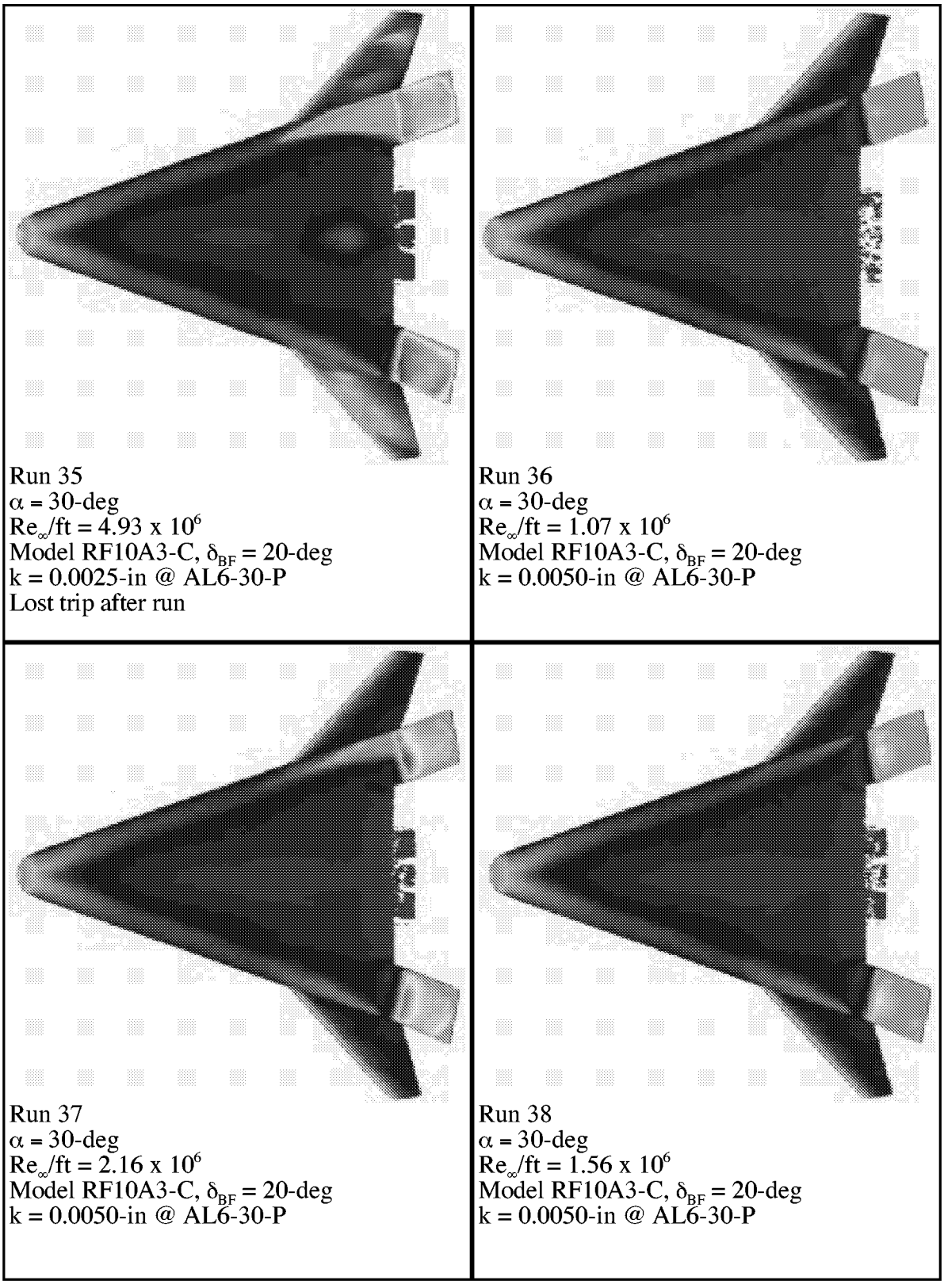

Run 35
α = 30-deg
Re_∞/ft = 4.93 x 10^6
Model RF10A3-C, δ_{BF} = 20-deg
k = 0.0025-in @ AL6-30-P
Lost trip after run

Run 36
α = 30-deg
Re_∞/ft = 1.07 x 10^6
Model RF10A3-C, δ_{BF} = 20-deg
k = 0.0050-in @ AL6-30-P

Run 37
α = 30-deg
Re_∞/ft = 2.16 x 10^6
Model RF10A3-C, δ_{BF} = 20-deg
k = 0.0050-in @ AL6-30-P

Run 38
α = 30-deg
Re_∞/ft = 1.56 x 10^6
Model RF10A3-C, δ_{BF} = 20-deg
k = 0.0050-in @ AL6-30-P

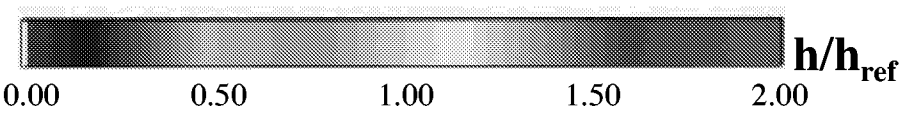

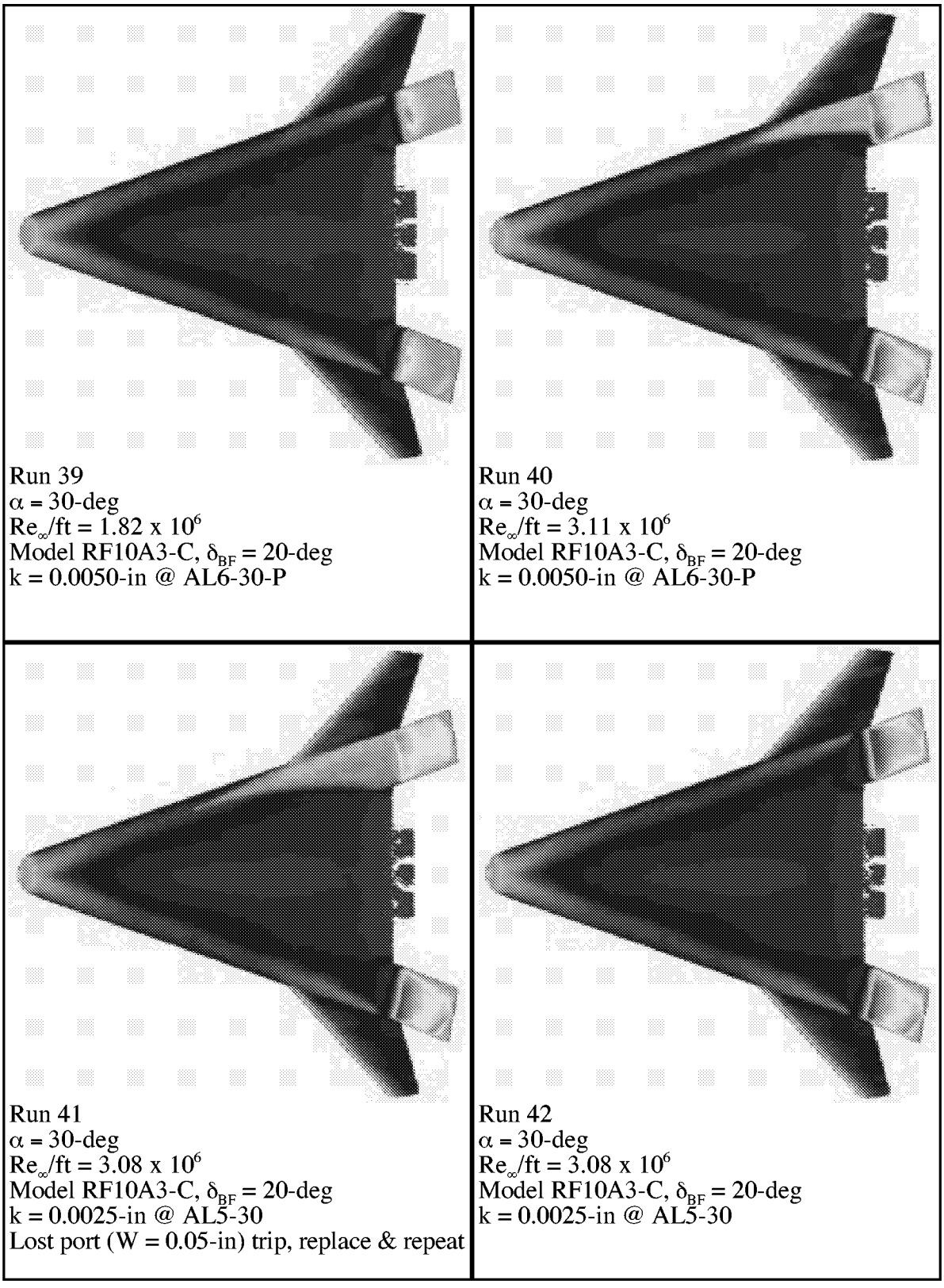

Run 39
α = 30-deg
Re_∞/ft = 1.82 x 10^6
Model RF10A3-C, δ_{BF} = 20-deg
k = 0.0050-in @ AL6-30-P

Run 40
α = 30-deg
Re_∞/ft = 3.11 x 10^6
Model RF10A3-C, δ_{BF} = 20-deg
k = 0.0050-in @ AL6-30-P

Run 41
α = 30-deg
Re_∞/ft = 3.08 x 10^6
Model RF10A3-C, δ_{BF} = 20-deg
k = 0.0025-in @ AL5-30
Lost port (W = 0.05-in) trip, replace & repeat

Run 42
α = 30-deg
Re_∞/ft = 3.08 x 10^6
Model RF10A3-C, δ_{BF} = 20-deg
k = 0.0025-in @ AL5-30

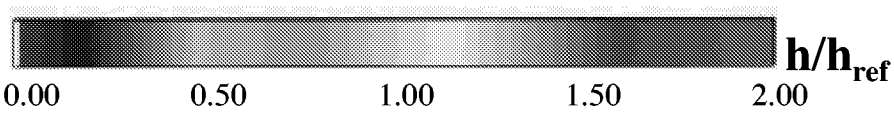

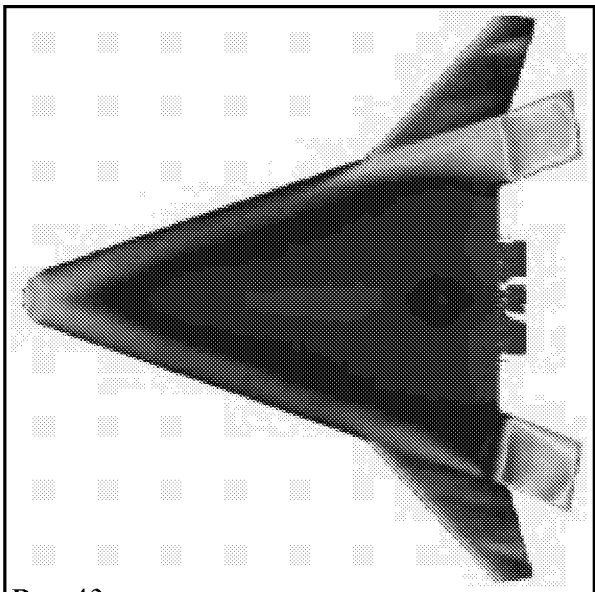

Run 43
α = 30-deg
Re_∞/ft = 4.15 x 10^6
Model RF10A3-C, δ_{BF} = 20-deg
k = 0.0025-in @ AL5-30
Port trip corner sticking up after run

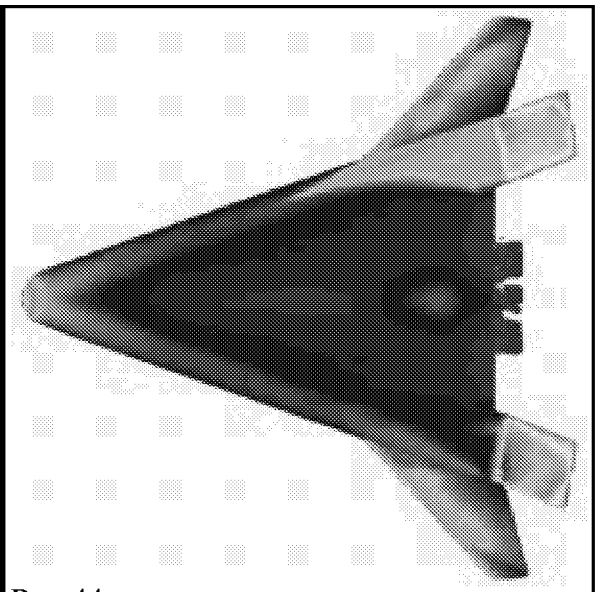

Run 44
α = 30-deg
Re_∞/ft = 4.96 x 10^6
Model RF10A3-C, δ_{BF} = 20-deg
k = 0.0025-in @ AL5-30
Port trip corner sticking up after run

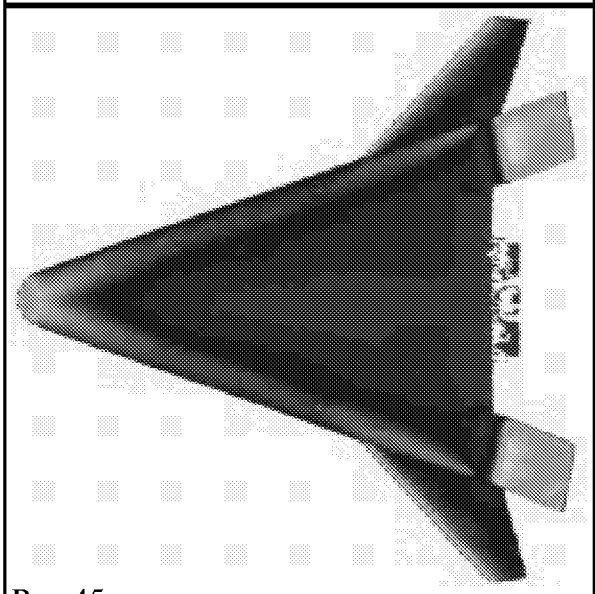

Run 45
α = 30-deg
Re_∞/ft = 1.50 x 10^6
Model RF10A3-C, δ_{BF} = 20-deg
k = Both @ AL6-30
Both = 0.0025-in port & 0.0050-in Starboard

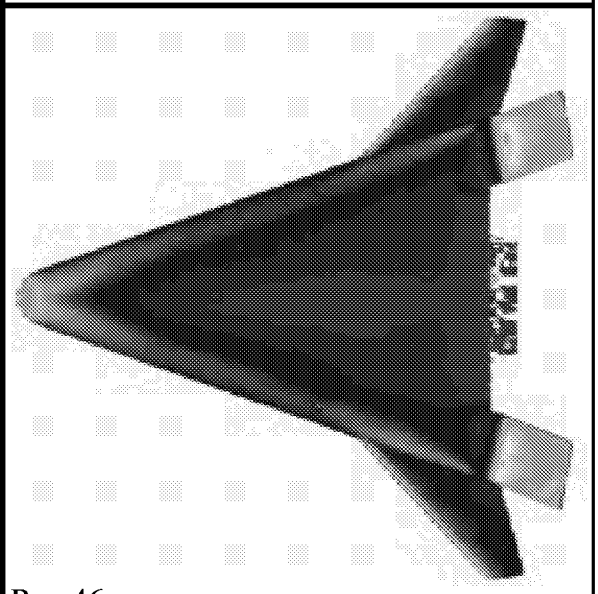

Run 46
α = 30-deg
Re_∞/ft = 1.78 x 10^6
Model RF10A3-C, δ_{BF} = 20-deg
k = Both @ AL6-30

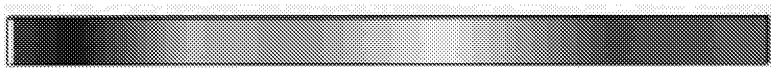

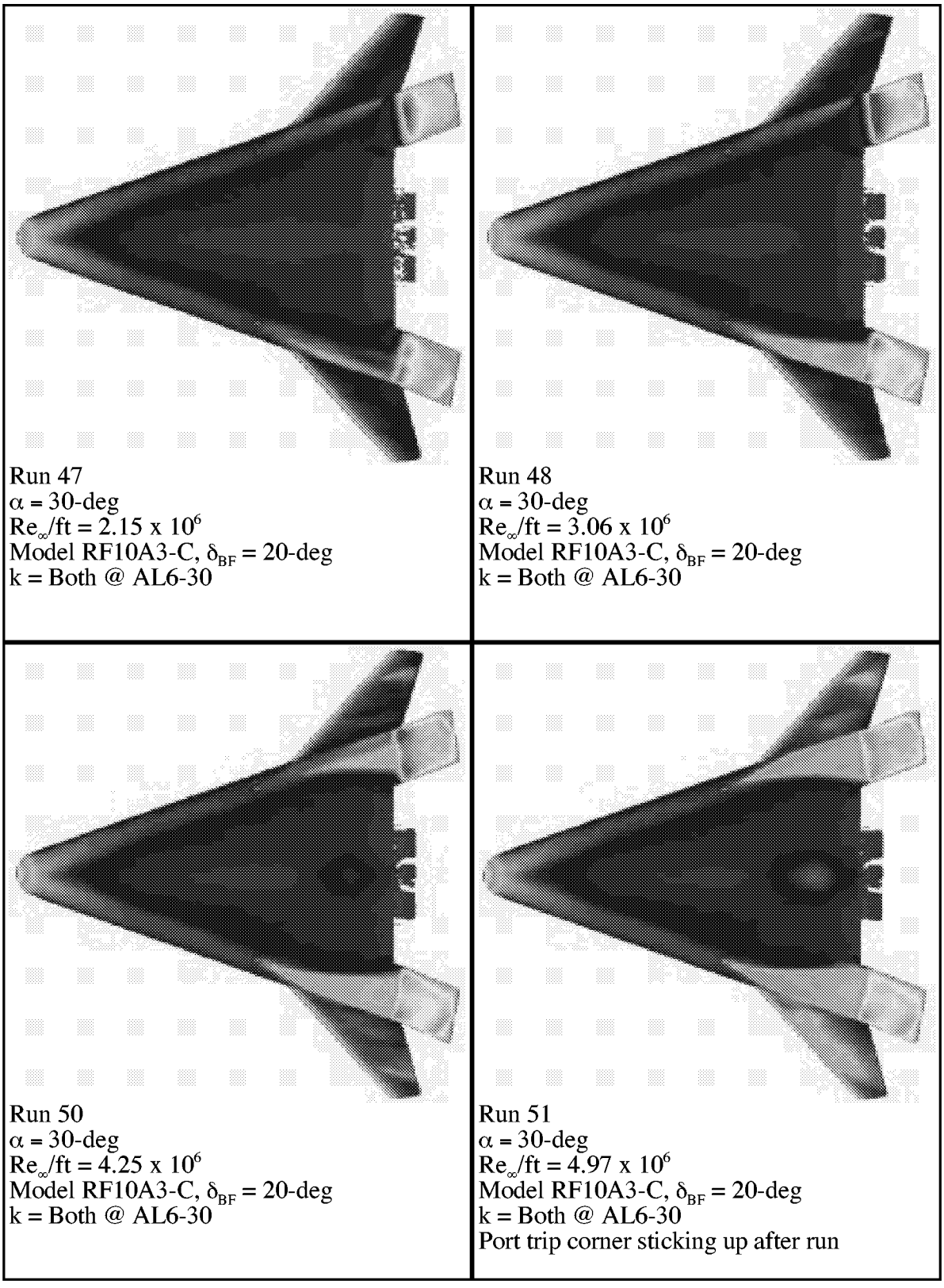

Run 47
α = 30-deg
Re_∞/ft = 2.15 x 10^6
Model RF10A3-C, δ_{BF} = 20-deg
k = Both @ AL6-30

Run 48
α = 30-deg
Re_∞/ft = 3.06 x 10^6
Model RF10A3-C, δ_{BF} = 20-deg
k = Both @ AL6-30

Run 50
α = 30-deg
Re_∞/ft = 4.25 x 10^6
Model RF10A3-C, δ_{BF} = 20-deg
k = Both @ AL6-30

Run 51
α = 30-deg
Re_∞/ft = 4.97 x 10^6
Model RF10A3-C, δ_{BF} = 20-deg
k = Both @ AL6-30
Port trip corner sticking up after run

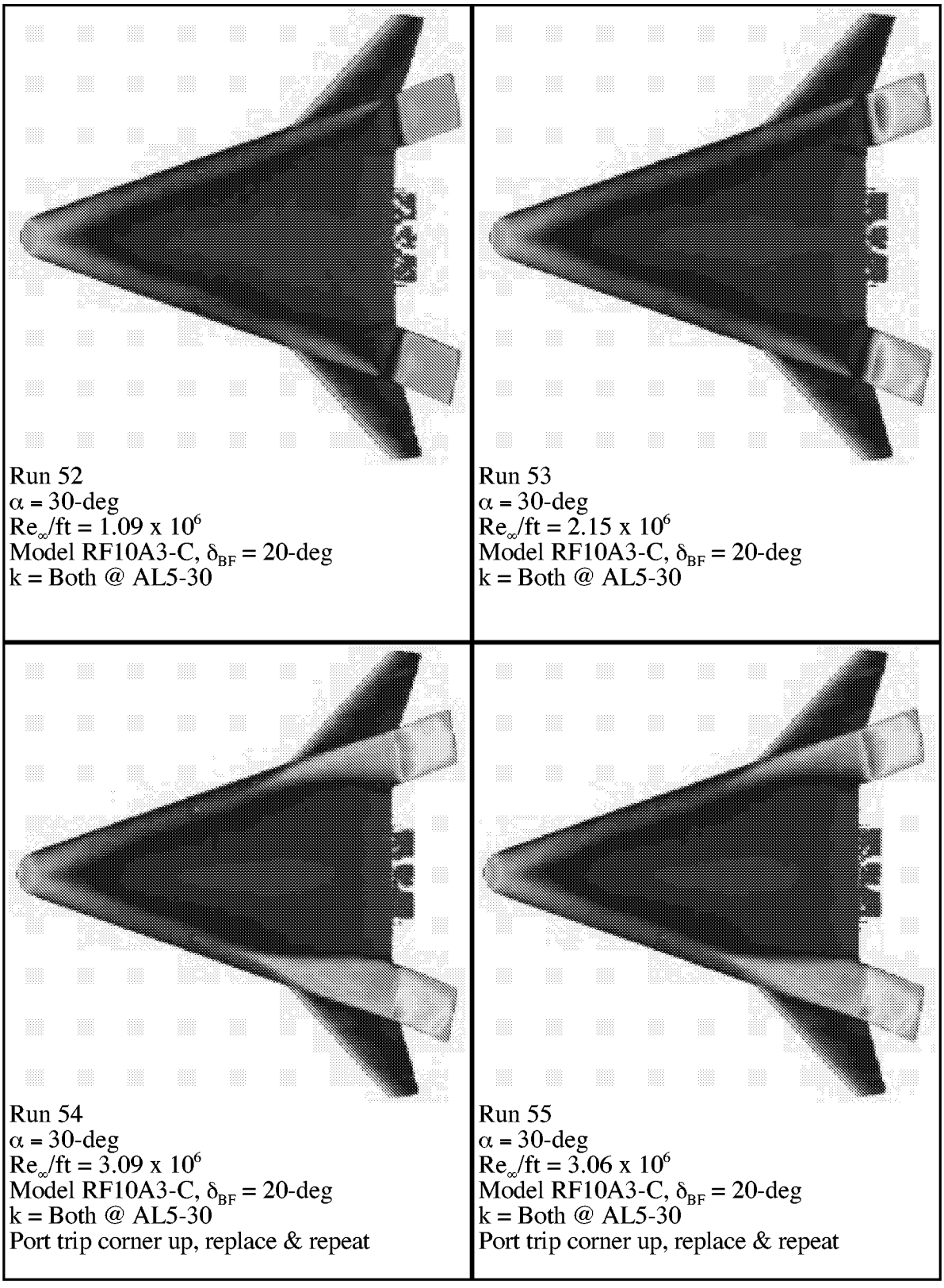

Run 52
α = 30-deg
Re_∞/ft = 1.09 x 10^6
Model RF10A3-C, δ_{BF} = 20-deg
k = Both @ AL5-30

Run 53
α = 30-deg
Re_∞/ft = 2.15 x 10^6
Model RF10A3-C, δ_{BF} = 20-deg
k = Both @ AL5-30

Run 54
α = 30-deg
Re_∞/ft = 3.09 x 10^6
Model RF10A3-C, δ_{BF} = 20-deg
k = Both @ AL5-30
Port trip corner up, replace & repeat

Run 55
α = 30-deg
Re_∞/ft = 3.06 x 10^6
Model RF10A3-C, δ_{BF} = 20-deg
k = Both @ AL5-30
Port trip corner up, replace & repeat

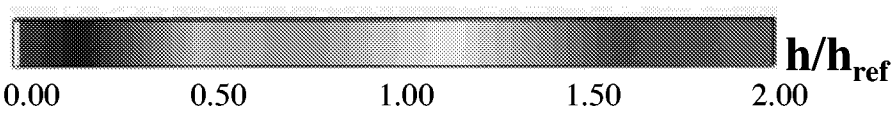

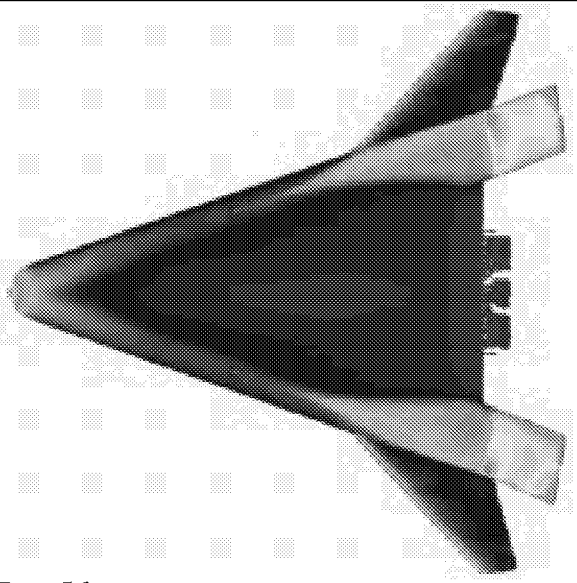

Run 56
α = 30-deg
Re_∞/ft = 3.09 x 10^6
Model RF10A3-C, δ_{BF} = 20-deg
k = Both @ AL5-30
Port trip corner up, replace & repeat

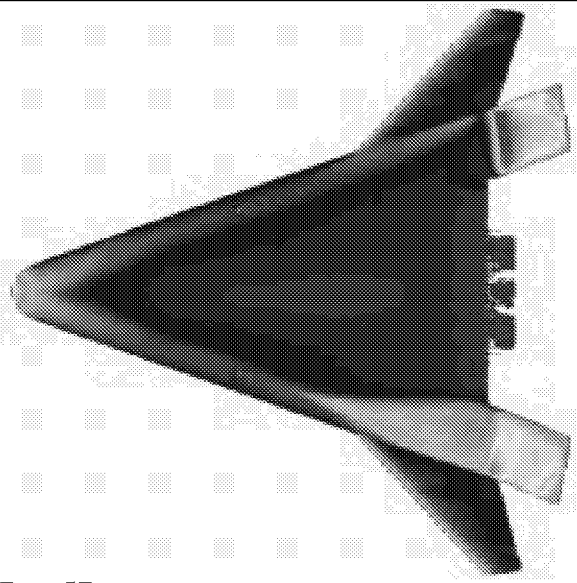

Run 57
α = 30-deg
Re_∞/ft = 3.11 x 10^6
Model RF10A3-C, δ_{BF} = 20-deg
k = Both @ AL5-30

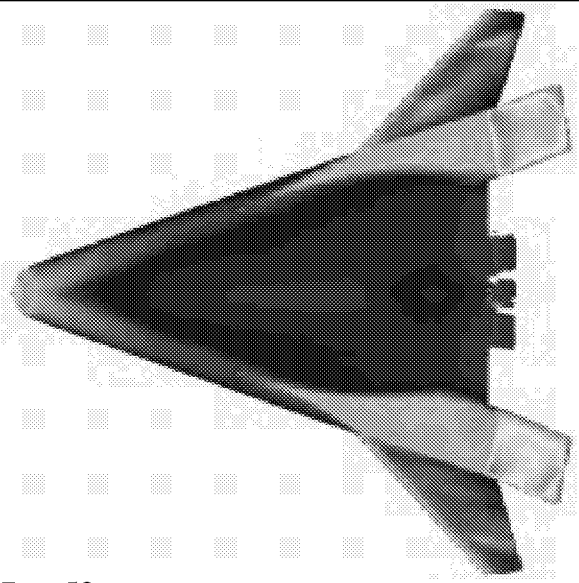

Run 58
α = 30-deg
Re_∞/ft = 4.26 x 10^6
Model RF10A3-C, δ_{BF} = 20-deg
k = Both @ AL5-30

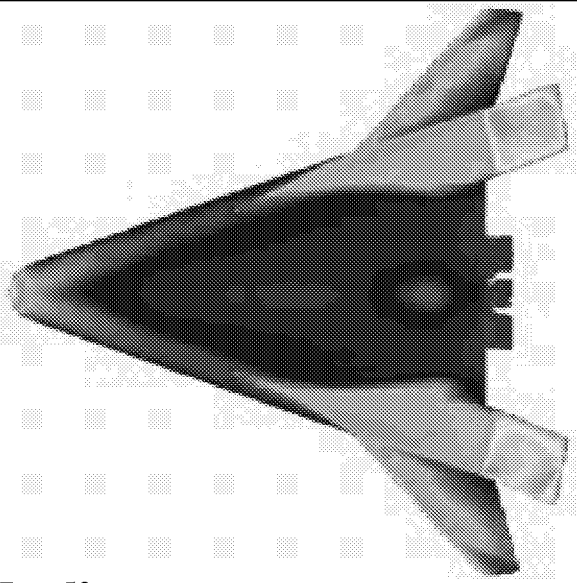

Run 59
α = 30-deg
Re_∞/ft = 4.94 x 10^6
Model RF10A3-C, δ_{BF} = 20-deg
k = Both @ AL5-30

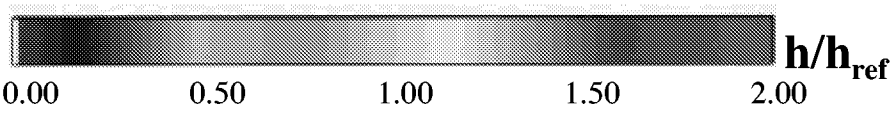

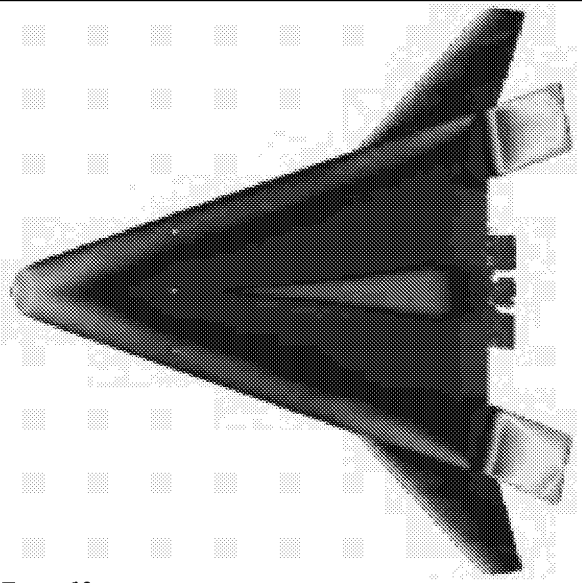

Run 60
α = 30-deg
Re_∞/ft = 3.09 x 10^6
Model RF10A3-C, δ_{BF} = 20-deg
k = 0.0025-in @ AL4-30 and CL4
CL trip corner sticking up after run

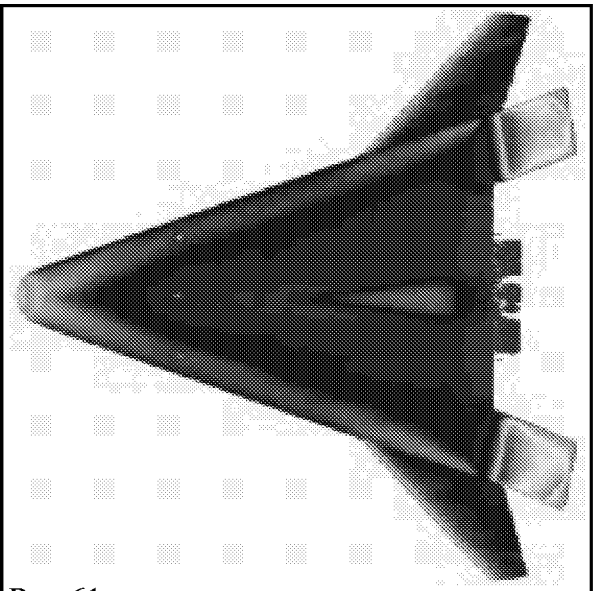

Run 61
α = 30-deg
Re_∞/ft = 3.07 x 10^6
Model RF10A3-C, δ_{BF} = 20-deg
k = 0.0025-in @ AL4-30 and CL4
CL trip corner sticking up after run

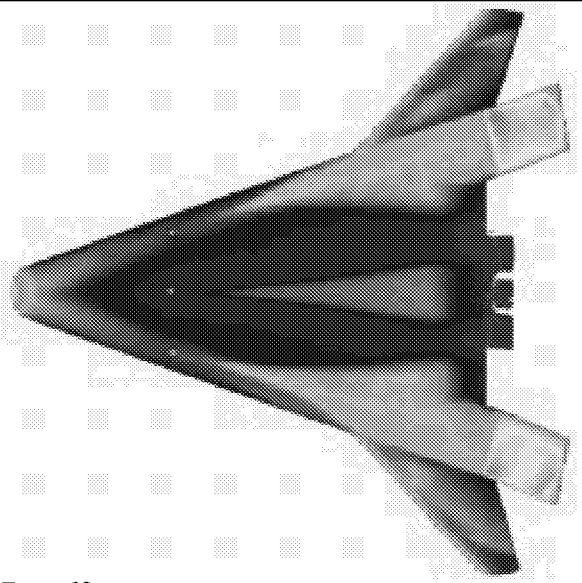

Run 62
α = 30-deg
Re_∞/ft = 4.22 x 10^6
Model RF10A3-C, δ_{BF} = 20-deg
k = 0.0025-in @ AL4-30 and CL4
Lost STBD trip, replace & repeat

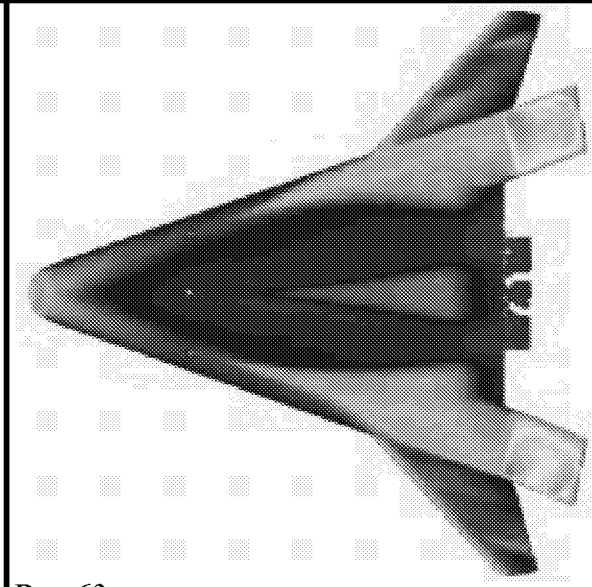

Run 63
α = 30-deg
Re_∞/ft = 4.16 x 10^6
Model RF10A3-C, δ_{BF} = 20-deg
k = 0.0025-in @ AL4-30 and CL4
Decided to change out model

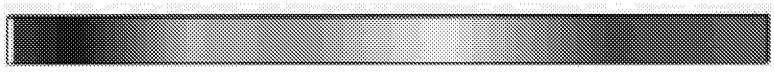

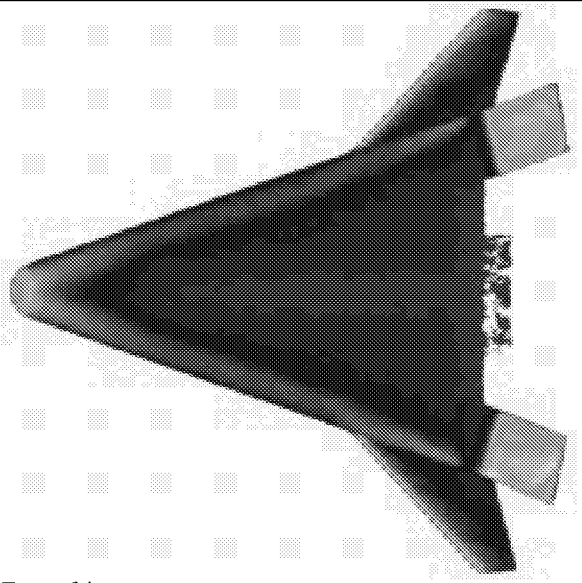

Run 64
α = 30-deg
Re_∞/ft = 1.08 x 10^6
Model RF10A3-D, δ_{BF} = 20-deg
New model baseline

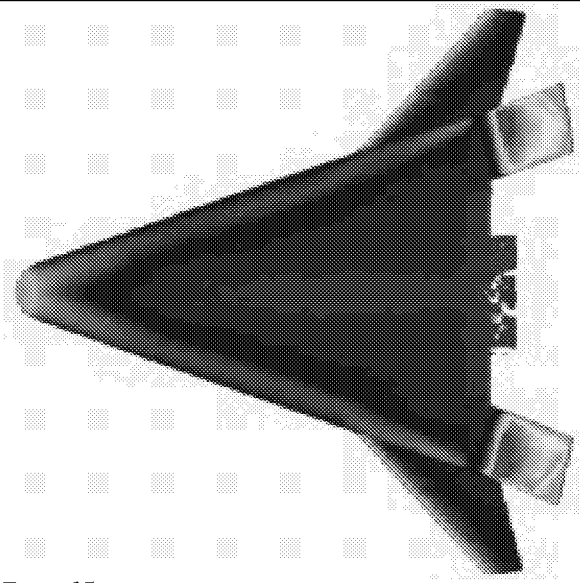

Run 65
α = 30-deg
Re_∞/ft = 2.15 x 10^6
Model RF10A3-D, δ_{BF} = 20-deg
New model baseline

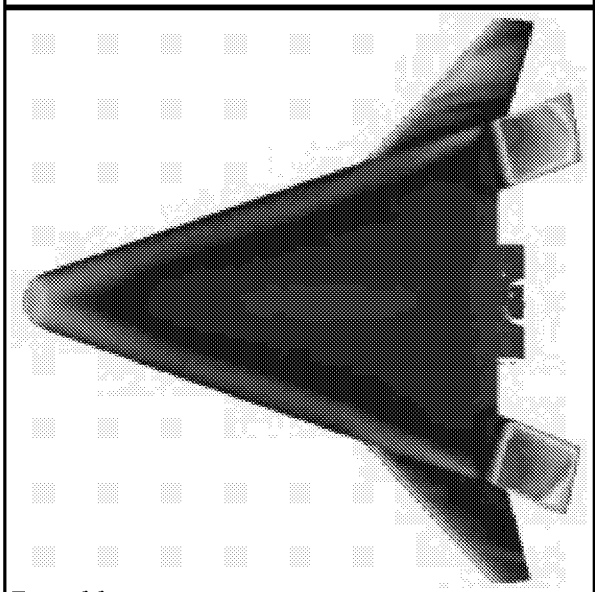

Run 66
α = 30-deg
Re_∞/ft = 3.07 x 10^6
Model RF10A3-D, δ_{BF} = 20-deg
New model baseline

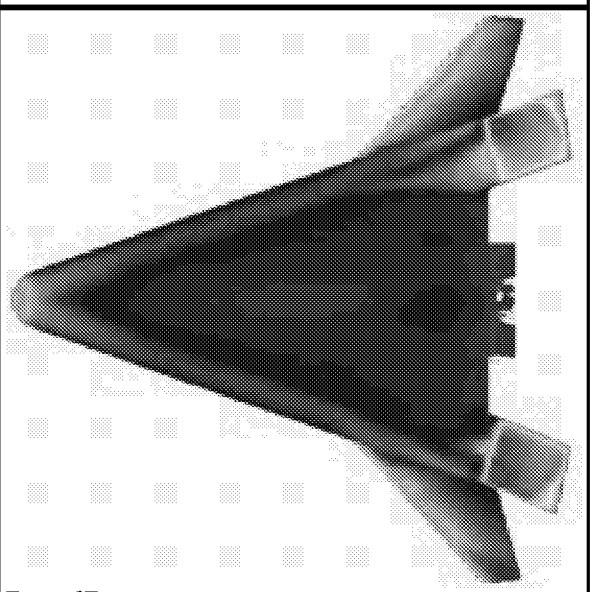

Run 67
α = 30-deg
Re_∞/ft = 4.28 x 10^6
Model RF10A3-D, δ_{BF} = 20-deg
New model baseline
Surface defect, wipe down and repeat

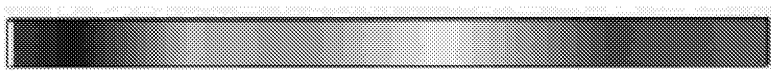

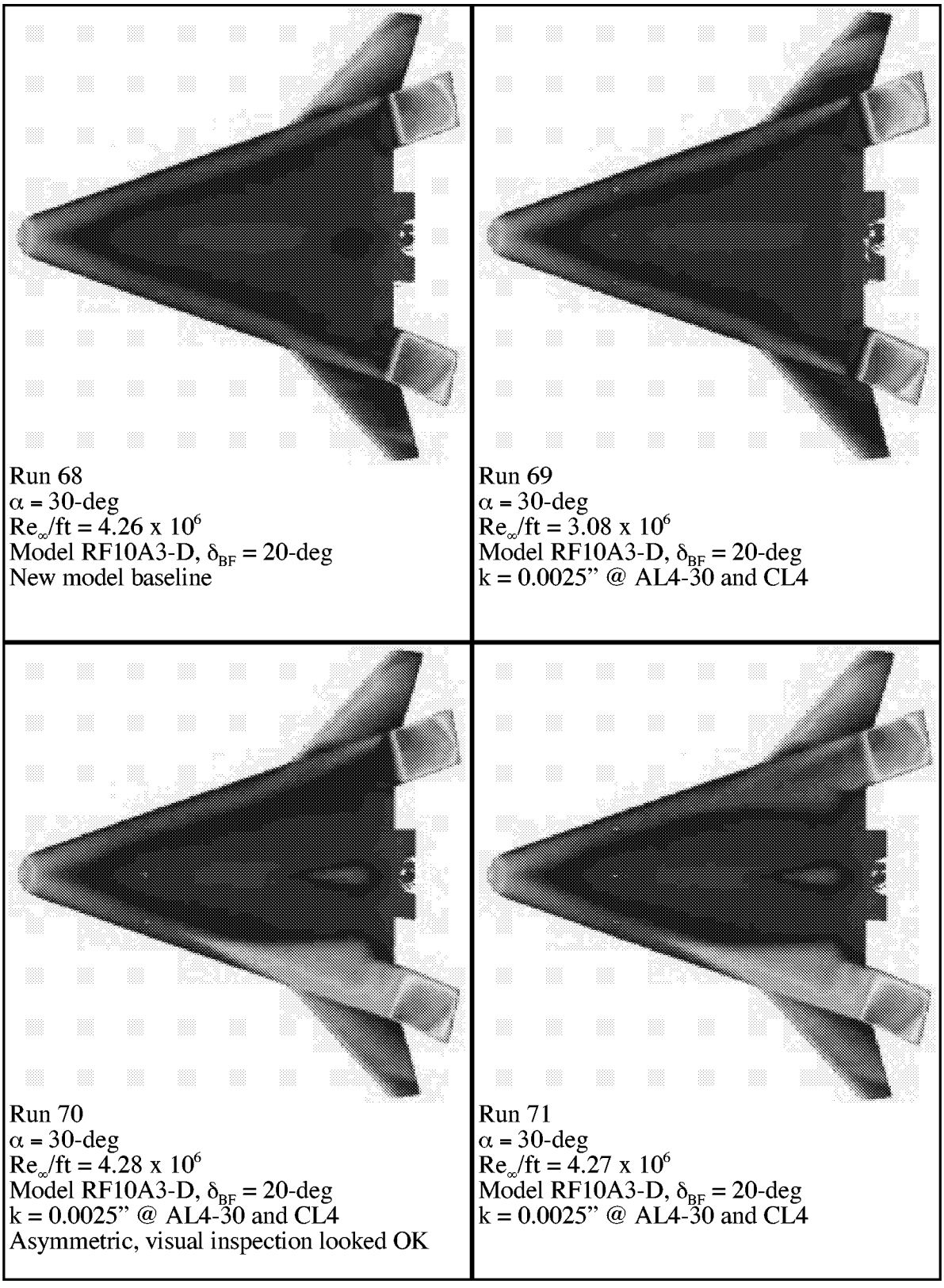

Run 68
α = 30-deg
Re_∞/ft = 4.26 x 10^6
Model RF10A3-D, δ_{BF} = 20-deg
New model baseline

Run 69
α = 30-deg
Re_∞/ft = 3.08 x 10^6
Model RF10A3-D, δ_{BF} = 20-deg
k = 0.0025" @ AL4-30 and CL4

Run 70
α = 30-deg
Re_∞/ft = 4.28 x 10^6
Model RF10A3-D, δ_{BF} = 20-deg
k = 0.0025" @ AL4-30 and CL4
Asymmetric, visual inspection looked OK

Run 71
α = 30-deg
Re_∞/ft = 4.27 x 10^6
Model RF10A3-D, δ_{BF} = 20-deg
k = 0.0025" @ AL4-30 and CL4

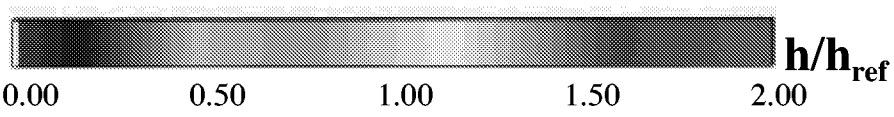

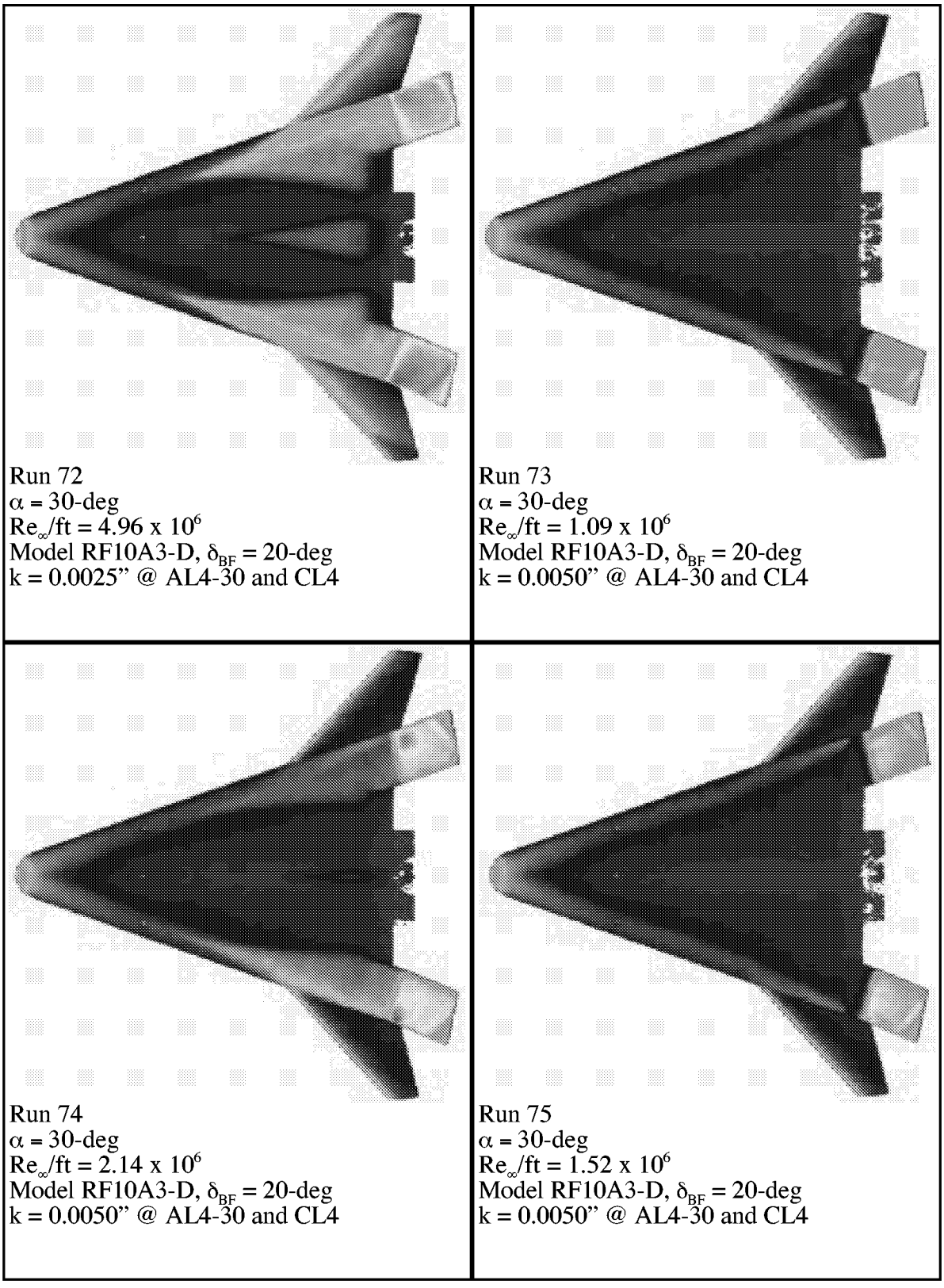

Run 72
α = 30-deg
Re_∞/ft = 4.96 x 10^6
Model RF10A3-D, δ_{BF} = 20-deg
k = 0.0025" @ AL4-30 and CL4

Run 73
α = 30-deg
Re_∞/ft = 1.09 x 10^6
Model RF10A3-D, δ_{BF} = 20-deg
k = 0.0050" @ AL4-30 and CL4

Run 74
α = 30-deg
Re_∞/ft = 2.14 x 10^6
Model RF10A3-D, δ_{BF} = 20-deg
k = 0.0050" @ AL4-30 and CL4

Run 75
α = 30-deg
Re_∞/ft = 1.52 x 10^6
Model RF10A3-D, δ_{BF} = 20-deg
k = 0.0050" @ AL4-30 and CL4

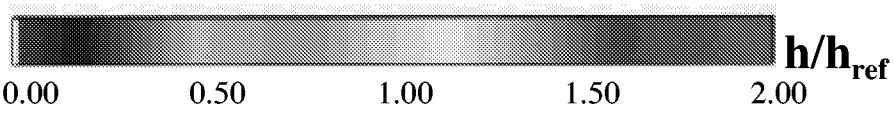

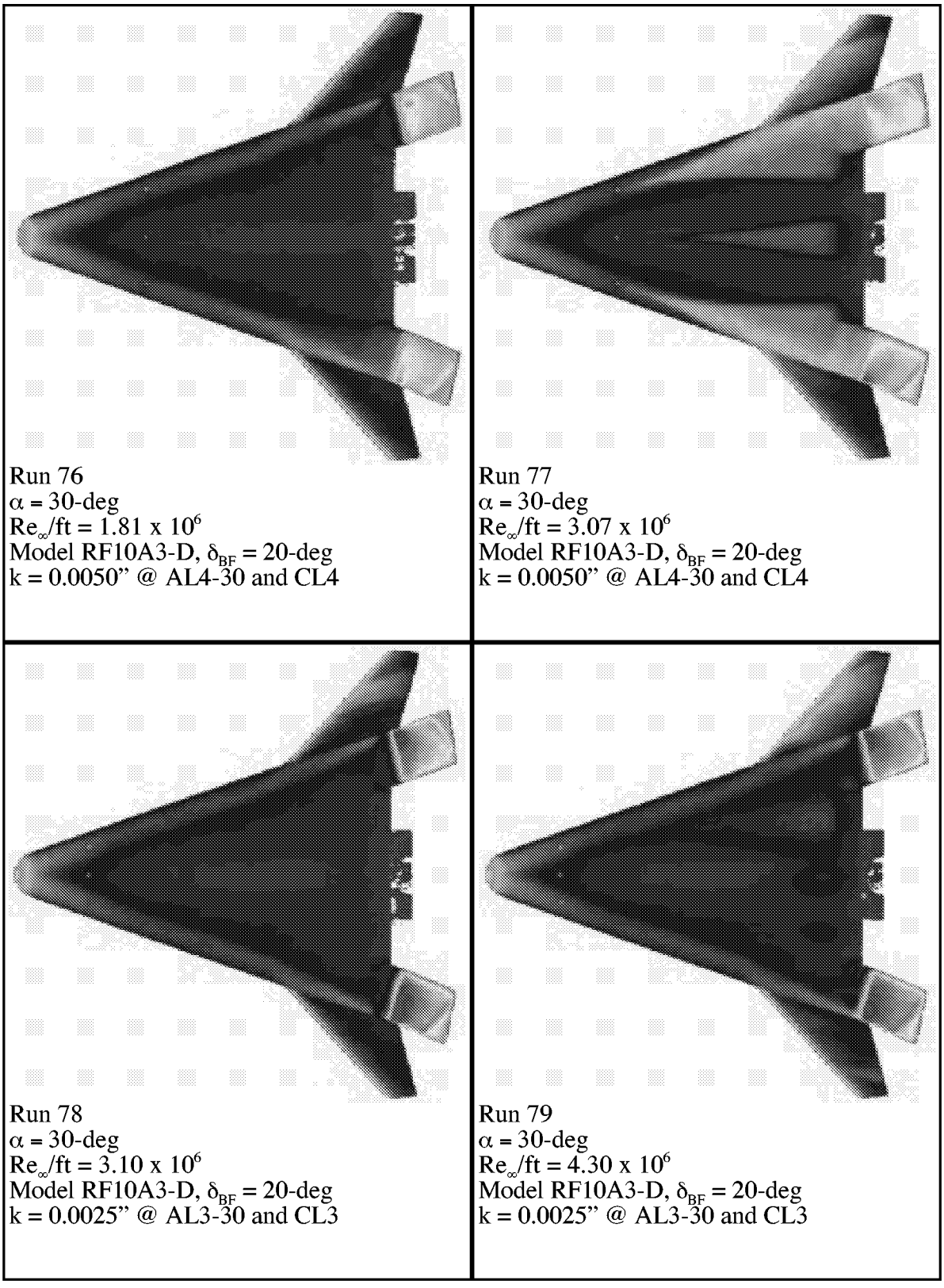

Run 76
α = 30-deg
Re_∞/ft = 1.81 x 10^6
Model RF10A3-D, δ_{BF} = 20-deg
k = 0.0050" @ AL4-30 and CL4

Run 77
α = 30-deg
Re_∞/ft = 3.07 x 10^6
Model RF10A3-D, δ_{BF} = 20-deg
k = 0.0050" @ AL4-30 and CL4

Run 78
α = 30-deg
Re_∞/ft = 3.10 x 10^6
Model RF10A3-D, δ_{BF} = 20-deg
k = 0.0025" @ AL3-30 and CL3

Run 79
α = 30-deg
Re_∞/ft = 4.30 x 10^6
Model RF10A3-D, δ_{BF} = 20-deg
k = 0.0025" @ AL3-30 and CL3

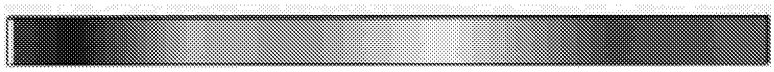

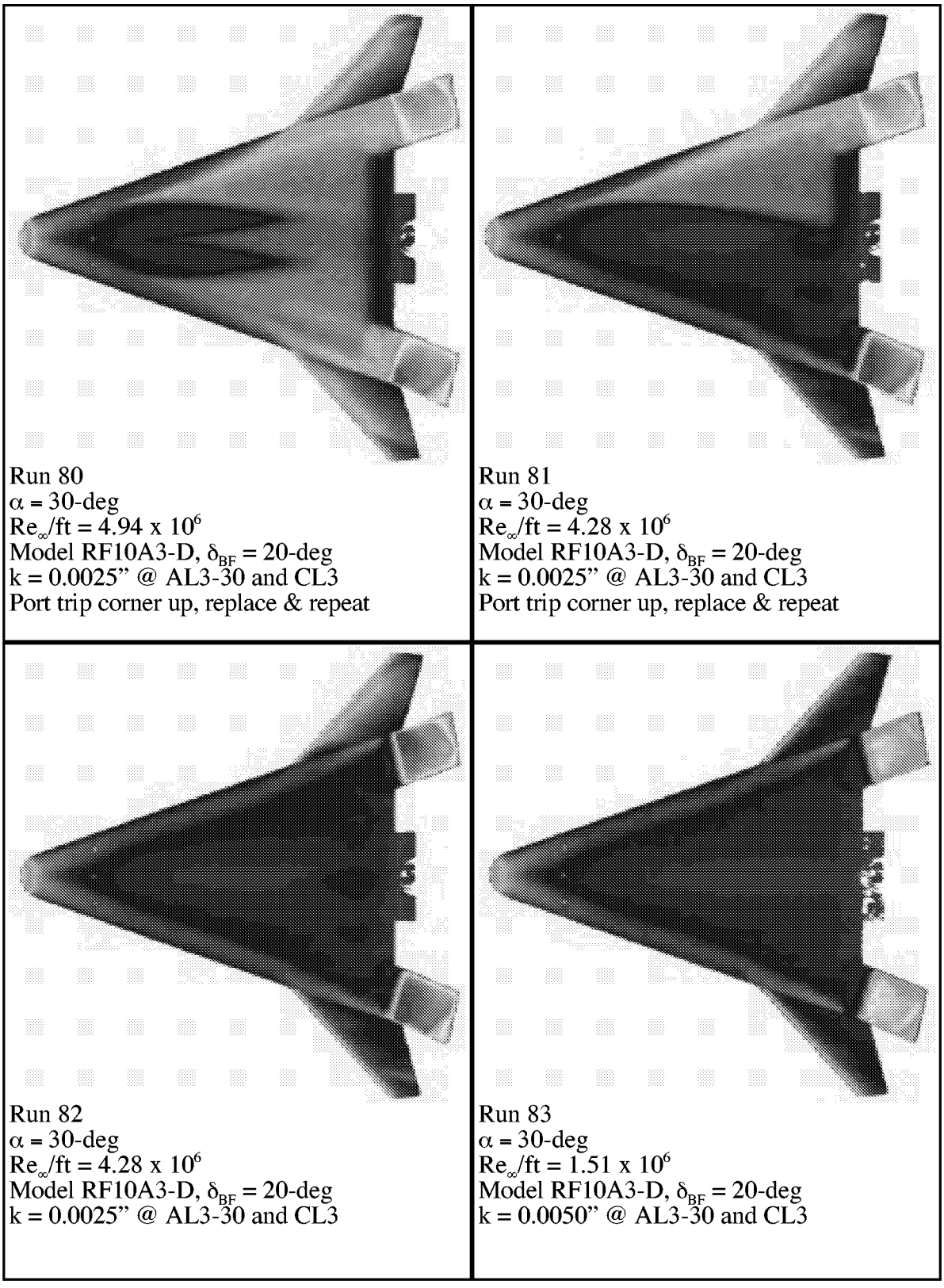

Run 80
α = 30-deg
Re_∞/ft = 4.94 x 10^6
Model RF10A3-D, δ_{BF} = 20-deg
k = 0.0025" @ AL3-30 and CL3
Port trip corner up, replace & repeat

Run 81
α = 30-deg
Re_∞/ft = 4.28 x 10^6
Model RF10A3-D, δ_{BF} = 20-deg
k = 0.0025" @ AL3-30 and CL3
Port trip corner up, replace & repeat

Run 82
α = 30-deg
Re_∞/ft = 4.28 x 10^6
Model RF10A3-D, δ_{BF} = 20-deg
k = 0.0025" @ AL3-30 and CL3

Run 83
α = 30-deg
Re_∞/ft = 1.51 x 10^6
Model RF10A3-D, δ_{BF} = 20-deg
k = 0.0050" @ AL3-30 and CL3

h/h_{ref}

0.00 0.50 1.00 1.50 2.00

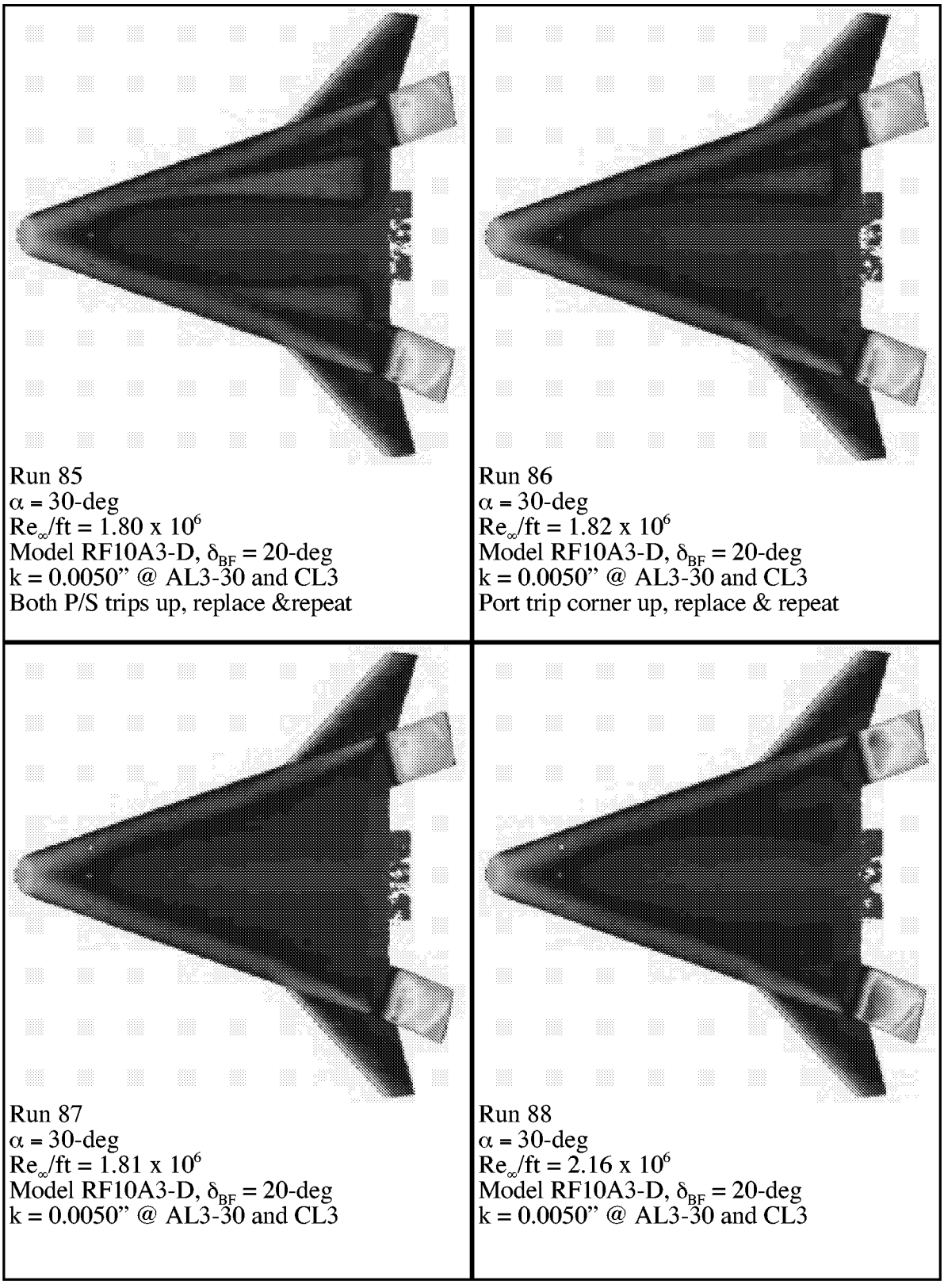

Run 85
α = 30-deg
Re_∞/ft = 1.80 x 10^6
Model RF10A3-D, δ_{BF} = 20-deg
k = 0.0050" @ AL3-30 and CL3
Both P/S trips up, replace &repeat

Run 86
α = 30-deg
Re_∞/ft = 1.82 x 10^6
Model RF10A3-D, δ_{BF} = 20-deg
k = 0.0050" @ AL3-30 and CL3
Port trip corner up, replace & repeat

Run 87
α = 30-deg
Re_∞/ft = 1.81 x 10^6
Model RF10A3-D, δ_{BF} = 20-deg
k = 0.0050" @ AL3-30 and CL3

Run 88
α = 30-deg
Re_∞/ft = 2.16 x 10^6
Model RF10A3-D, δ_{BF} = 20-deg
k = 0.0050" @ AL3-30 and CL3

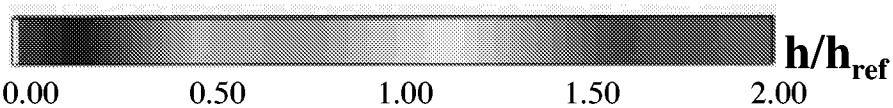

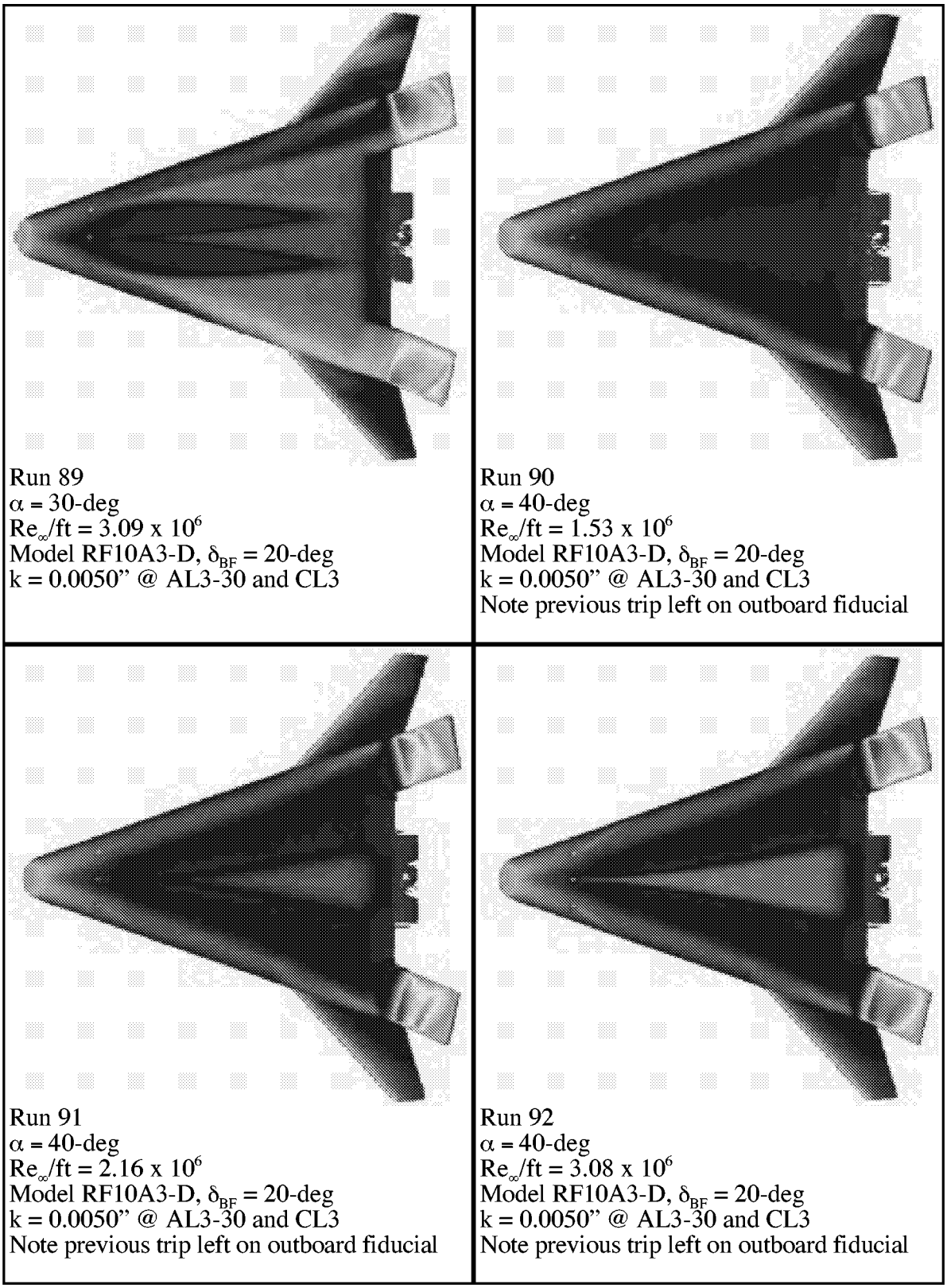

Run 89
α = 30-deg
Re_∞/ft = 3.09 x 10^6
Model RF10A3-D, δ_{BF} = 20-deg
k = 0.0050" @ AL3-30 and CL3

Run 90
α = 40-deg
Re_∞/ft = 1.53 x 10^6
Model RF10A3-D, δ_{BF} = 20-deg
k = 0.0050" @ AL3-30 and CL3
Note previous trip left on outboard fiducial

Run 91
α = 40-deg
Re_∞/ft = 2.16 x 10^6
Model RF10A3-D, δ_{BF} = 20-deg
k = 0.0050" @ AL3-30 and CL3
Note previous trip left on outboard fiducial

Run 92
α = 40-deg
Re_∞/ft = 3.08 x 10^6
Model RF10A3-D, δ_{BF} = 20-deg
k = 0.0050" @ AL3-30 and CL3
Note previous trip left on outboard fiducial

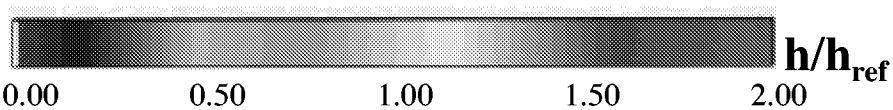

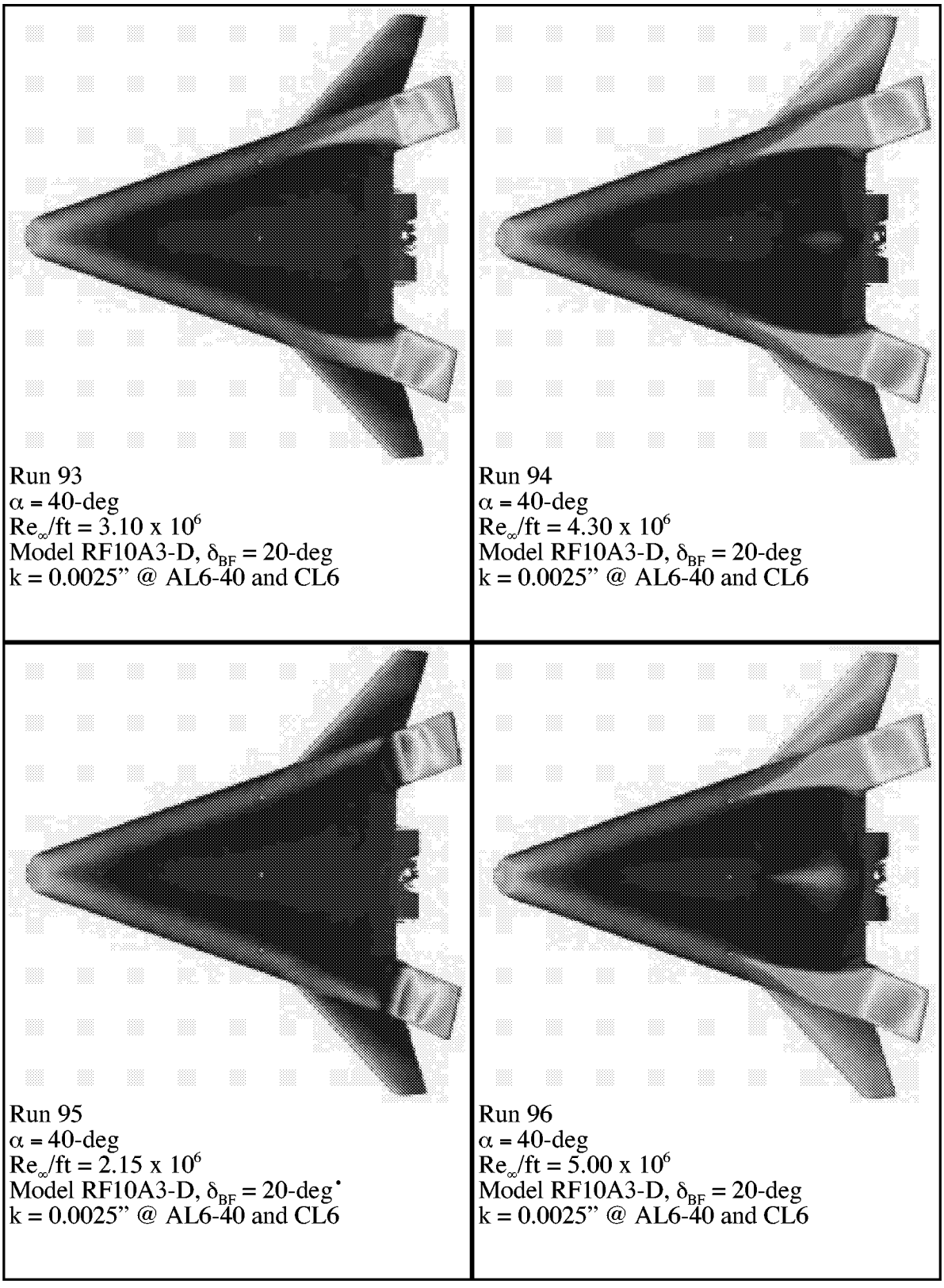

Run 93
α = 40-deg
Re_∞/ft = 3.10 x 10^6
Model RF10A3-D, δ_{BF} = 20-deg
k = 0.0025" @ AL6-40 and CL6

Run 94
α = 40-deg
Re_∞/ft = 4.30 x 10^6
Model RF10A3-D, δ_{BF} = 20-deg
k = 0.0025" @ AL6-40 and CL6

Run 95
α = 40-deg
Re_∞/ft = 2.15 x 10^6
Model RF10A3-D, δ_{BF} = 20-deg•
k = 0.0025" @ AL6-40 and CL6

Run 96
α = 40-deg
Re_∞/ft = 5.00 x 10^6
Model RF10A3-D, δ_{BF} = 20-deg
k = 0.0025" @ AL6-40 and CL6

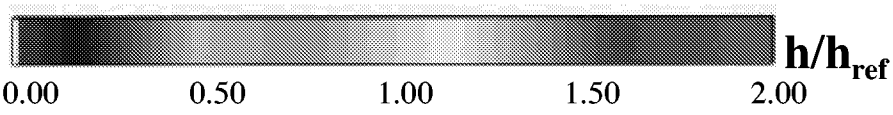

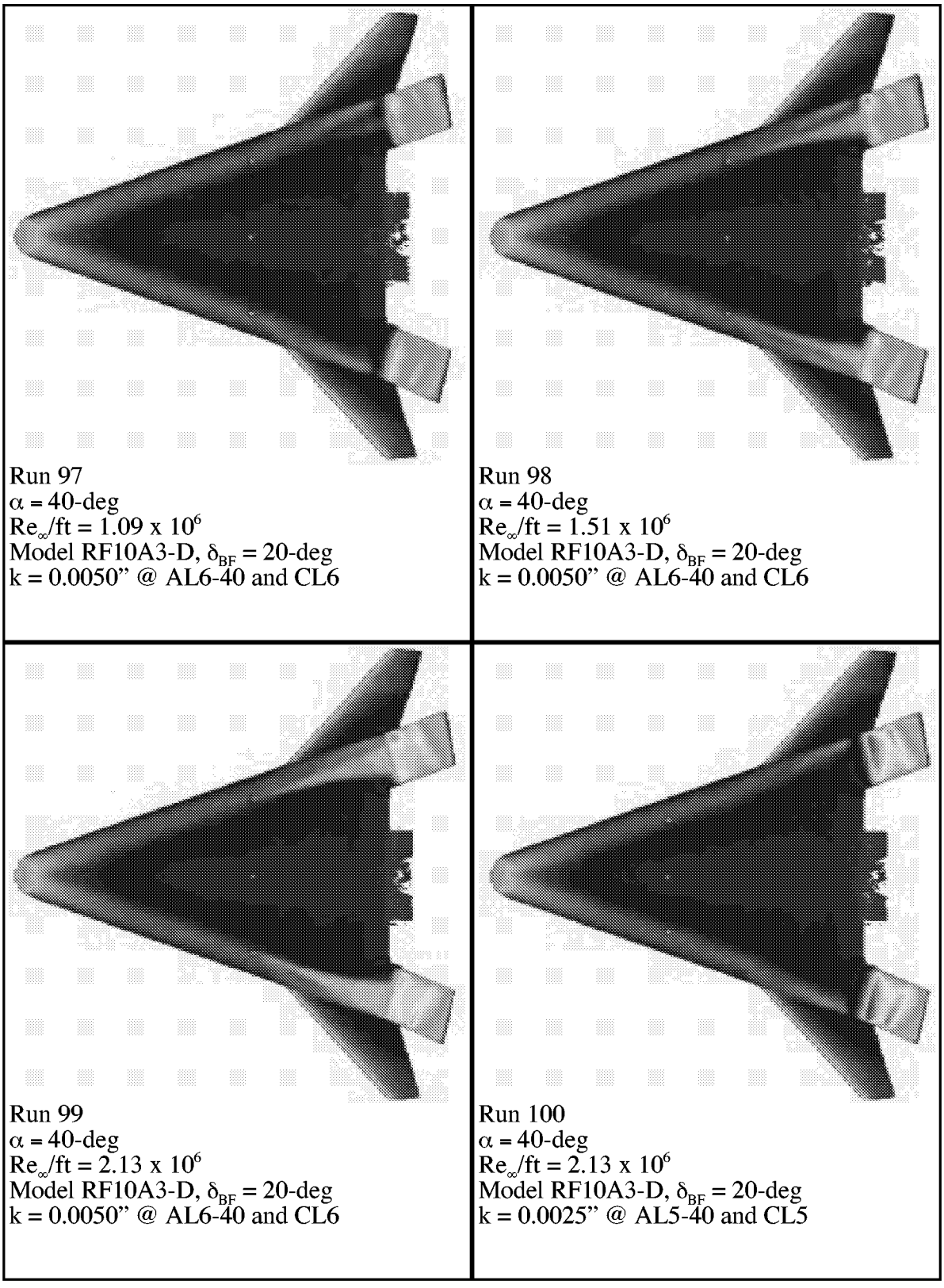

Run 97
α = 40-deg
Re_∞/ft = 1.09 x 10^6
Model RF10A3-D, δ_{BF} = 20-deg
k = 0.0050" @ AL6-40 and CL6

Run 98
α = 40-deg
Re_∞/ft = 1.51 x 10^6
Model RF10A3-D, δ_{BF} = 20-deg
k = 0.0050" @ AL6-40 and CL6

Run 99
α = 40-deg
Re_∞/ft = 2.13 x 10^6
Model RF10A3-D, δ_{BF} = 20-deg
k = 0.0050" @ AL6-40 and CL6

Run 100
α = 40-deg
Re_∞/ft = 2.13 x 10^6
Model RF10A3-D, δ_{BF} = 20-deg
k = 0.0025" @ AL5-40 and CL5

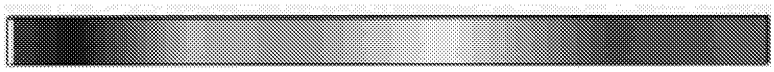

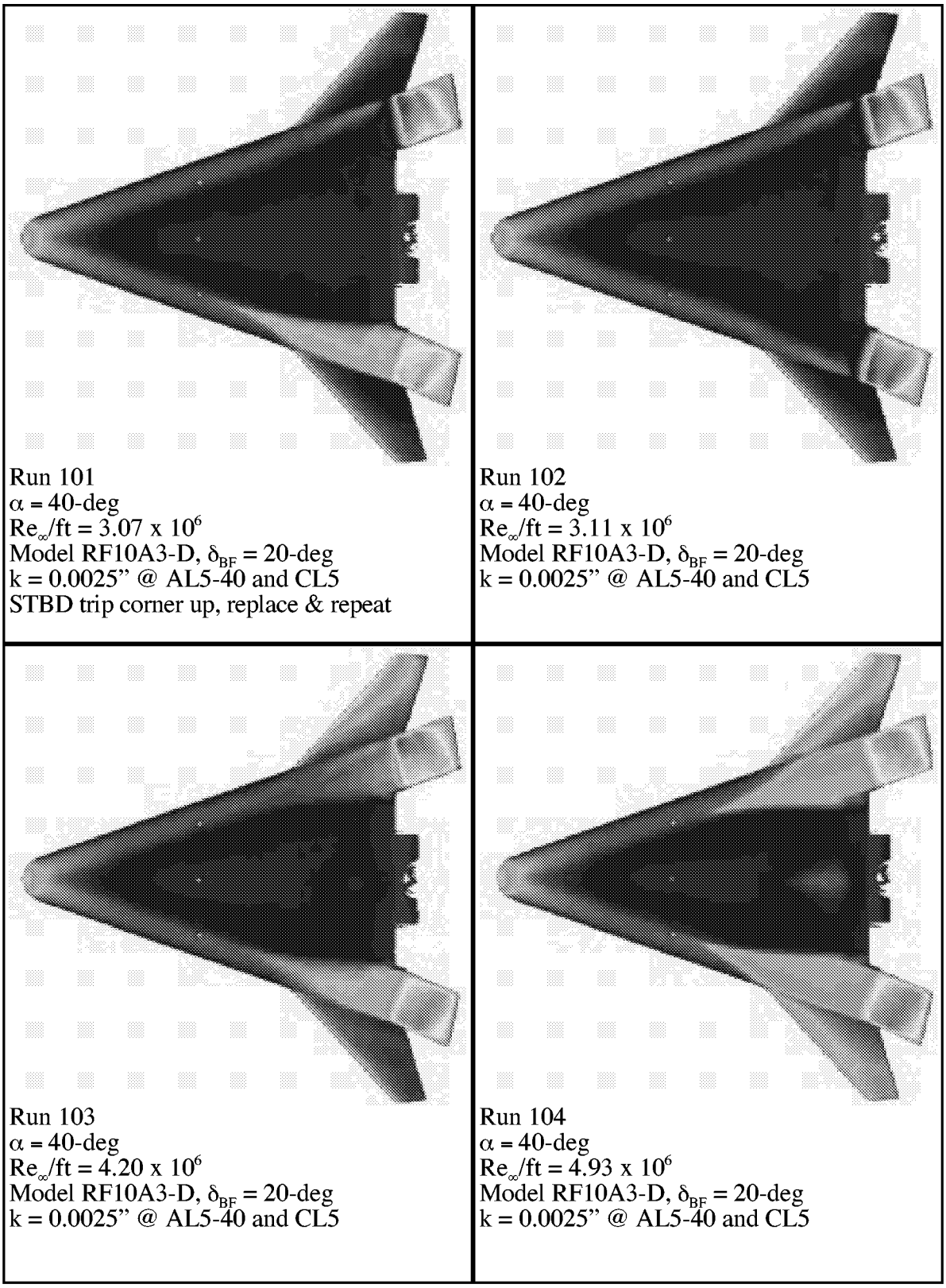

Run 101
α = 40-deg
Re_∞/ft = 3.07 x 10^6
Model RF10A3-D, δ_{BF} = 20-deg
k = 0.0025" @ AL5-40 and CL5
STBD trip corner up, replace & repeat

Run 102
α = 40-deg
Re_∞/ft = 3.11 x 10^6
Model RF10A3-D, δ_{BF} = 20-deg
k = 0.0025" @ AL5-40 and CL5

Run 103
α = 40-deg
Re_∞/ft = 4.20 x 10^6
Model RF10A3-D, δ_{BF} = 20-deg
k = 0.0025" @ AL5-40 and CL5

Run 104
α = 40-deg
Re_∞/ft = 4.93 x 10^6
Model RF10A3-D, δ_{BF} = 20-deg
k = 0.0025" @ AL5-40 and CL5

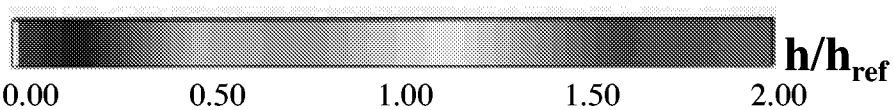

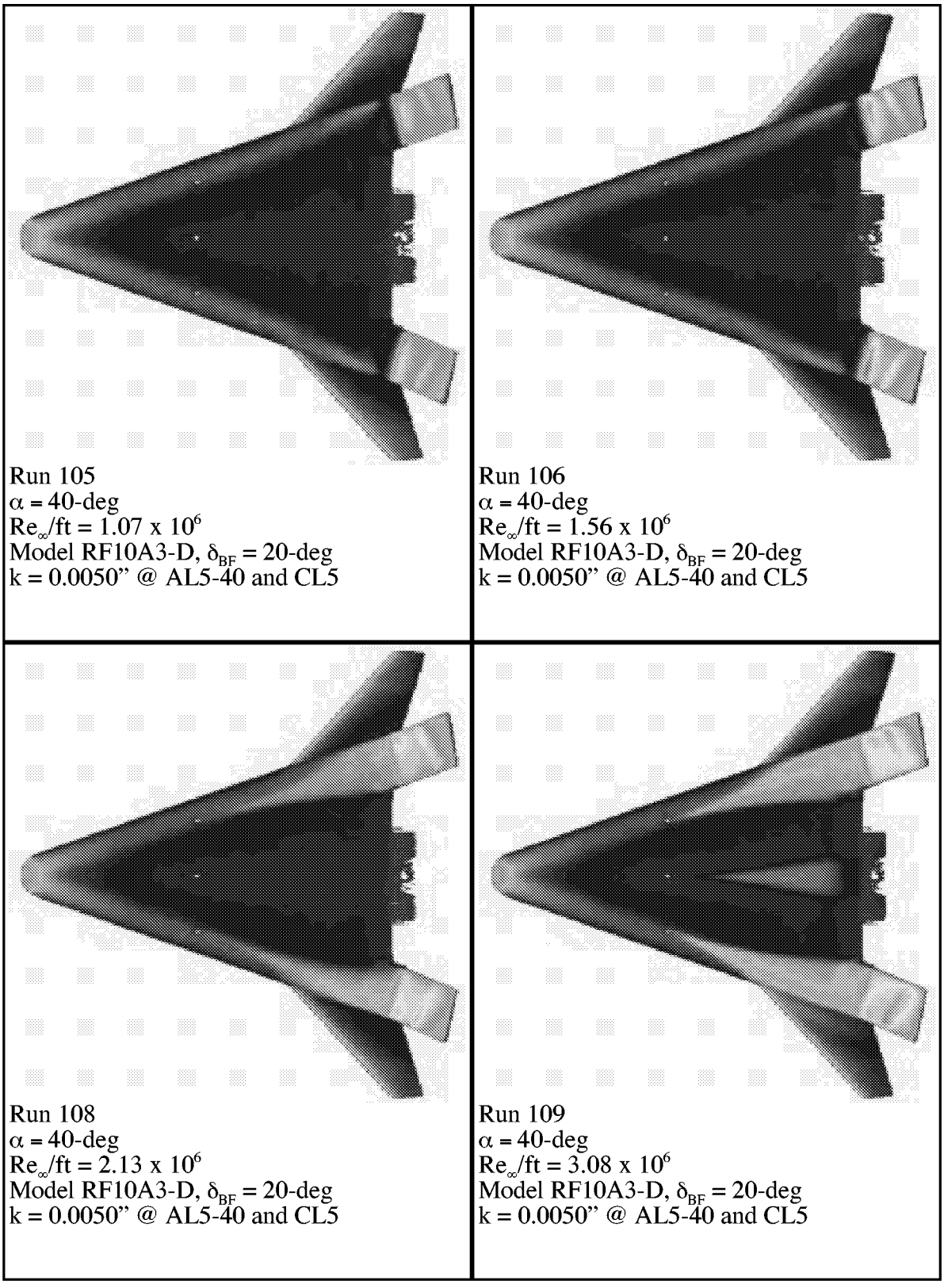

Run 105
α = 40-deg
Re_∞/ft = 1.07 x 10^6
Model RF10A3-D, δ_{BF} = 20-deg
k = 0.0050" @ AL5-40 and CL5

Run 106
α = 40-deg
Re_∞/ft = 1.56 x 10^6
Model RF10A3-D, δ_{BF} = 20-deg
k = 0.0050" @ AL5-40 and CL5

Run 108
α = 40-deg
Re_∞/ft = 2.13 x 10^6
Model RF10A3-D, δ_{BF} = 20-deg
k = 0.0050" @ AL5-40 and CL5

Run 109
α = 40-deg
Re_∞/ft = 3.08 x 10^6
Model RF10A3-D, δ_{BF} = 20-deg
k = 0.0050" @ AL5-40 and CL5

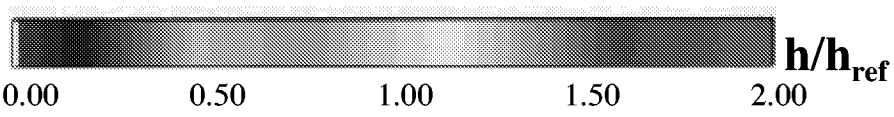

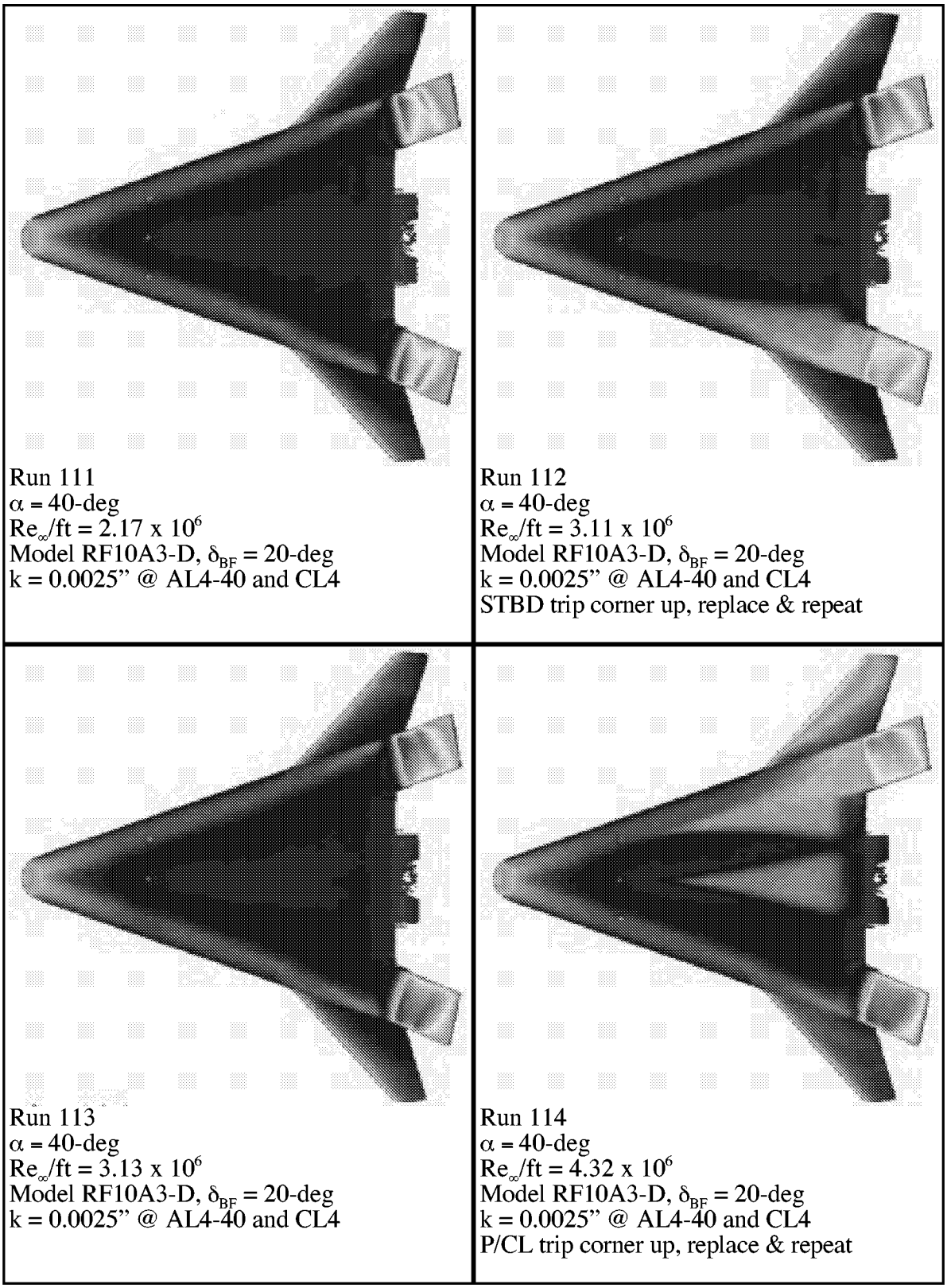

Run 111
α = 40-deg
Re_∞/ft = 2.17 x 10^6
Model RF10A3-D, δ_{BF} = 20-deg
k = 0.0025" @ AL4-40 and CL4

Run 112
α = 40-deg
Re_∞/ft = 3.11 x 10^6
Model RF10A3-D, δ_{BF} = 20-deg
k = 0.0025" @ AL4-40 and CL4
STBD trip corner up, replace & repeat

Run 113
α = 40-deg
Re_∞/ft = 3.13 x 10^6
Model RF10A3-D, δ_{BF} = 20-deg
k = 0.0025" @ AL4-40 and CL4

Run 114
α = 40-deg
Re_∞/ft = 4.32 x 10^6
Model RF10A3-D, δ_{BF} = 20-deg
k = 0.0025" @ AL4-40 and CL4
P/CL trip corner up, replace & repeat

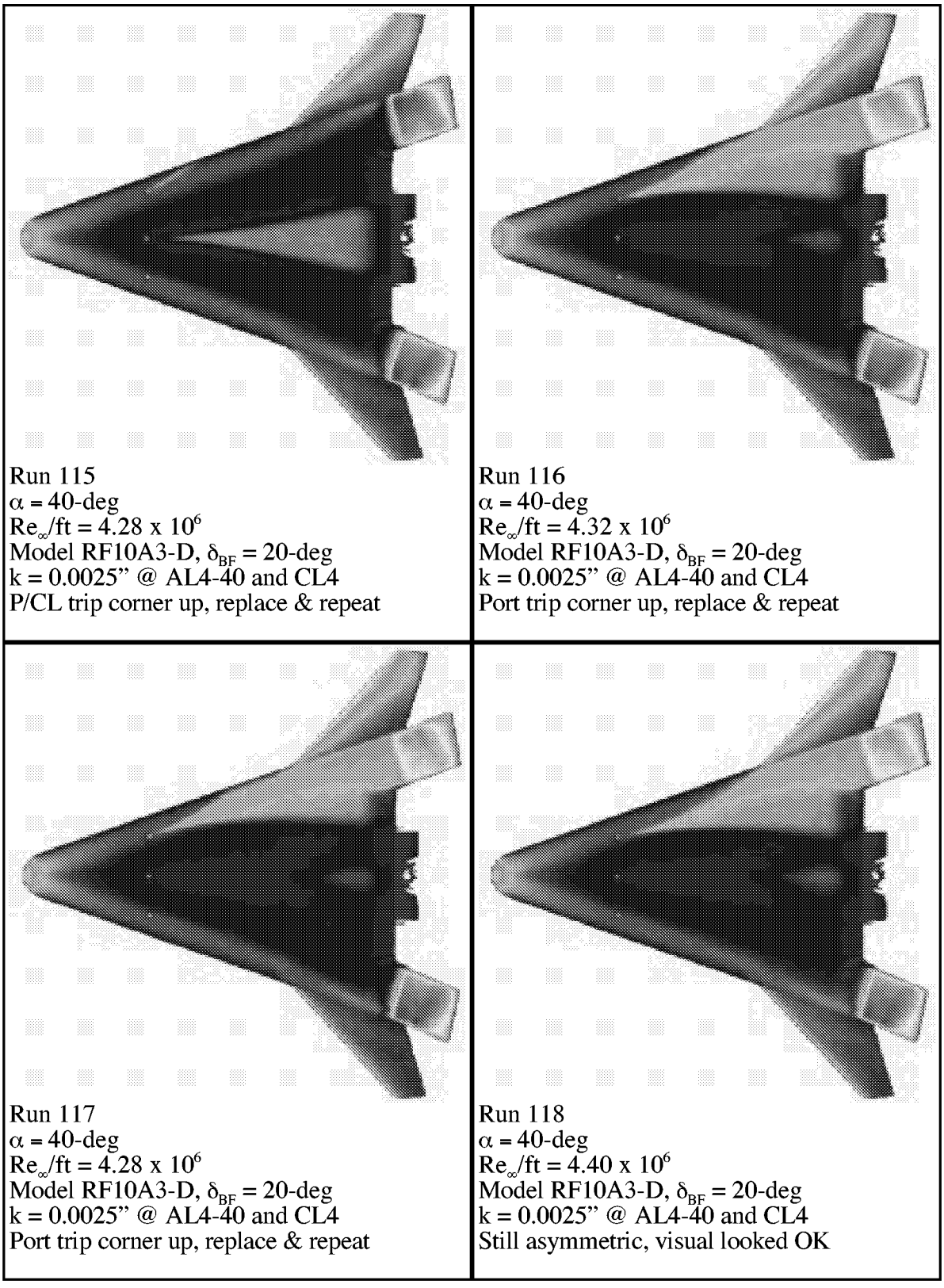

Run 115
α = 40-deg
Re_∞/ft = 4.28 x 10^6
Model RF10A3-D, δ_{BF} = 20-deg
k = 0.0025" @ AL4-40 and CL4
P/CL trip corner up, replace & repeat

Run 116
α = 40-deg
Re_∞/ft = 4.32 x 10^6
Model RF10A3-D, δ_{BF} = 20-deg
k = 0.0025" @ AL4-40 and CL4
Port trip corner up, replace & repeat

Run 117
α = 40-deg
Re_∞/ft = 4.28 x 10^6
Model RF10A3-D, δ_{BF} = 20-deg
k = 0.0025" @ AL4-40 and CL4
Port trip corner up, replace & repeat

Run 118
α = 40-deg
Re_∞/ft = 4.40 x 10^6
Model RF10A3-D, δ_{BF} = 20-deg
k = 0.0025" @ AL4-40 and CL4
Still asymmetric, visual looked OK

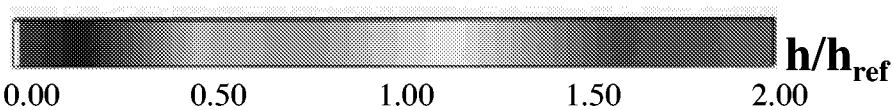

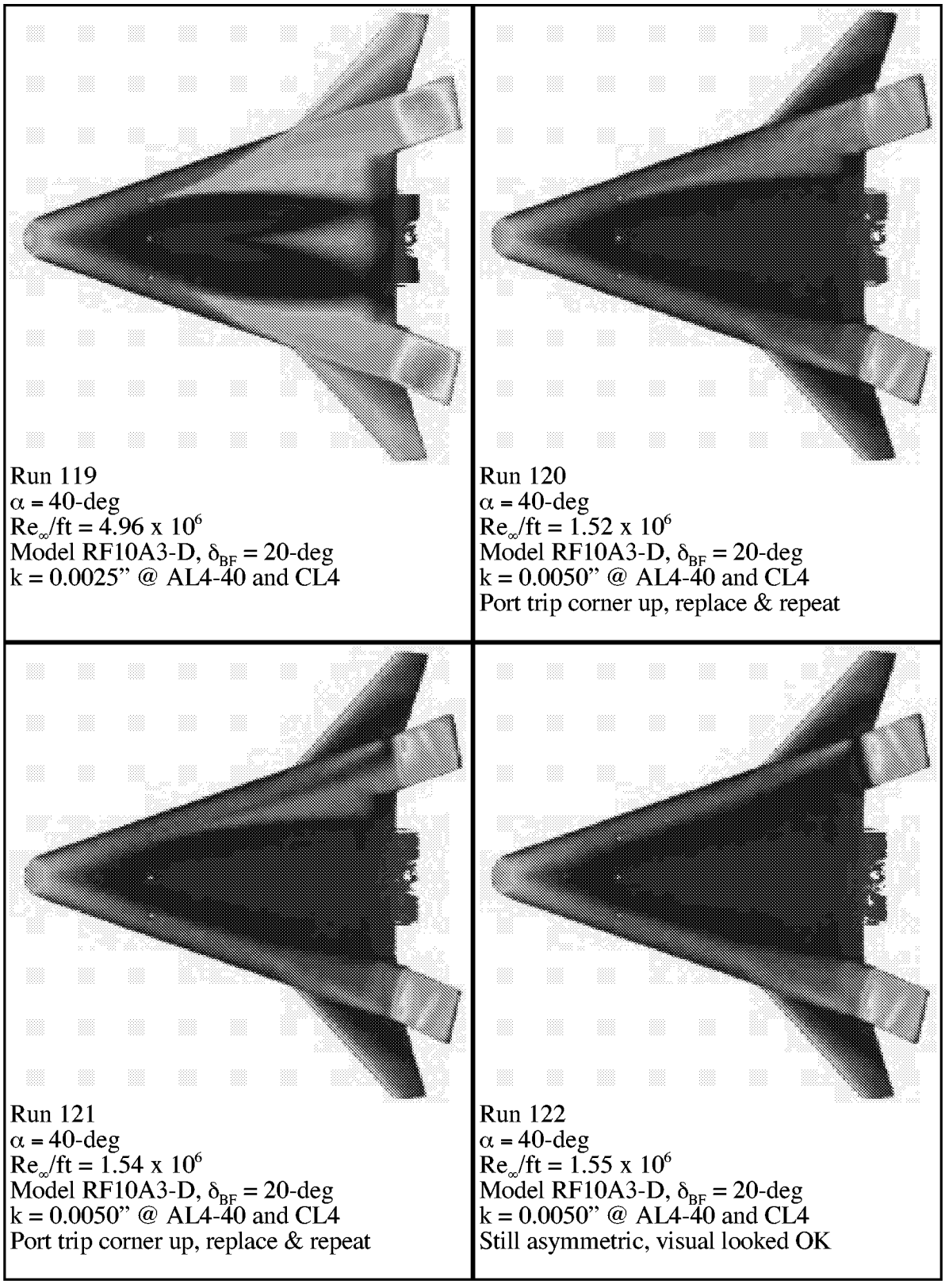

Run 119
α = 40-deg
Re_∞/ft = 4.96 x 10^6
Model RF10A3-D, δ_{BF} = 20-deg
k = 0.0025" @ AL4-40 and CL4

Run 120
α = 40-deg
Re_∞/ft = 1.52 x 10^6
Model RF10A3-D, δ_{BF} = 20-deg
k = 0.0050" @ AL4-40 and CL4
Port trip corner up, replace & repeat

Run 121
α = 40-deg
Re_∞/ft = 1.54 x 10^6
Model RF10A3-D, δ_{BF} = 20-deg
k = 0.0050" @ AL4-40 and CL4
Port trip corner up, replace & repeat

Run 122
α = 40-deg
Re_∞/ft = 1.55 x 10^6
Model RF10A3-D, δ_{BF} = 20-deg
k = 0.0050" @ AL4-40 and CL4
Still asymmetric, visual looked OK

h/h_{ref}

0.00 0.50 1.00 1.50 2.00

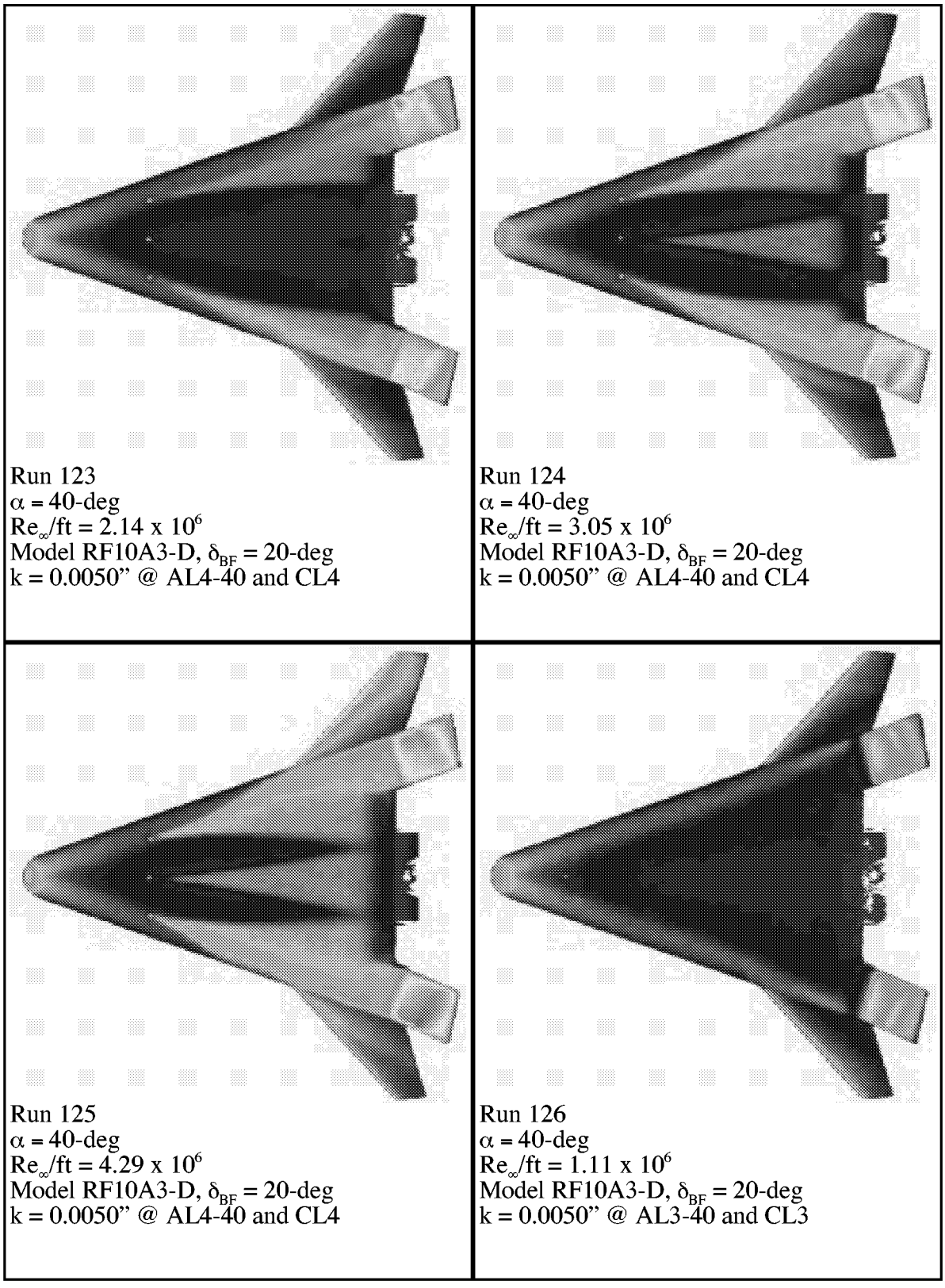

Run 123
α = 40-deg
Re_∞/ft = 2.14 x 10^6
Model RF10A3-D, δ_{BF} = 20-deg
k = 0.0050" @ AL4-40 and CL4

Run 124
α = 40-deg
Re_∞/ft = 3.05 x 10^6
Model RF10A3-D, δ_{BF} = 20-deg
k = 0.0050" @ AL4-40 and CL4

Run 125
α = 40-deg
Re_∞/ft = 4.29 x 10^6
Model RF10A3-D, δ_{BF} = 20-deg
k = 0.0050" @ AL4-40 and CL4

Run 126
α = 40-deg
Re_∞/ft = 1.11 x 10^6
Model RF10A3-D, δ_{BF} = 20-deg
k = 0.0050" @ AL3-40 and CL3

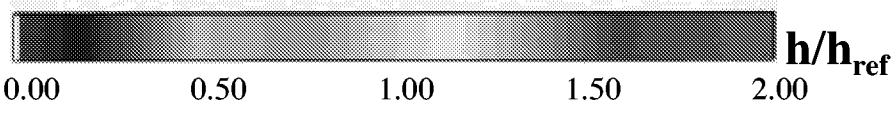

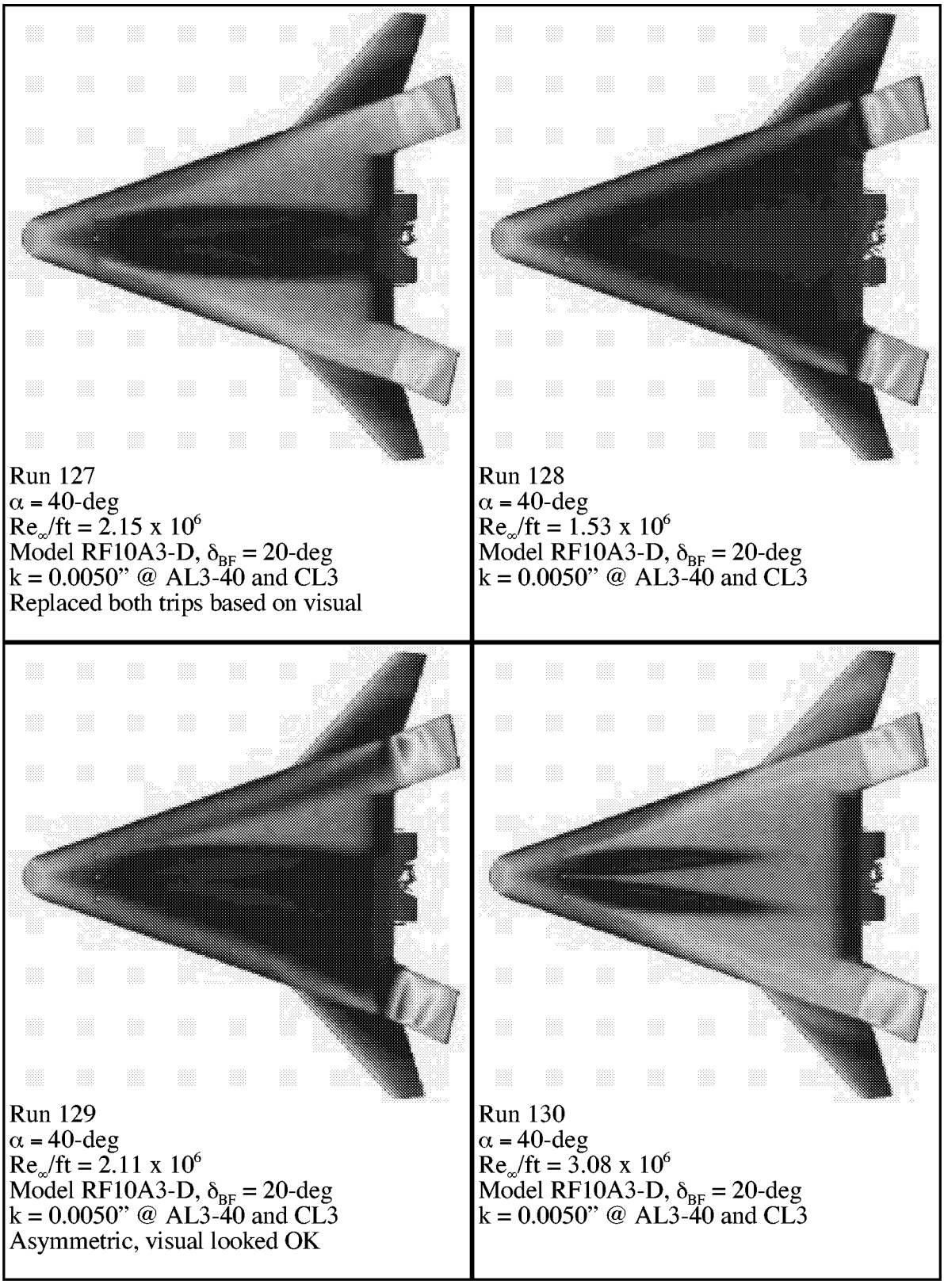

Run 127
α = 40-deg
Re_∞/ft = 2.15 x 10^6
Model RF10A3-D, δ_{BF} = 20-deg
k = 0.0050" @ AL3-40 and CL3
Replaced both trips based on visual

Run 128
α = 40-deg
Re_∞/ft = 1.53 x 10^6
Model RF10A3-D, δ_{BF} = 20-deg
k = 0.0050" @ AL3-40 and CL3

Run 129
α = 40-deg
Re_∞/ft = 2.11 x 10^6
Model RF10A3-D, δ_{BF} = 20-deg
k = 0.0050" @ AL3-40 and CL3
Asymmetric, visual looked OK

Run 130
α = 40-deg
Re_∞/ft = 3.08 x 10^6
Model RF10A3-D, δ_{BF} = 20-deg
k = 0.0050" @ AL3-40 and CL3

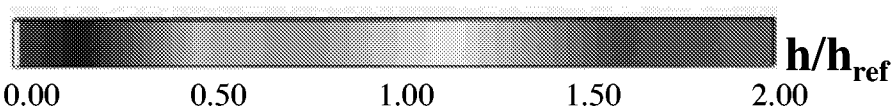

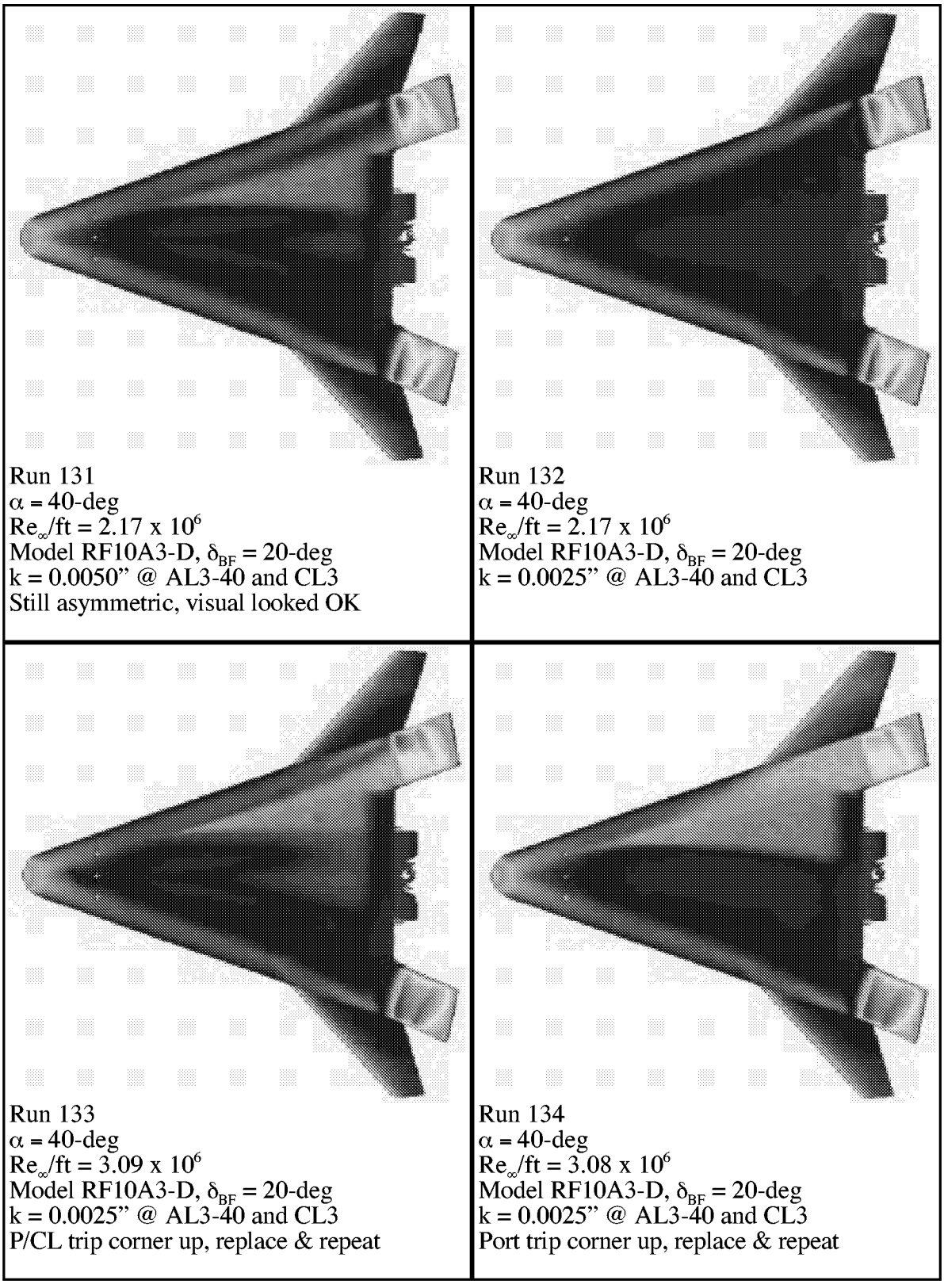

Run 131
α = 40-deg
Re_∞/ft = 2.17 x 10^6
Model RF10A3-D, δ_{BF} = 20-deg
k = 0.0050" @ AL3-40 and CL3
Still asymmetric, visual looked OK

Run 132
α = 40-deg
Re_∞/ft = 2.17 x 10^6
Model RF10A3-D, δ_{BF} = 20-deg
k = 0.0025" @ AL3-40 and CL3

Run 133
α = 40-deg
Re_∞/ft = 3.09 x 10^6
Model RF10A3-D, δ_{BF} = 20-deg
k = 0.0025" @ AL3-40 and CL3
P/CL trip corner up, replace & repeat

Run 134
α = 40-deg
Re_∞/ft = 3.08 x 10^6
Model RF10A3-D, δ_{BF} = 20-deg
k = 0.0025" @ AL3-40 and CL3
Port trip corner up, replace & repeat

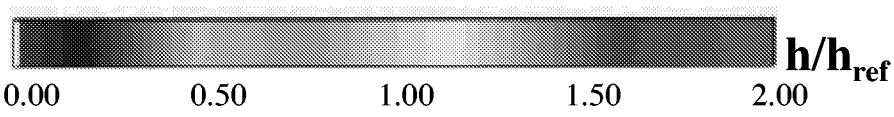

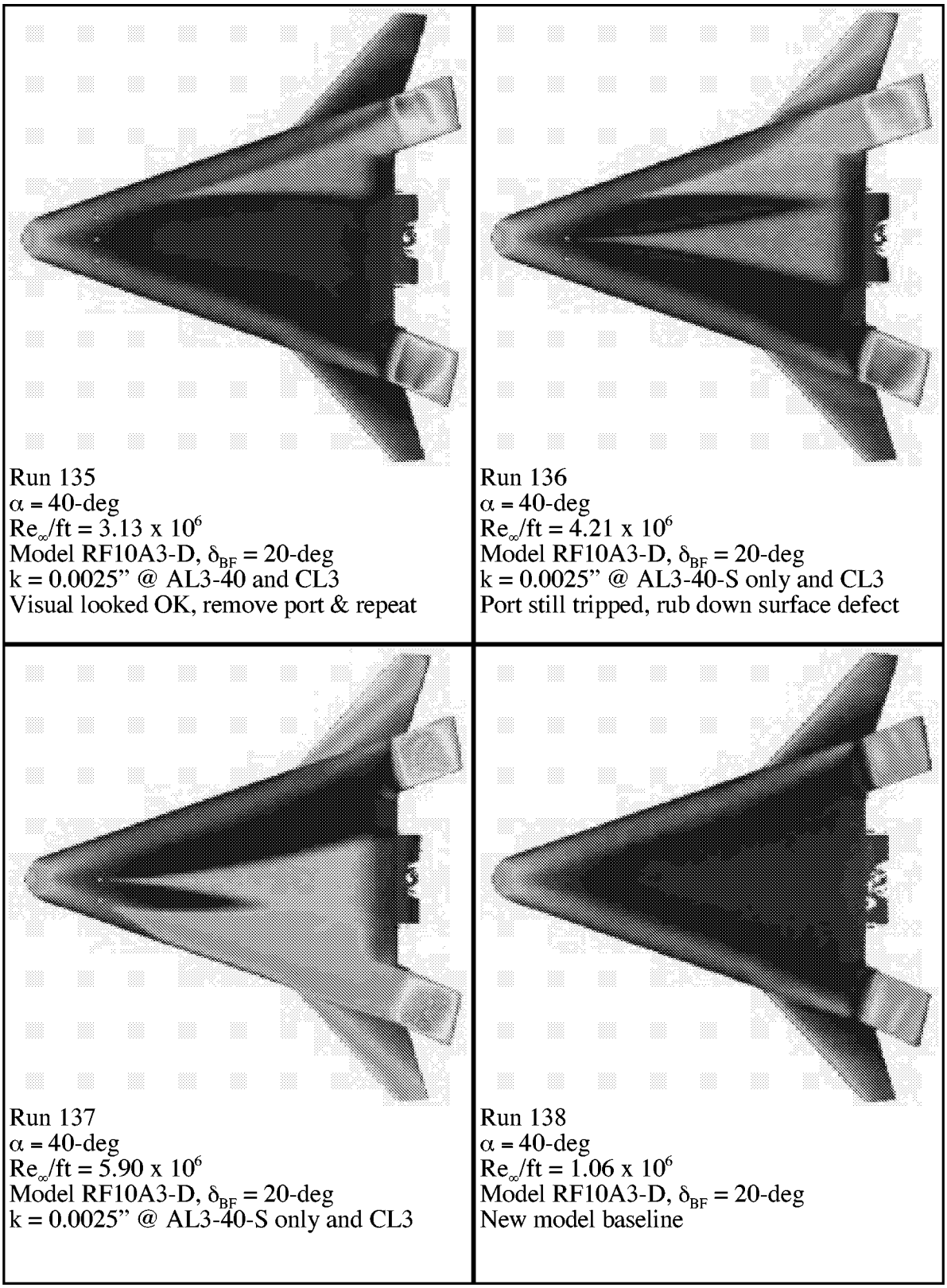

Run 135
α = 40-deg
Re_∞/ft = 3.13 x 10^6
Model RF10A3-D, δ_{BF} = 20-deg
k = 0.0025" @ AL3-40 and CL3
Visual looked OK, remove port & repeat

Run 136
α = 40-deg
Re_∞/ft = 4.21 x 10^6
Model RF10A3-D, δ_{BF} = 20-deg
k = 0.0025" @ AL3-40-S only and CL3
Port still tripped, rub down surface defect

Run 137
α = 40-deg
Re_∞/ft = 5.90 x 10^6
Model RF10A3-D, δ_{BF} = 20-deg
k = 0.0025" @ AL3-40-S only and CL3

Run 138
α = 40-deg
Re_∞/ft = 1.06 x 10^6
Model RF10A3-D, δ_{BF} = 20-deg
New model baseline

h/h_{ref}

0.00 0.50 1.00 1.50 2.00

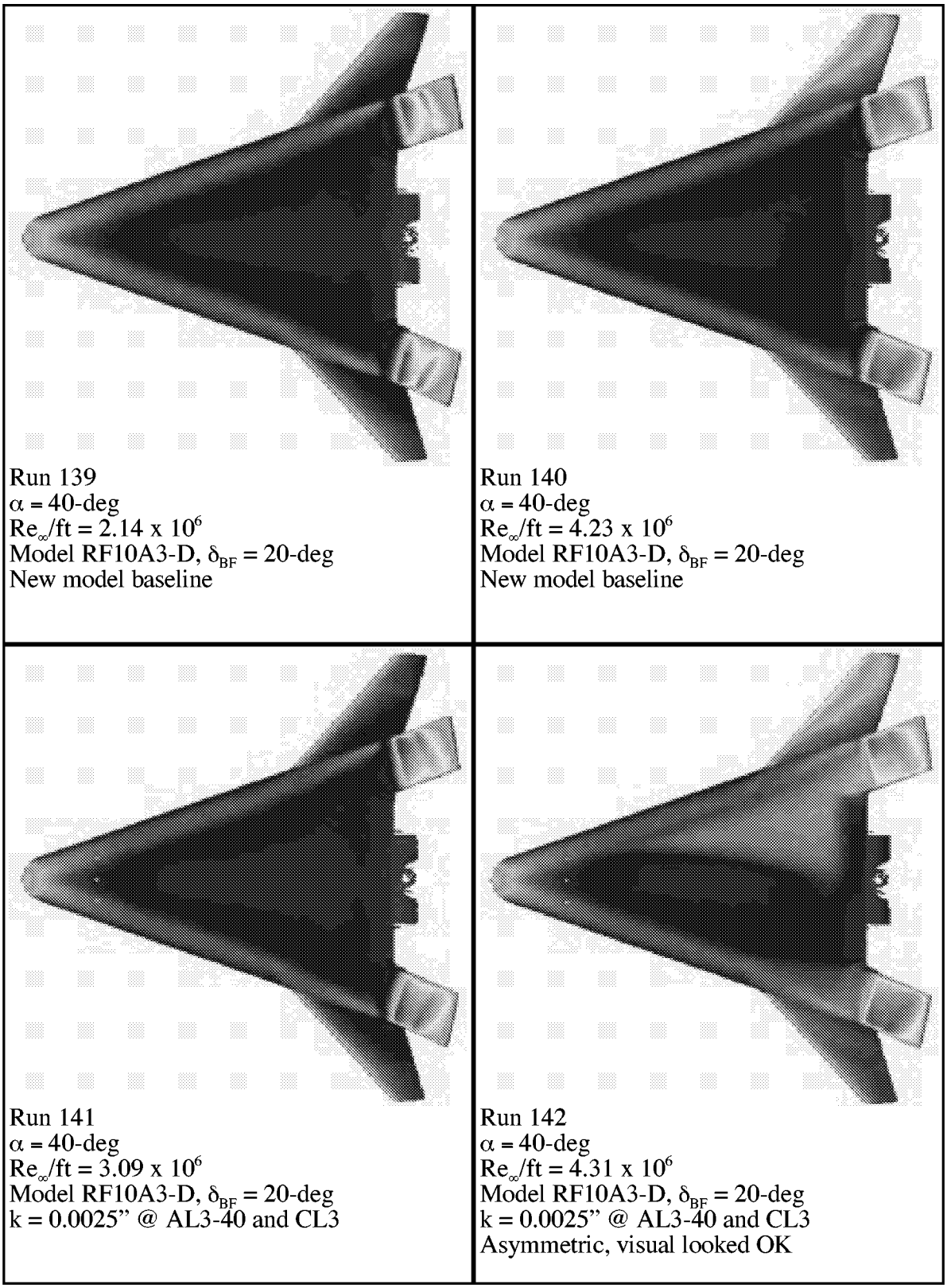

Run 139
α = 40-deg
Re_∞/ft = 2.14 x 10^6
Model RF10A3-D, δ_{BF} = 20-deg
New model baseline

Run 140
α = 40-deg
Re_∞/ft = 4.23 x 10^6
Model RF10A3-D, δ_{BF} = 20-deg
New model baseline

Run 141
α = 40-deg
Re_∞/ft = 3.09 x 10^6
Model RF10A3-D, δ_{BF} = 20-deg
k = 0.0025" @ AL3-40 and CL3

Run 142
α = 40-deg
Re_∞/ft = 4.31 x 10^6
Model RF10A3-D, δ_{BF} = 20-deg
k = 0.0025" @ AL3-40 and CL3
Asymmetric, visual looked OK

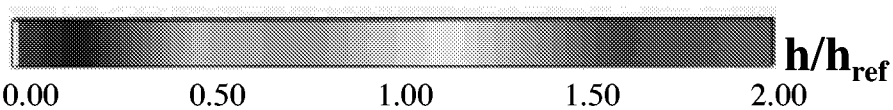

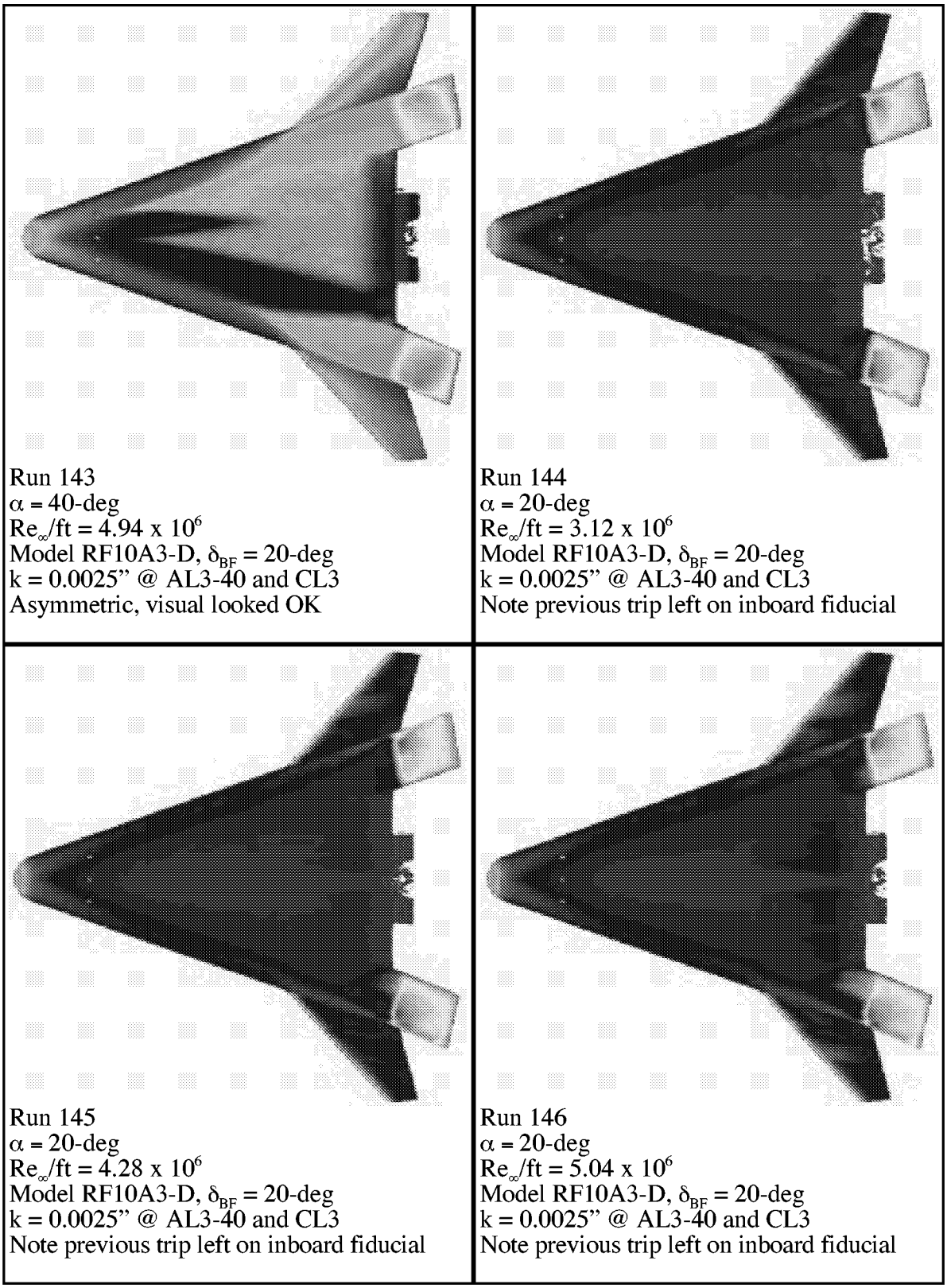

Run 143
α = 40-deg
Re_∞/ft = 4.94 x 10^6
Model RF10A3-D, δ_{BF} = 20-deg
k = 0.0025" @ AL3-40 and CL3
Asymmetric, visual looked OK

Run 144
α = 20-deg
Re_∞/ft = 3.12 x 10^6
Model RF10A3-D, δ_{BF} = 20-deg
k = 0.0025" @ AL3-40 and CL3
Note previous trip left on inboard fiducial

Run 145
α = 20-deg
Re_∞/ft = 4.28 x 10^6
Model RF10A3-D, δ_{BF} = 20-deg
k = 0.0025" @ AL3-40 and CL3
Note previous trip left on inboard fiducial

Run 146
α = 20-deg
Re_∞/ft = 5.04 x 10^6
Model RF10A3-D, δ_{BF} = 20-deg
k = 0.0025" @ AL3-40 and CL3
Note previous trip left on inboard fiducial

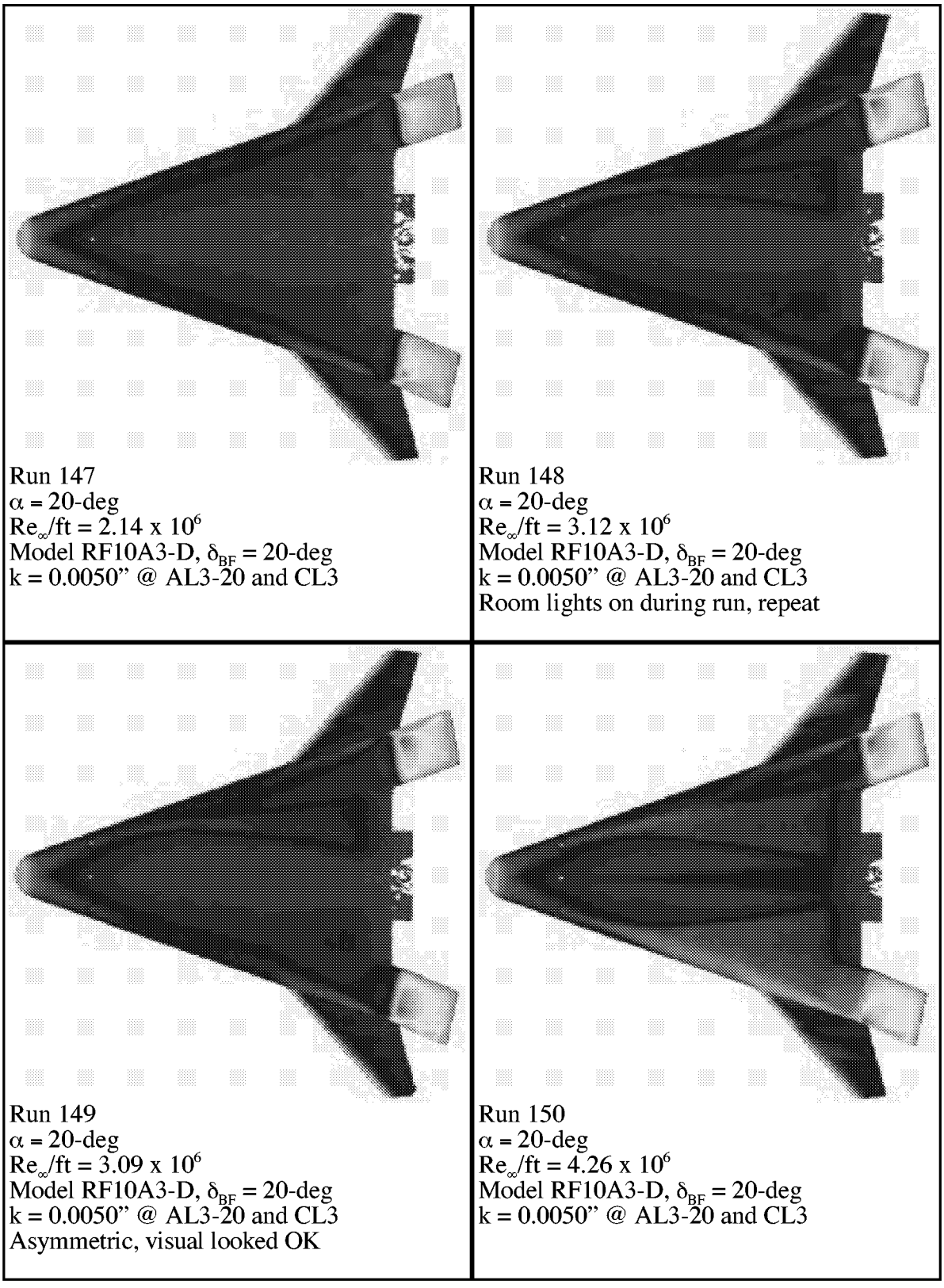

Run 147
α = 20-deg
Re_∞/ft = 2.14 x 10^6
Model RF10A3-D, δ_{BF} = 20-deg
k = 0.0050" @ AL3-20 and CL3

Run 148
α = 20-deg
Re_∞/ft = 3.12 x 10^6
Model RF10A3-D, δ_{BF} = 20-deg
k = 0.0050" @ AL3-20 and CL3
Room lights on during run, repeat

Run 149
α = 20-deg
Re_∞/ft = 3.09 x 10^6
Model RF10A3-D, δ_{BF} = 20-deg
k = 0.0050" @ AL3-20 and CL3
Asymmetric, visual looked OK

Run 150
α = 20-deg
Re_∞/ft = 4.26 x 10^6
Model RF10A3-D, δ_{BF} = 20-deg
k = 0.0050" @ AL3-20 and CL3

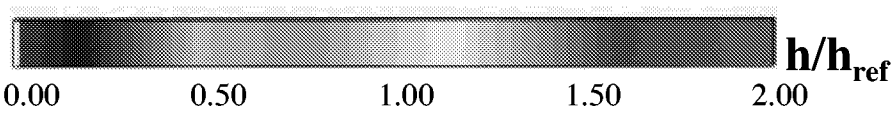

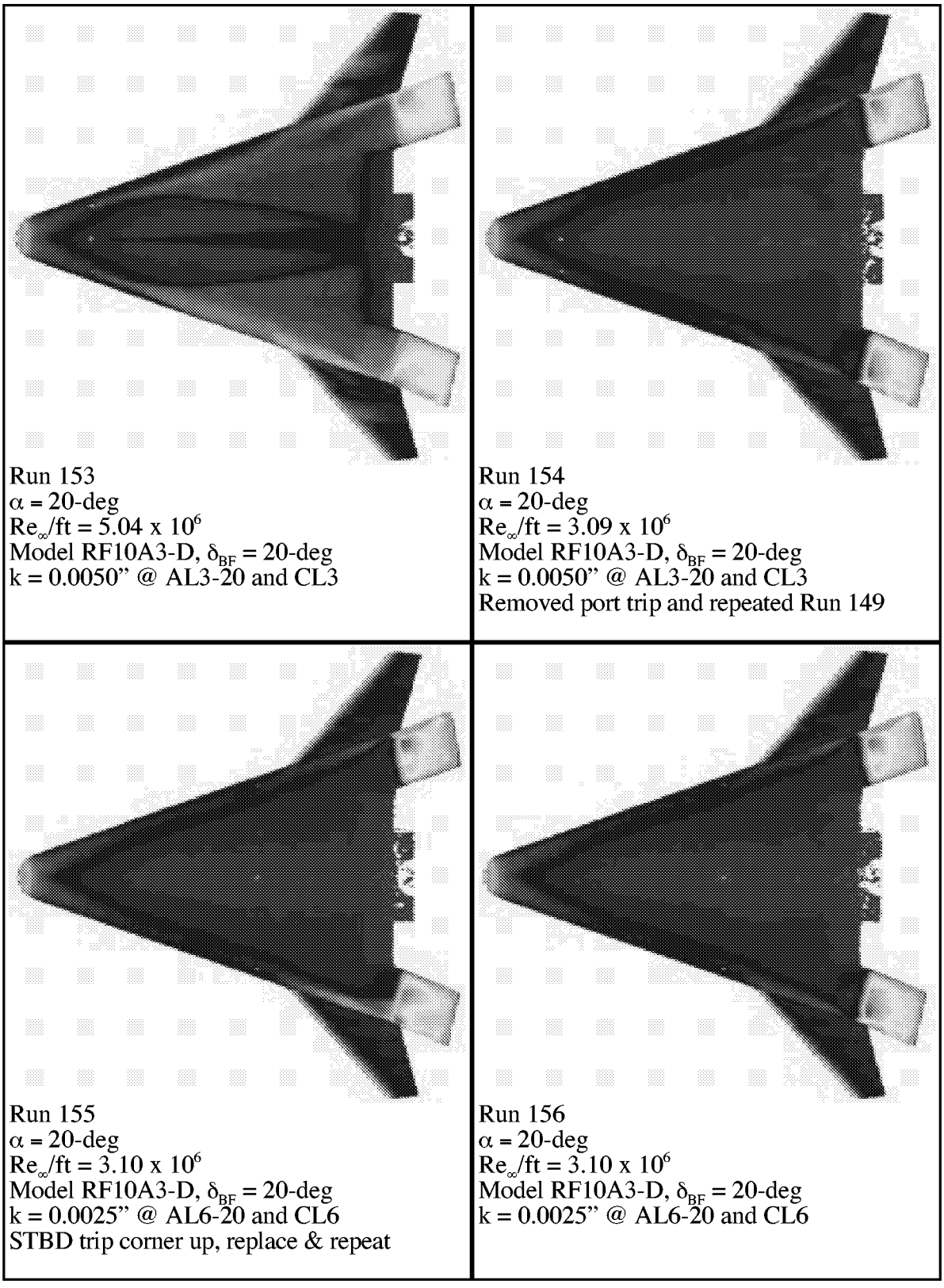

Run 153
α = 20-deg
Re_∞/ft = 5.04 x 10^6
Model RF10A3-D, δ_{BF} = 20-deg
k = 0.0050" @ AL3-20 and CL3

Run 154
α = 20-deg
Re_∞/ft = 3.09 x 10^6
Model RF10A3-D, δ_{BF} = 20-deg
k = 0.0050" @ AL3-20 and CL3
Removed port trip and repeated Run 149

Run 155
α = 20-deg
Re_∞/ft = 3.10 x 10^6
Model RF10A3-D, δ_{BF} = 20-deg
k = 0.0025" @ AL6-20 and CL6
STBD trip corner up, replace & repeat

Run 156
α = 20-deg
Re_∞/ft = 3.10 x 10^6
Model RF10A3-D, δ_{BF} = 20-deg
k = 0.0025" @ AL6-20 and CL6

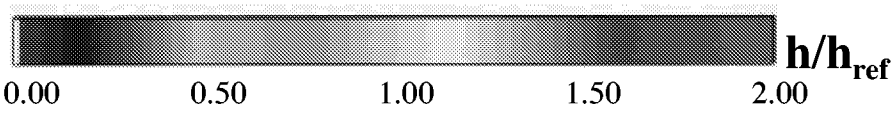

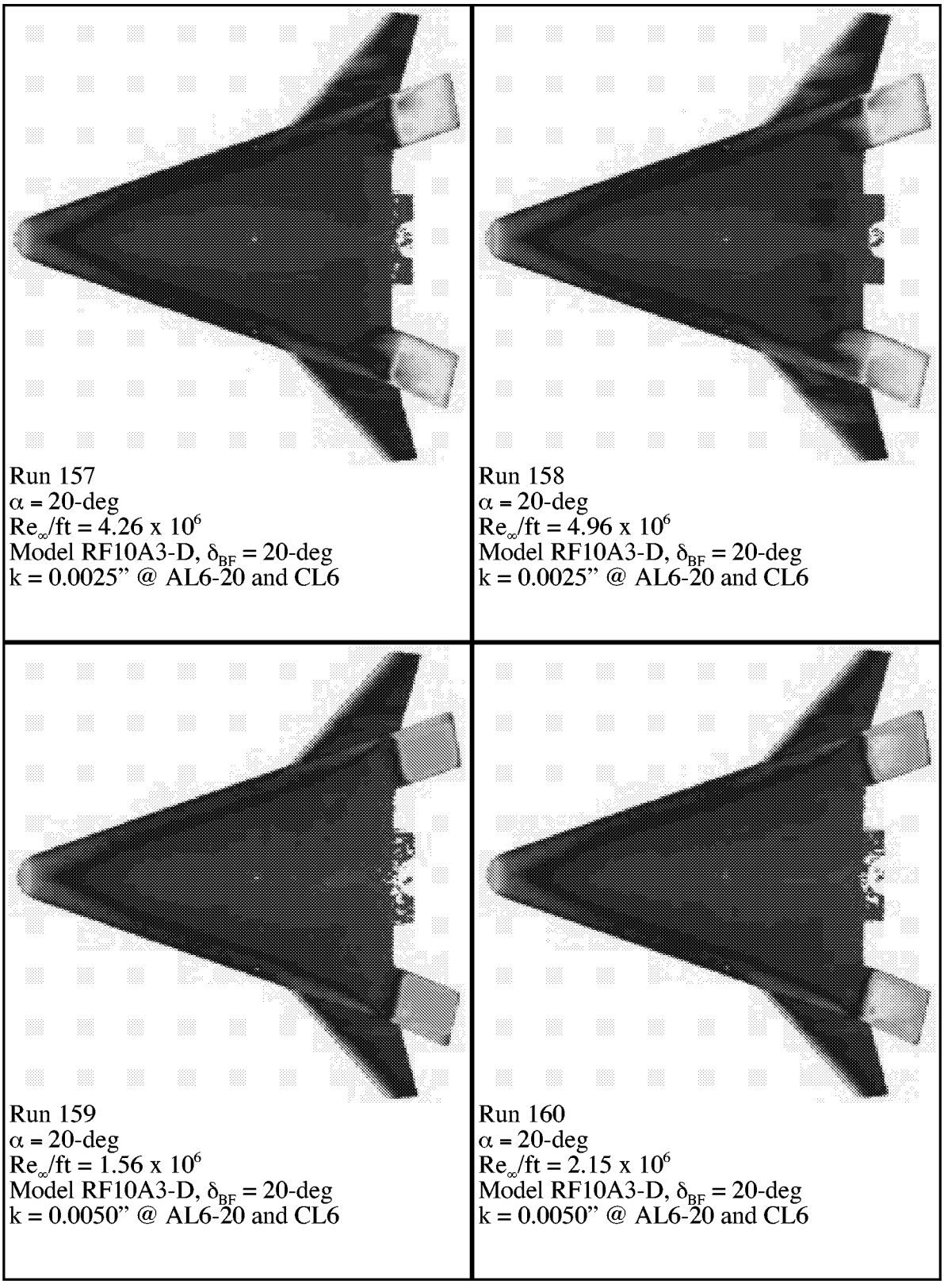

Run 157
α = 20-deg
Re_∞/ft = 4.26 x 10^6
Model RF10A3-D, δ_{BF} = 20-deg
k = 0.0025" @ AL6-20 and CL6

Run 158
α = 20-deg
Re_∞/ft = 4.96 x 10^6
Model RF10A3-D, δ_{BF} = 20-deg
k = 0.0025" @ AL6-20 and CL6

Run 159
α = 20-deg
Re_∞/ft = 1.56 x 10^6
Model RF10A3-D, δ_{BF} = 20-deg
k = 0.0050" @ AL6-20 and CL6

Run 160
α = 20-deg
Re_∞/ft = 2.15 x 10^6
Model RF10A3-D, δ_{BF} = 20-deg
k = 0.0050" @ AL6-20 and CL6

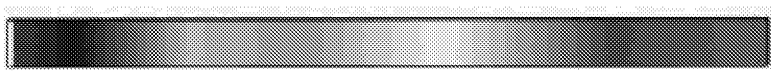

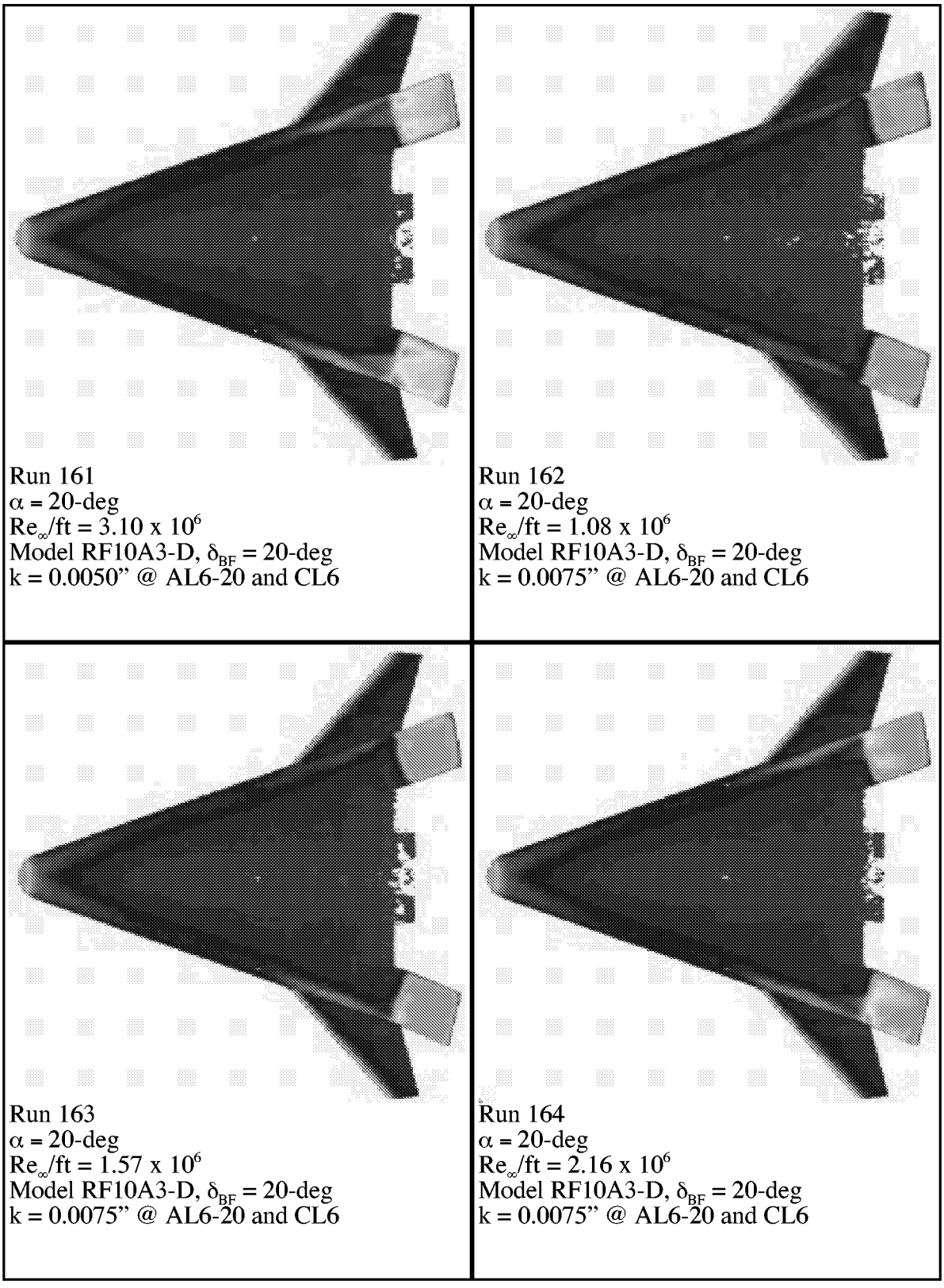

Run 161
α = 20-deg
Re_∞/ft = 3.10 x 10^6
Model RF10A3-D, δ_{BF} = 20-deg
k = 0.0050" @ AL6-20 and CL6

Run 162
α = 20-deg
Re_∞/ft = 1.08 x 10^6
Model RF10A3-D, δ_{BF} = 20-deg
k = 0.0075" @ AL6-20 and CL6

Run 163
α = 20-deg
Re_∞/ft = 1.57 x 10^6
Model RF10A3-D, δ_{BF} = 20-deg
k = 0.0075" @ AL6-20 and CL6

Run 164
α = 20-deg
Re_∞/ft = 2.16 x 10^6
Model RF10A3-D, δ_{BF} = 20-deg
k = 0.0075" @ AL6-20 and CL6

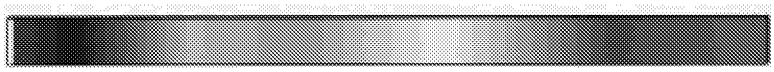

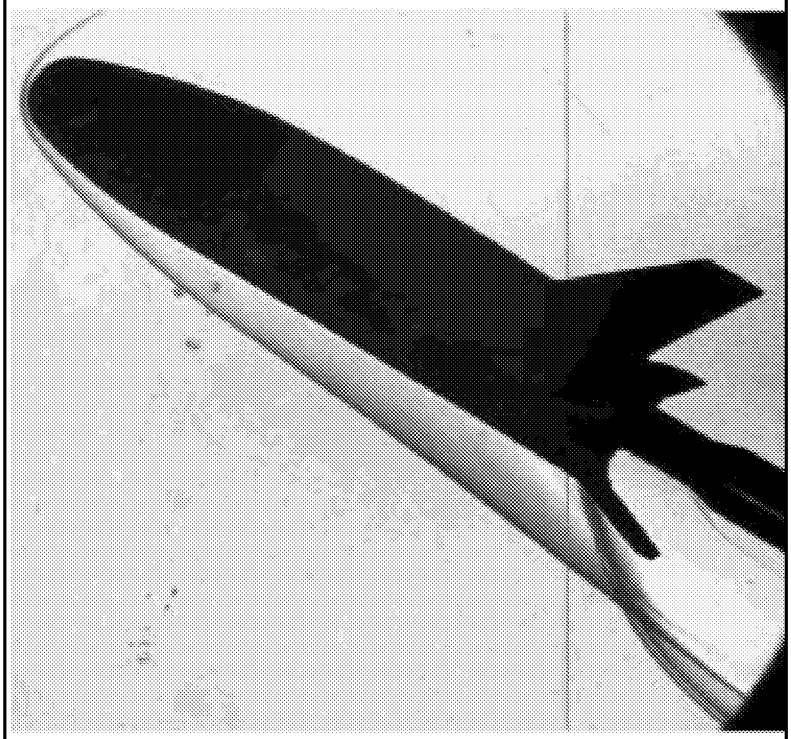

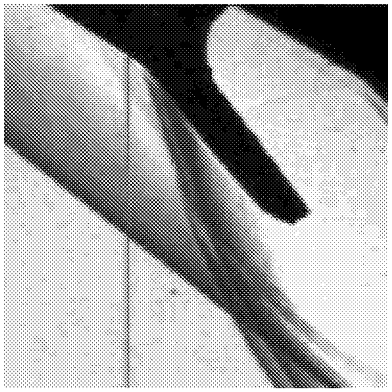

Run 174
α = 30-deg
Re_∞/ft = 3.12 x 10^6
δ_{BF} = 20-deg

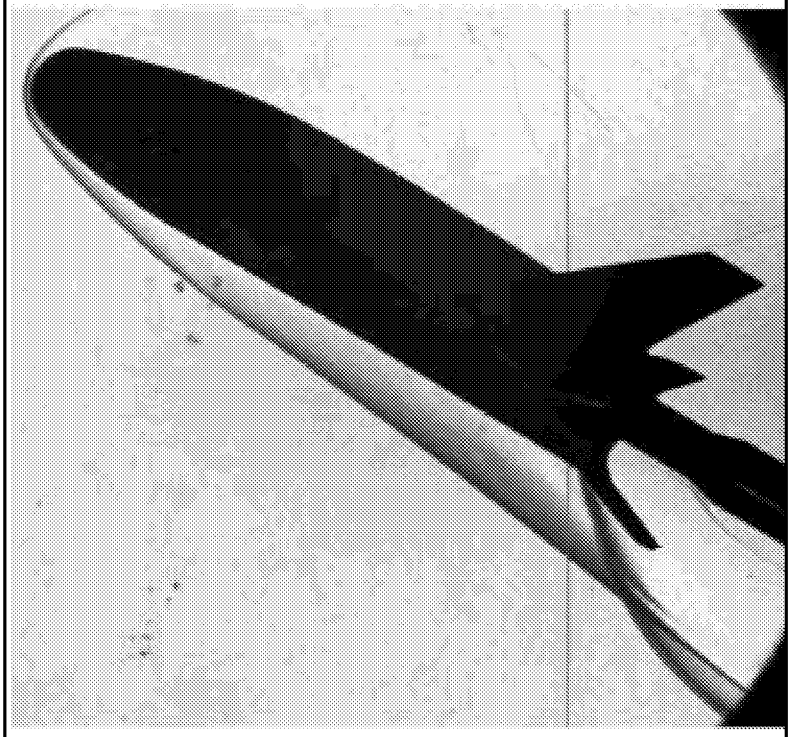

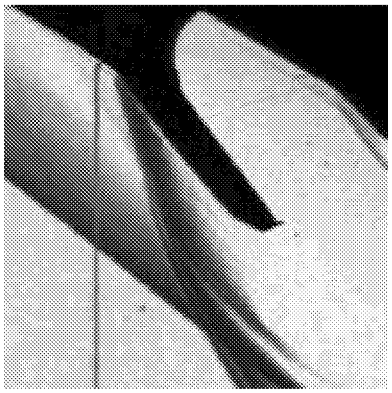

Run 175
α = 30-deg
Re_∞/ft = 4.35 x 10^6
δ_{BF} = 20-deg

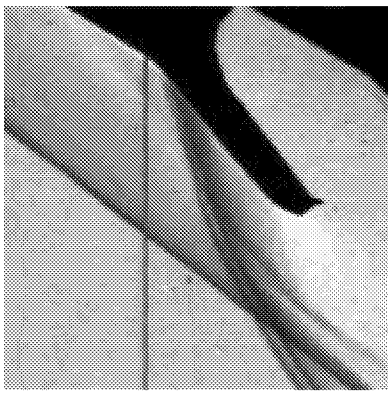

Run 176
α = 30-deg
Re_∞/ft = 1.13 x 10^6
δ_{BF} = 20-deg

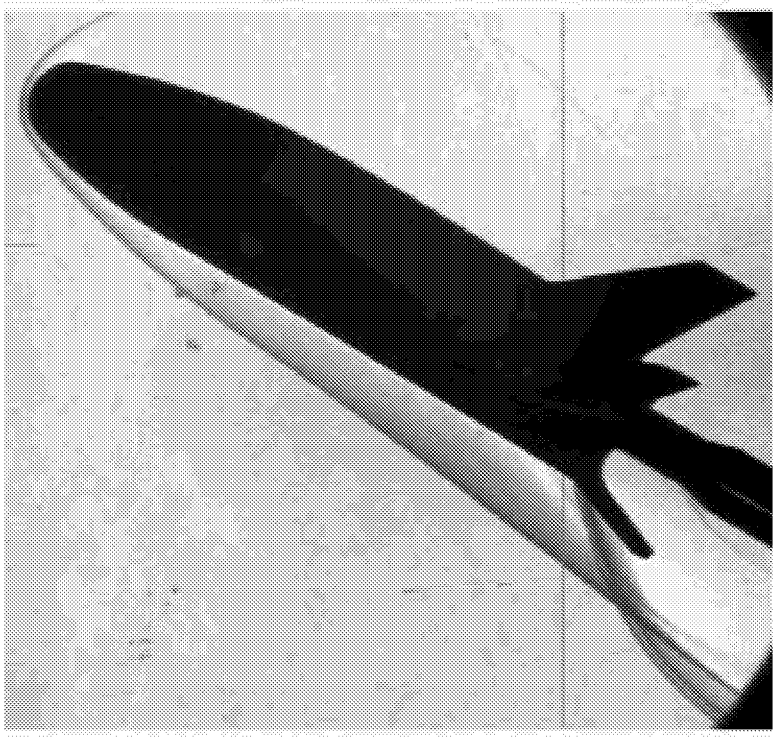

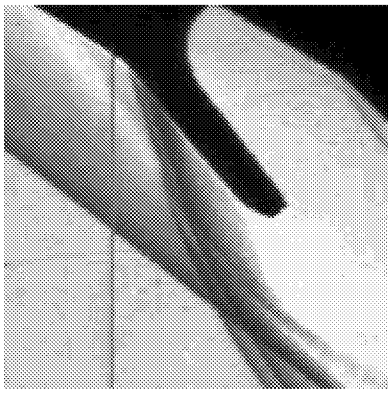

Run 177
α = 30-deg
Re_∞/ft = 2 x 10^6
δ_{BF} = 20-deg

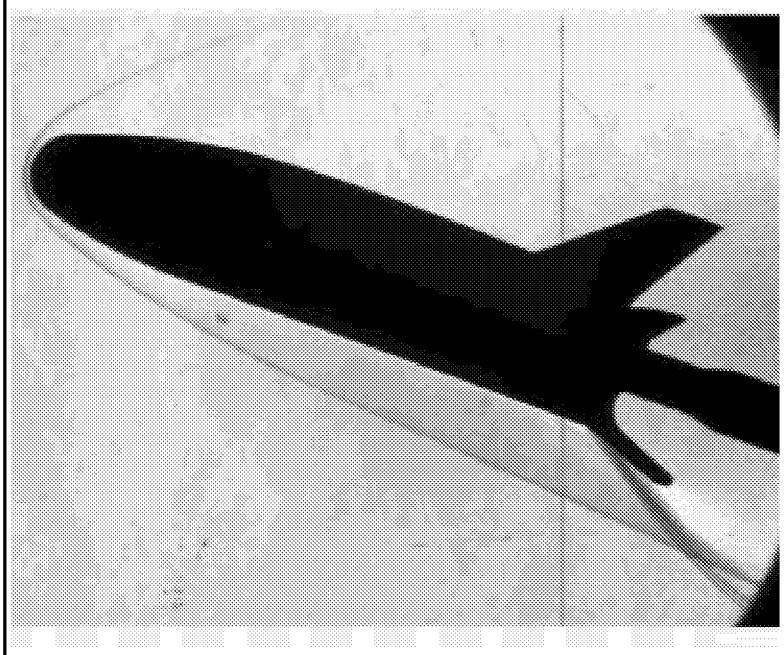

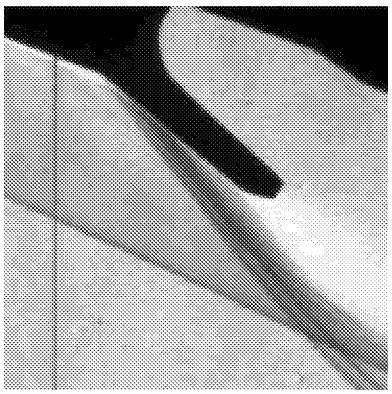

Run 182
α = 20-deg
Re_∞/ft = 1 x 10^6
δ_{BF} = 20-deg

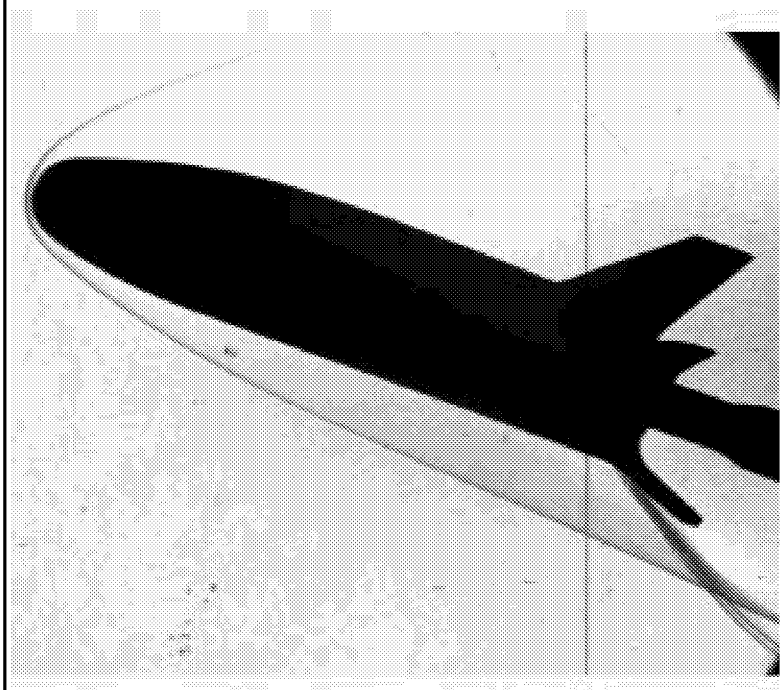

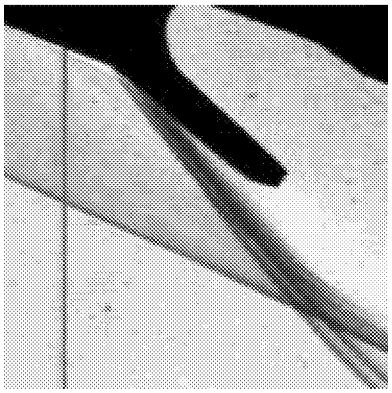

Run 182
α = 20-deg
Re_∞/ft = 2 x 10^6
δ_{BF} = 20-deg

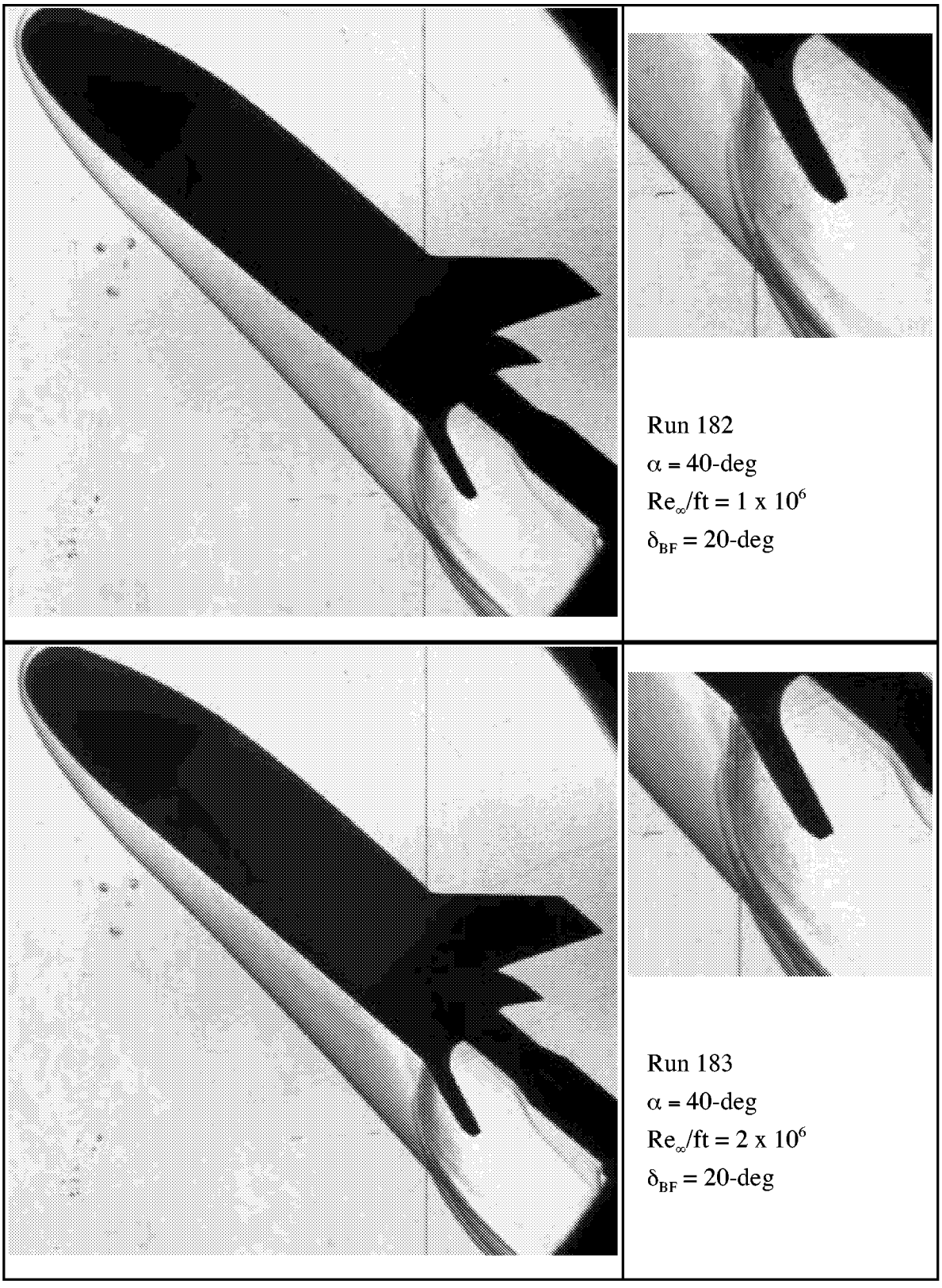

Run 182
α = 40-deg
Re_∞/ft = 1 x 10^6
δ_{BF} = 20-deg

Run 183
α = 40-deg
Re_∞/ft = 2 x 10^6
δ_{BF} = 20-deg

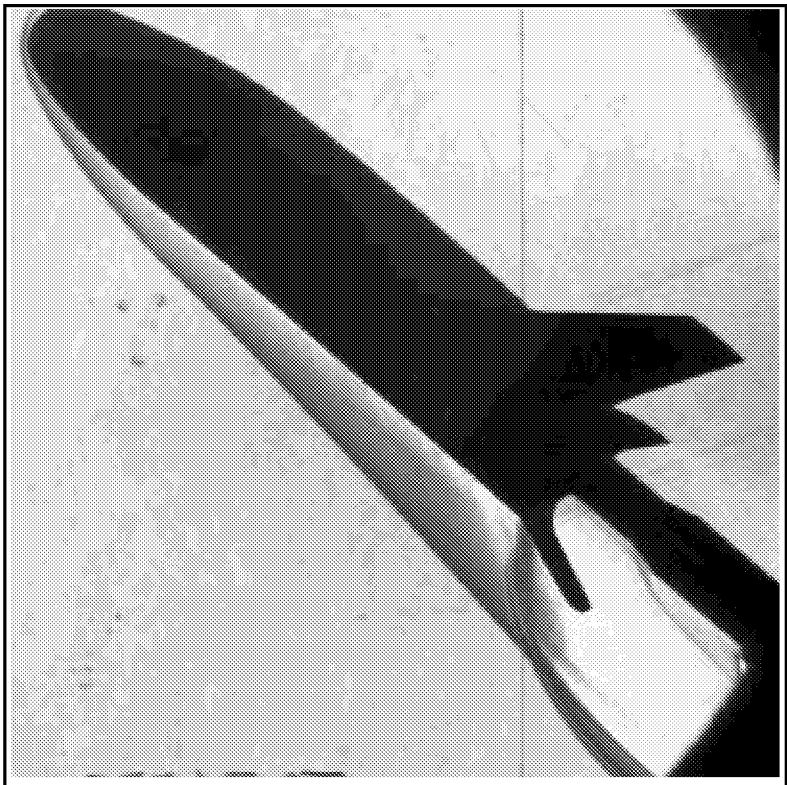

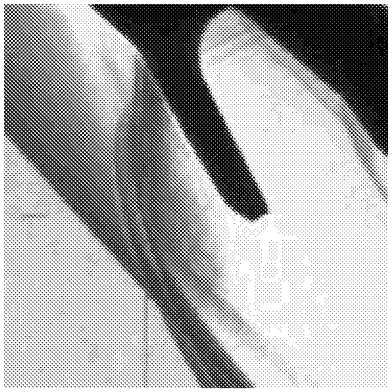

Run 183
α = 40-deg
Re_∞/ft = 3 x 10^6
δ_{BF} = 20-deg

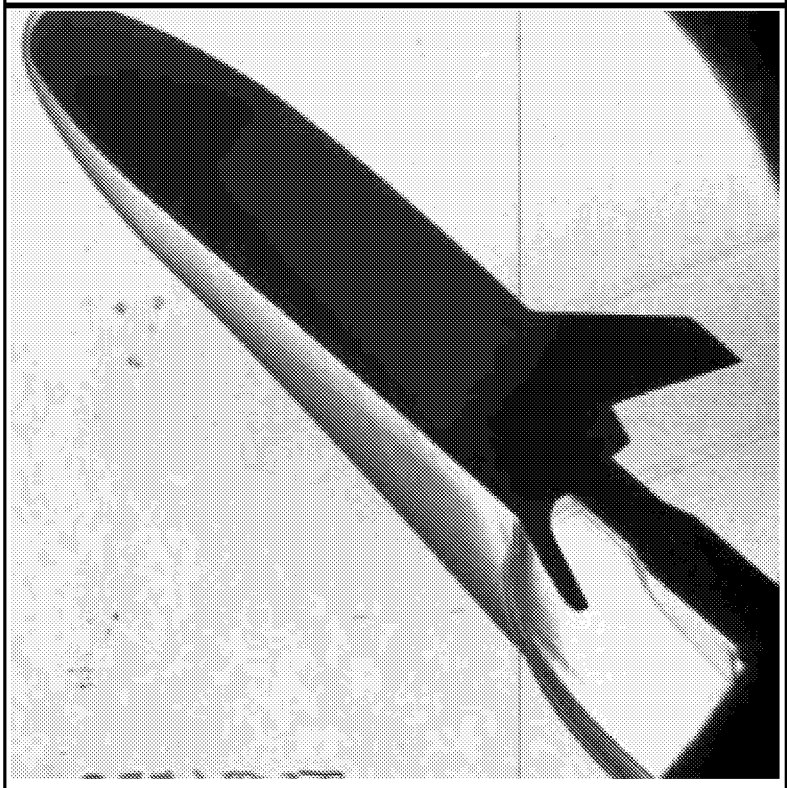

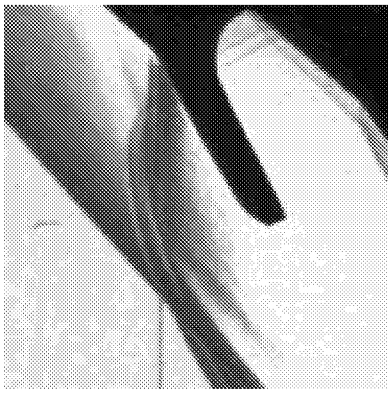

Run 183
α = 40-deg
Re_∞/ft = 4 x 10^6
δ_{BF} = 20-deg

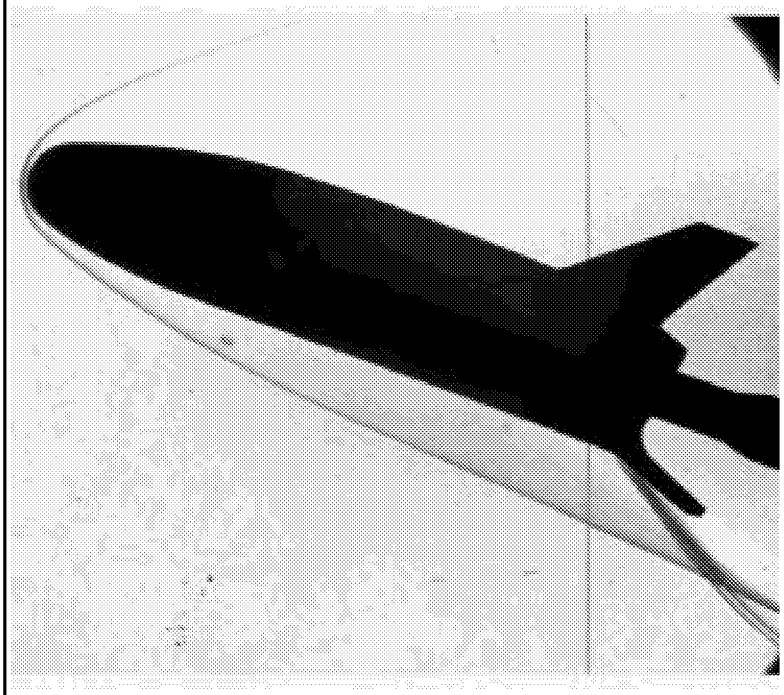

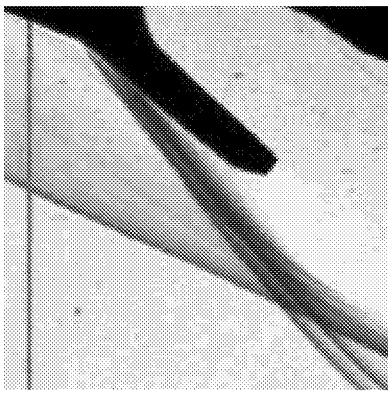

Run 184
α = 20-deg
Re_∞/ft = 3 x 10^6
δ_{BF} = 20-deg

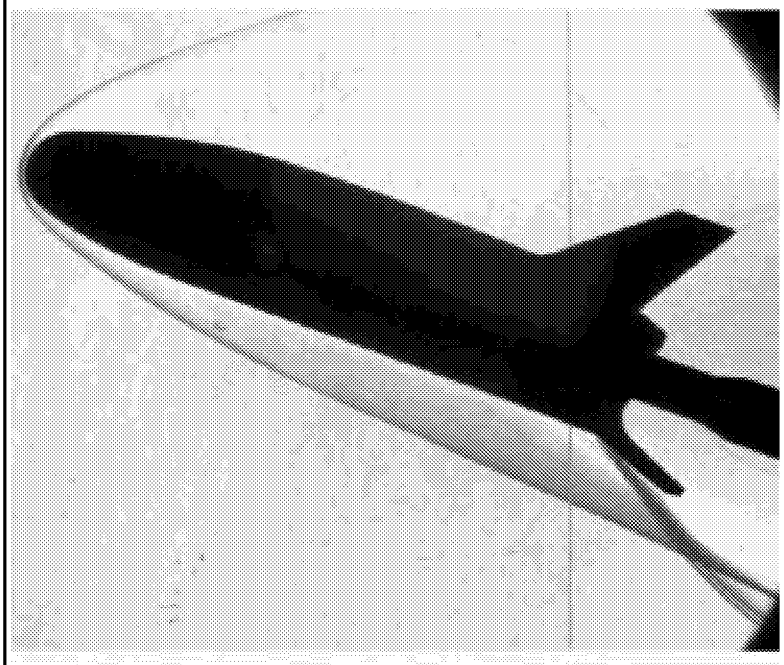

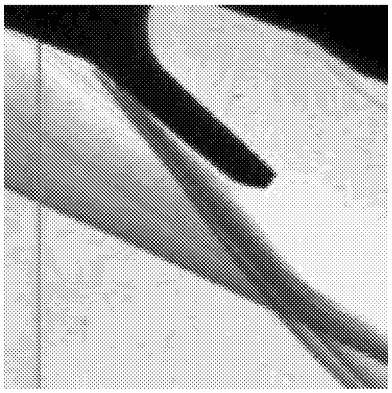

Run 184
α = 20-deg
Re_∞/ft = 4 x 10^6
δ_{BF} = 20-deg

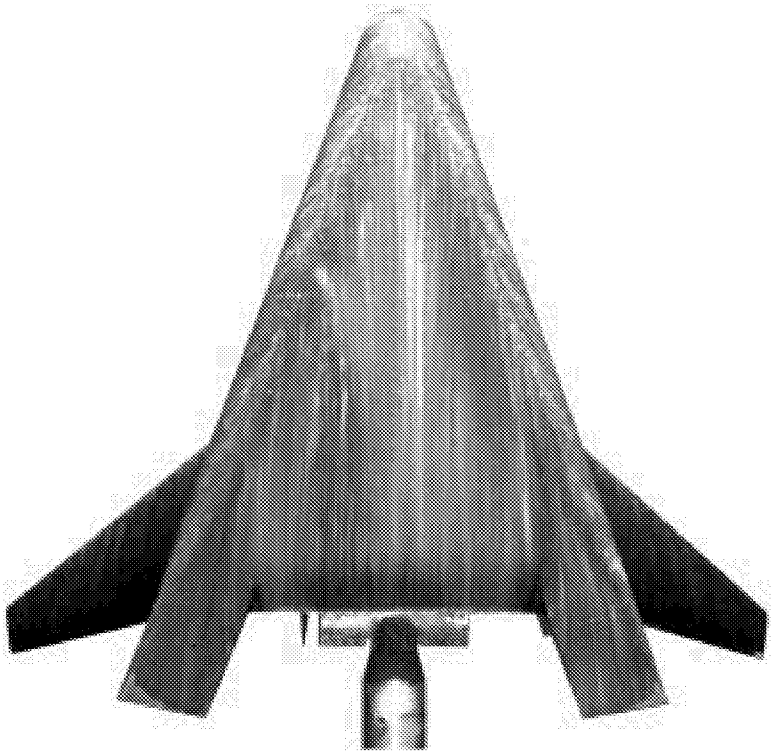

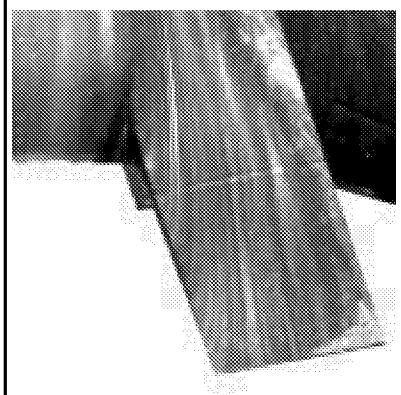

Run 1
α = 30-deg
Re_∞/ft = 4.24 x 10^6
δ_{BF} = 0-deg

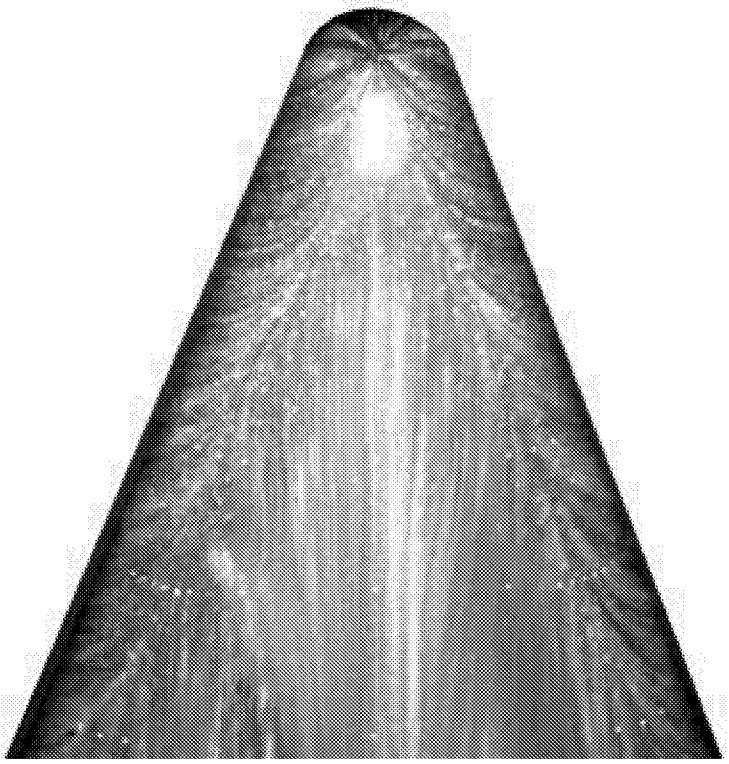

Run 1
α = 30-deg
Re_∞/ft = 4.24 x 10^6
δ_{BF} = 0-deg

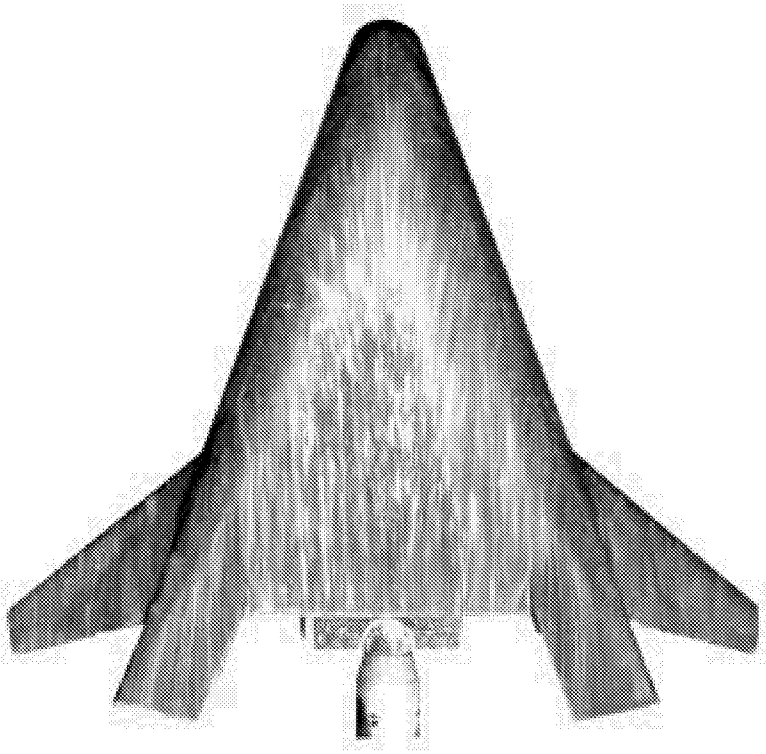

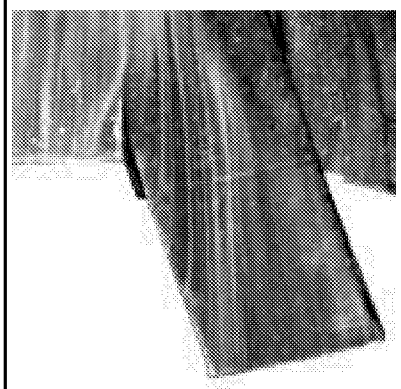

Run 2
α = 20-deg
Re_∞/ft = 4.37 x 10^6
δ_{BF} = 0-deg

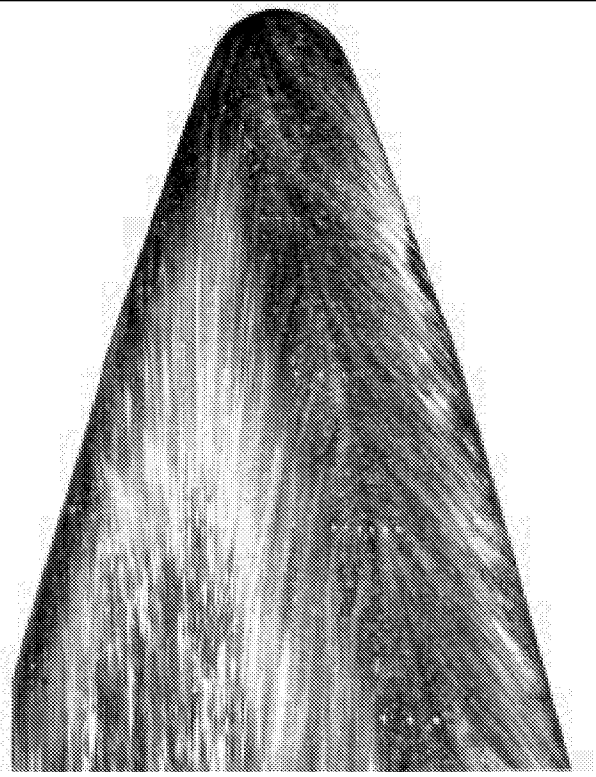

Run 2
α = 20-deg
Re_∞/ft = 4.37 x 10^6
δ_{BF} = 0-deg

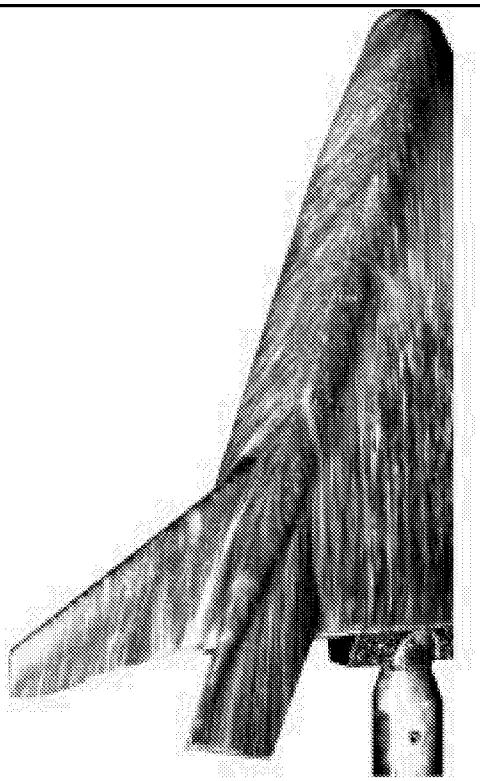

Run 2
α = 20-deg
Re_∞/ft = 4.37 x 10^6
δ_{BF} = 0-deg

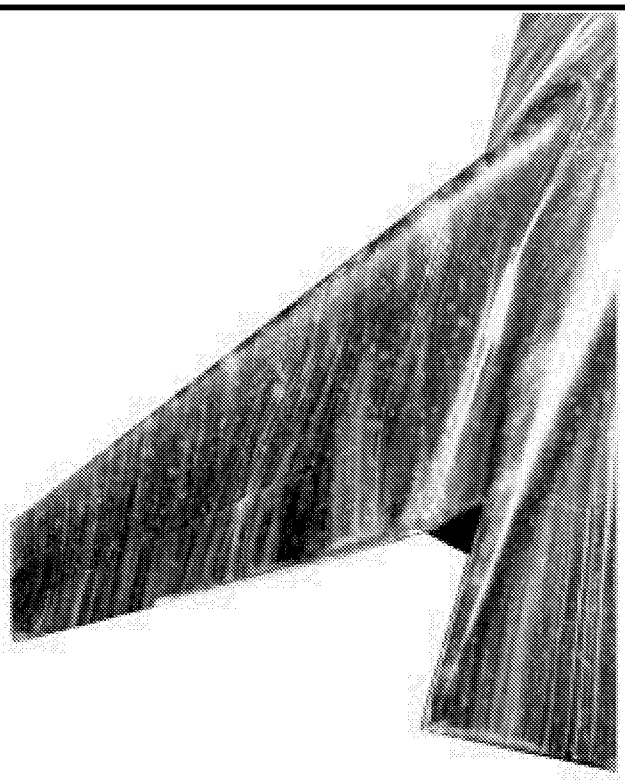

Run 2
α = 20-deg
Re_∞/ft = 4.37 x 10^6
δ_{BF} = 0-deg

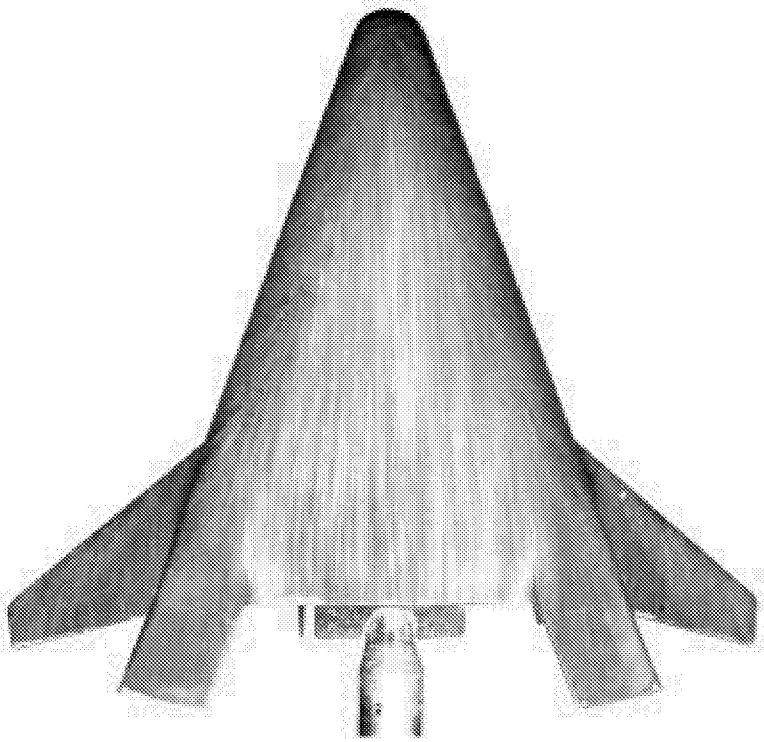

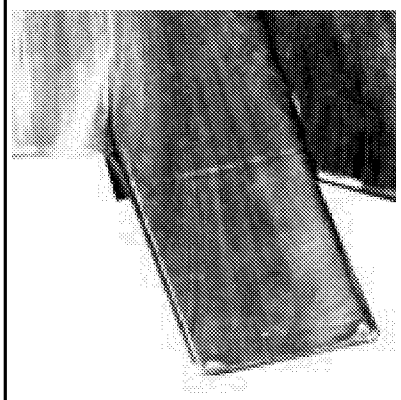

Run 3
α = 40-deg
Re_∞/ft = 4.37 x 10^6
δ_{BF} = 0-deg

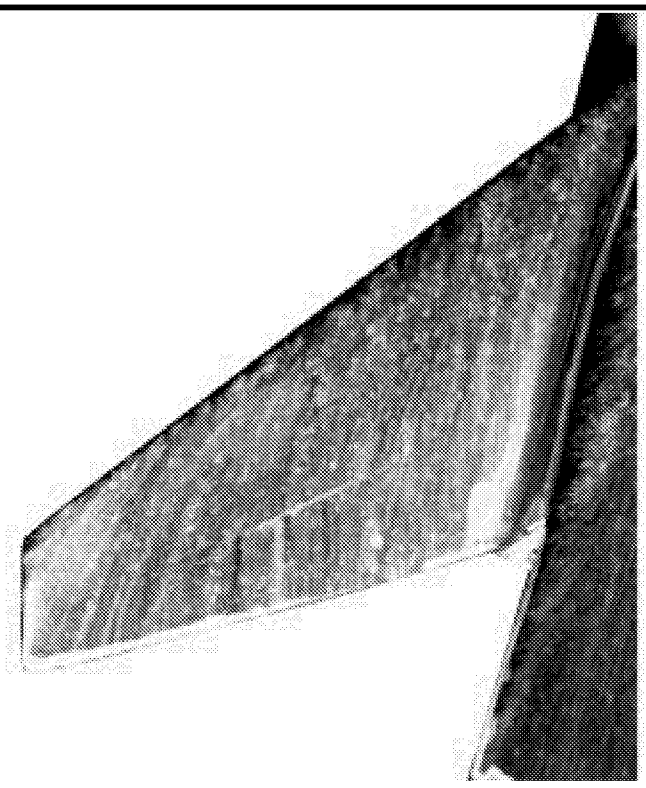

Run 3
α = 40-deg
Re_∞/ft = 4.37 x 10^6
δ_{BF} = 0-deg

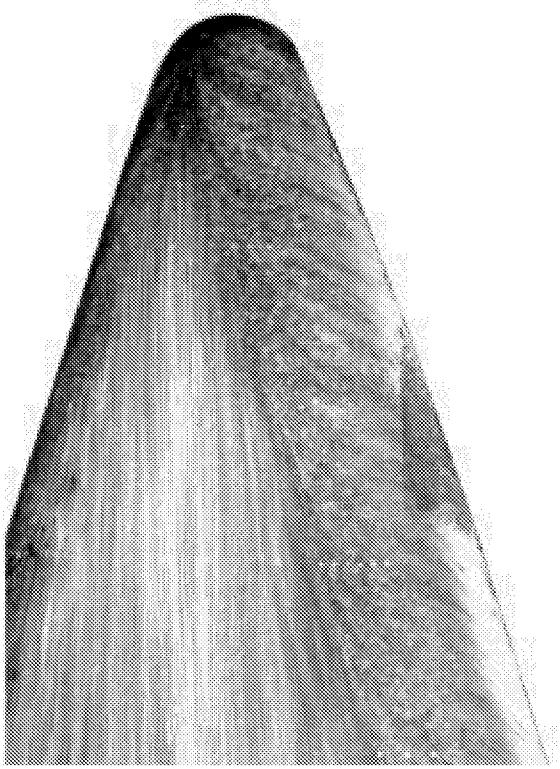

Run 3
α = 40-deg
Re_∞/ft = 4 x 10^6
δ_{BF} = 0-deg

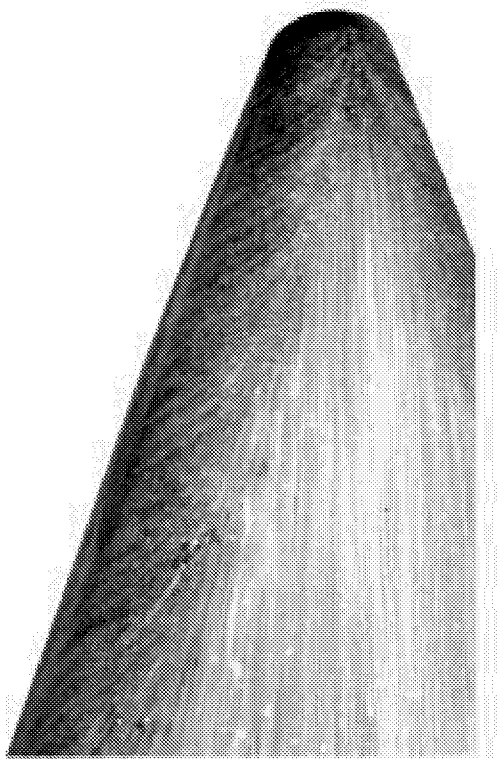

Run 3
α = 40-deg
Re_∞/ft = 4 x 10^6
δ_{BF} = 0-deg

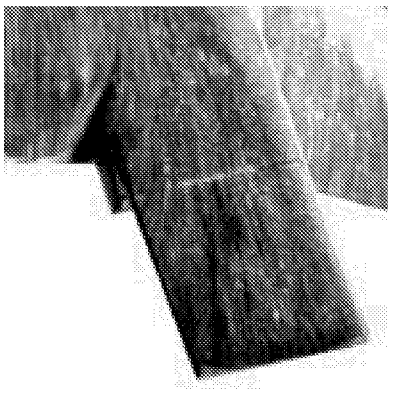

Run 4
α = 40-deg
Re_∞/ft = 4.31 x 10^6
δ_{BF} = 0-deg

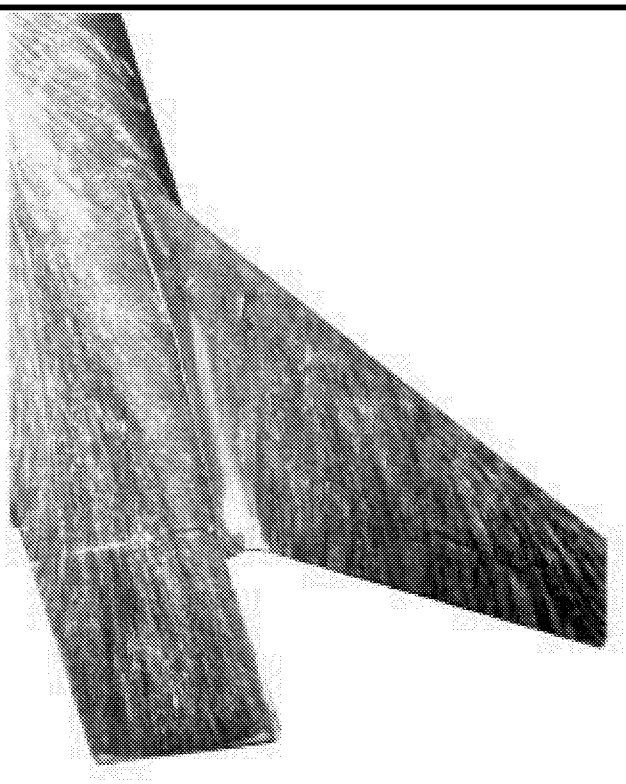

Run 4
α = 40-deg
Re_∞/ft = 4.31 x 10^6
δ_{BF} = 0-deg

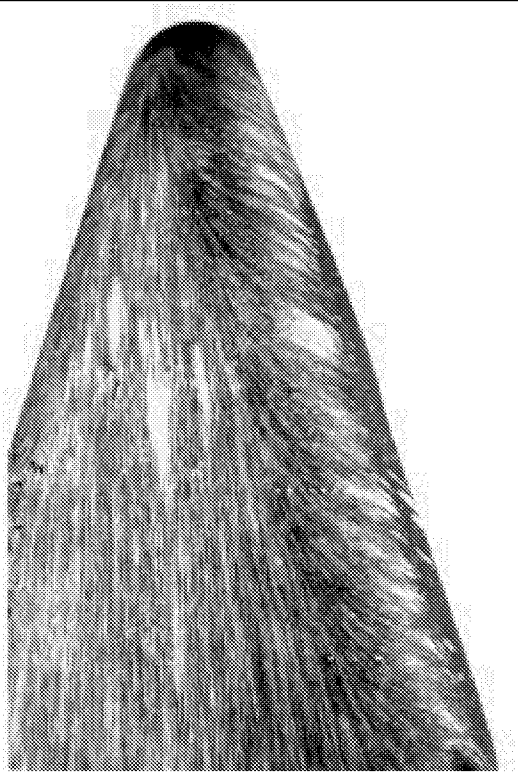

Run 4
α = 40-deg
Re_∞/ft = 4.31 x 10^6
δ_{BF} = 0-deg

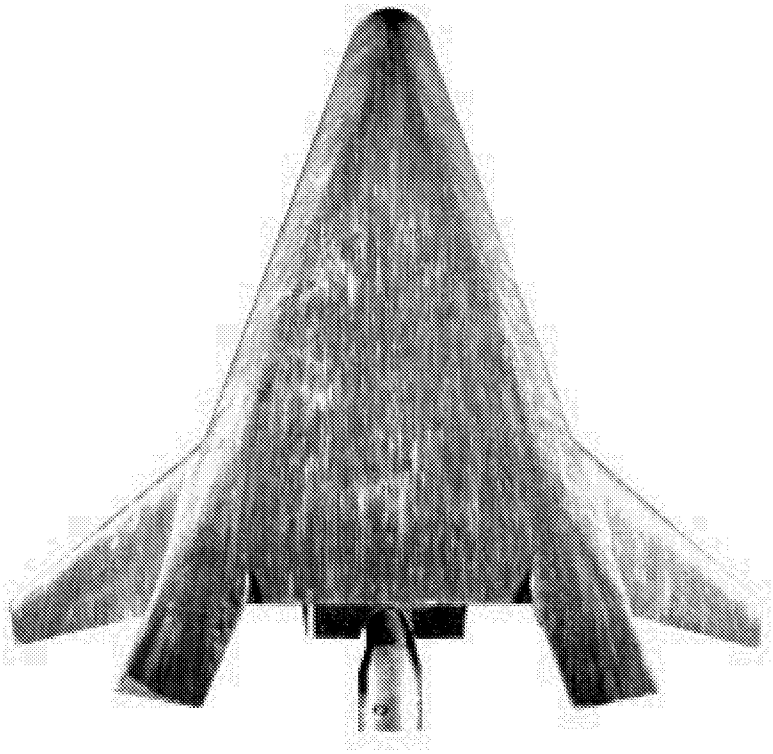

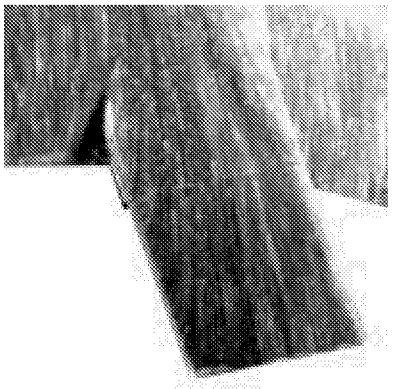

Run 5
α = 30-deg
Re_∞/ft = 4.32 x 10^6
δ_{BF} = 0-deg

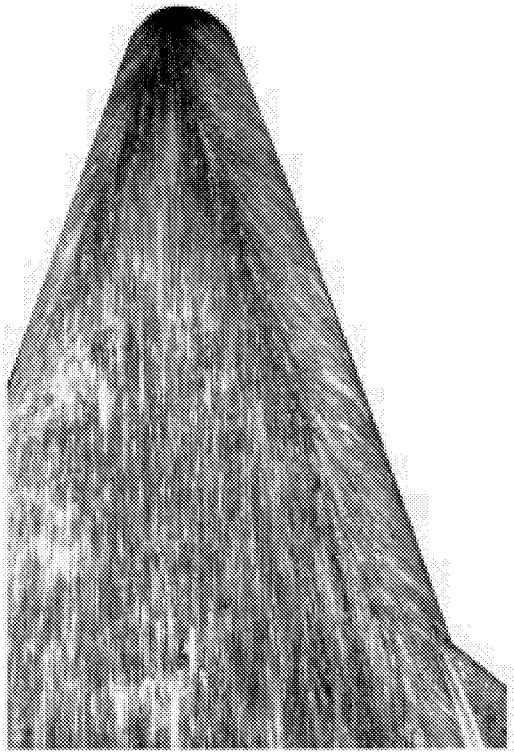

Run 5
α = 30-deg
Re_∞/ft = 4.32 x 10^6
δ_{BF} = 0-deg

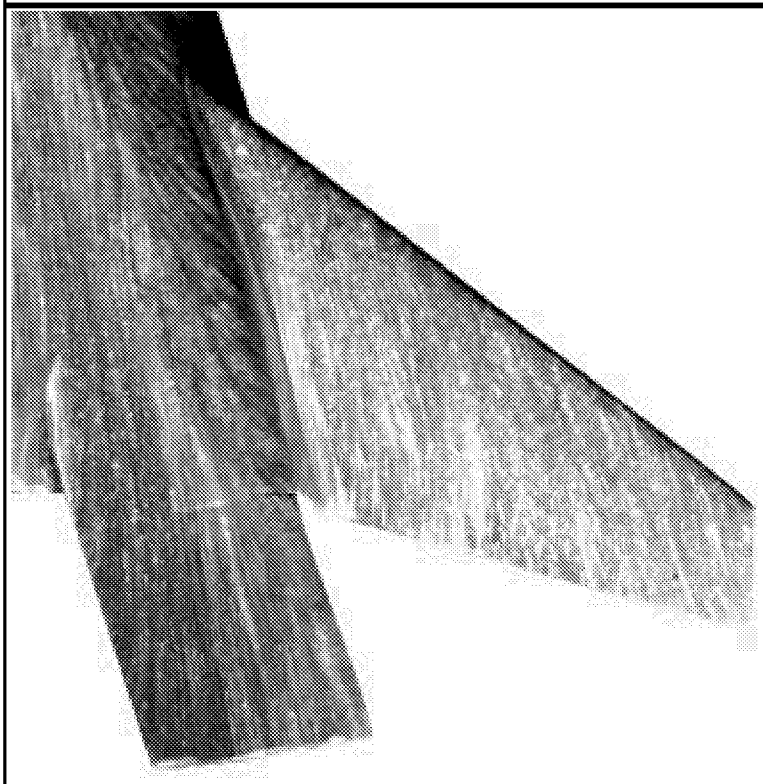

Run 5
α = 30-deg
Re_∞/ft = 4.32 x 10^6
δ_{BF} = 0-deg

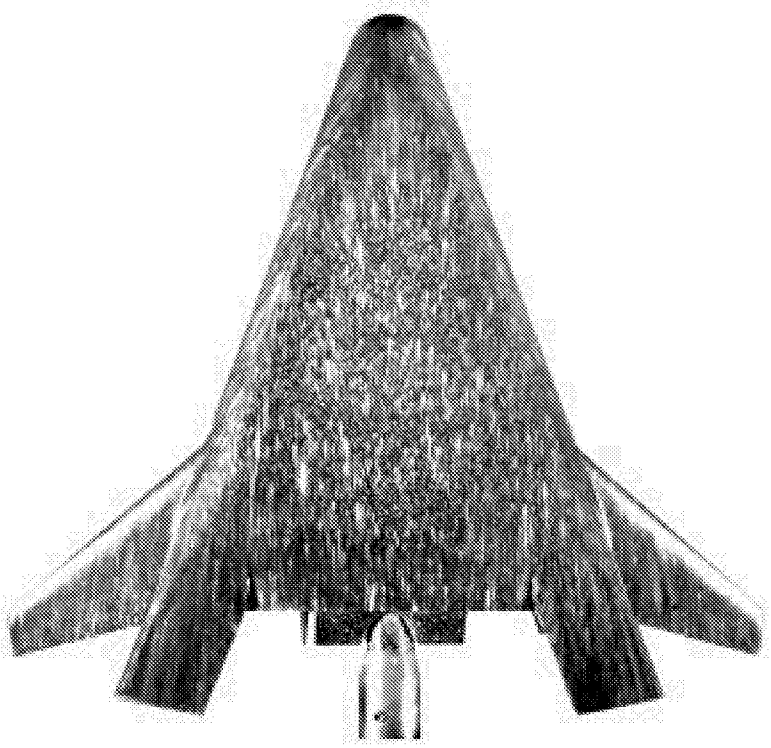

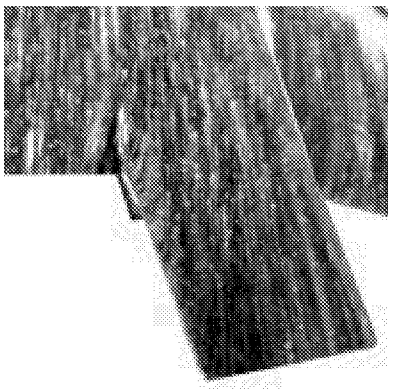

Run 6
α = 20-deg
Re_∞/ft = 4.34 x 10^6
δ_{BF} = 0-deg

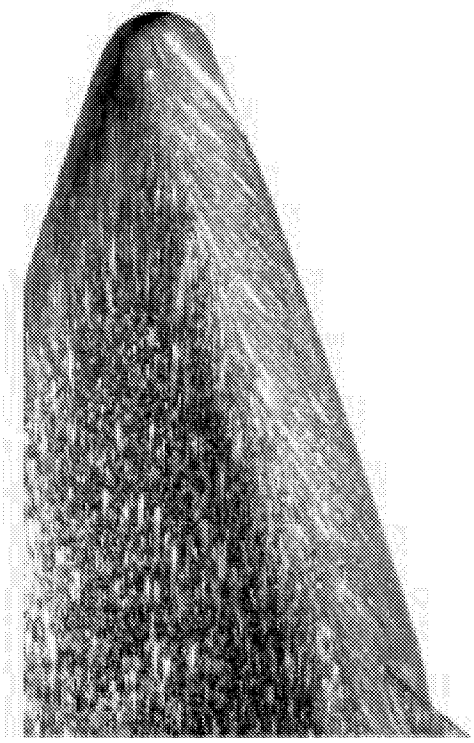

Run 6
α = 20-deg
Re_∞/ft = 4.34 x 10^6
δ_{BF} = 0-deg

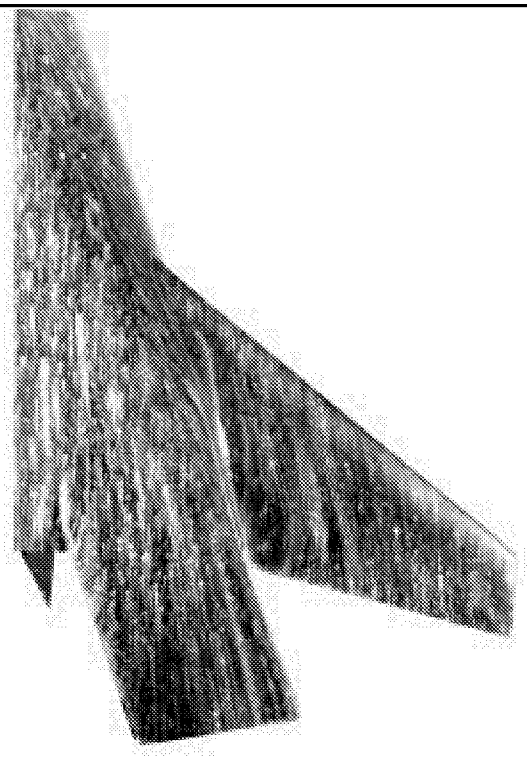

Run 6
α = 20-deg
Re_∞/ft = 4.34 x 10^6
δ_{BF} = 0-deg

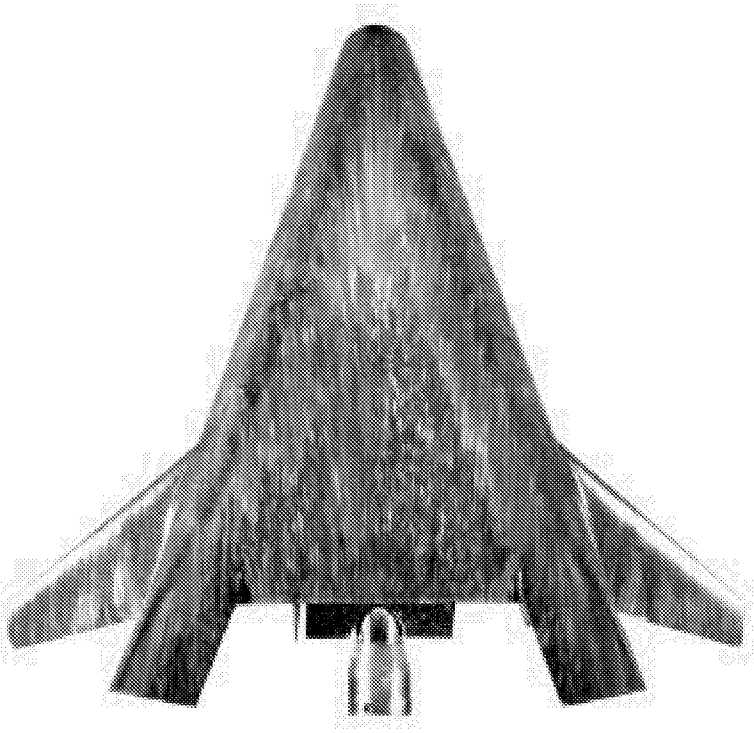

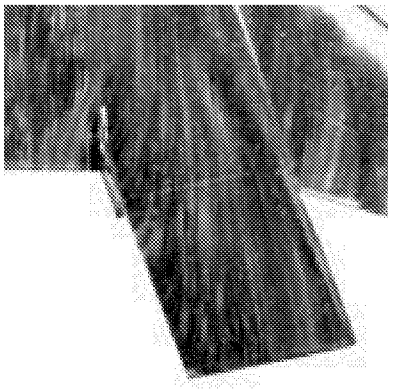

Run 7
α = 20-deg
Re_∞/ft = 2.18 x 10^6
δ_{BF} = 0-deg

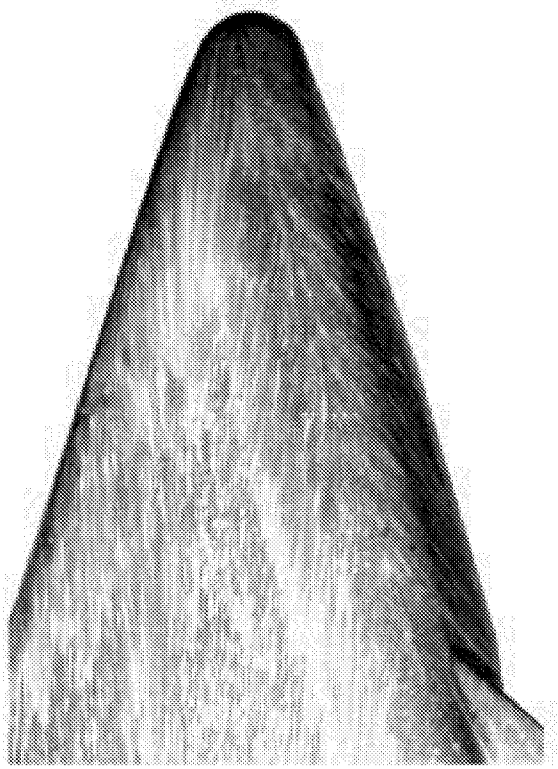

Run 7
α = 20-deg
Re_∞/ft = 2.18 x 10^6
δ_{BF} = 0-deg

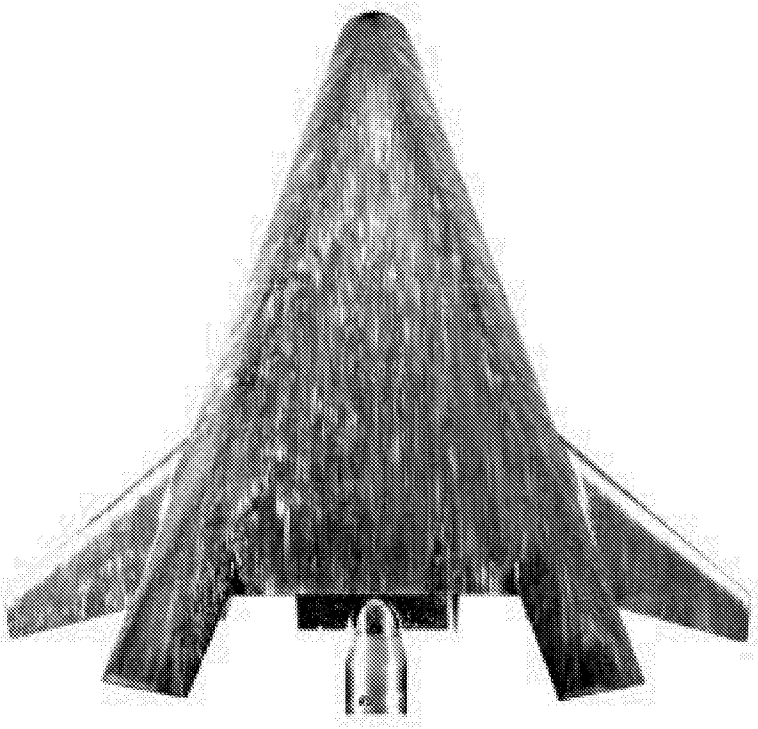

Run 8
α = 30-deg
Re_∞/ft = 2.21 x 10^6
δ_{BF} = 0-deg

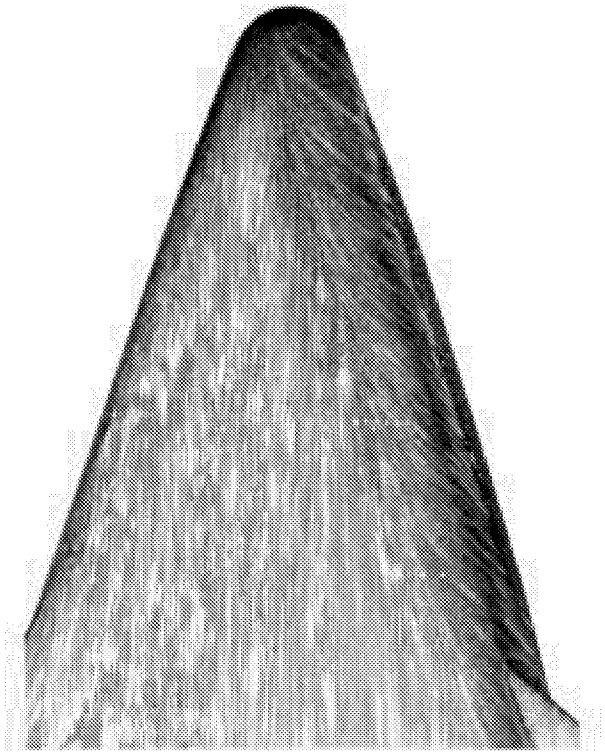

Run 8
α = 30-deg
Re_∞/ft = 2.21 x 10^6
δ_{BF} = 0-deg

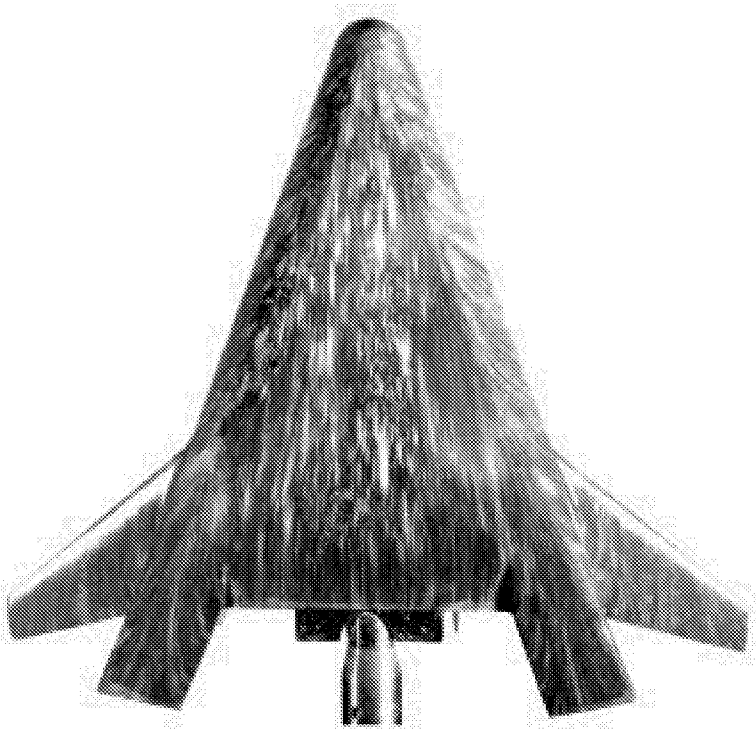

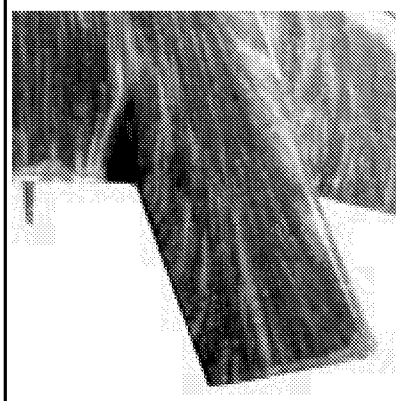

Run 9
α = 40-deg
Re_∞/ft = 2.19 x 10^6
δ_{BF} = 0-deg

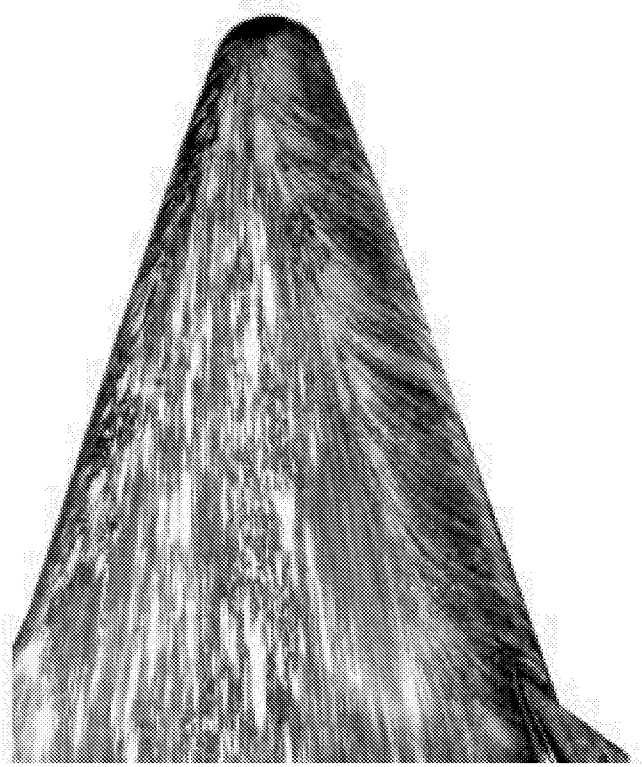

Run 9
α = 40-deg
Re_∞/ft = 2.19 x 10^6
δ_{BF} = 0-deg

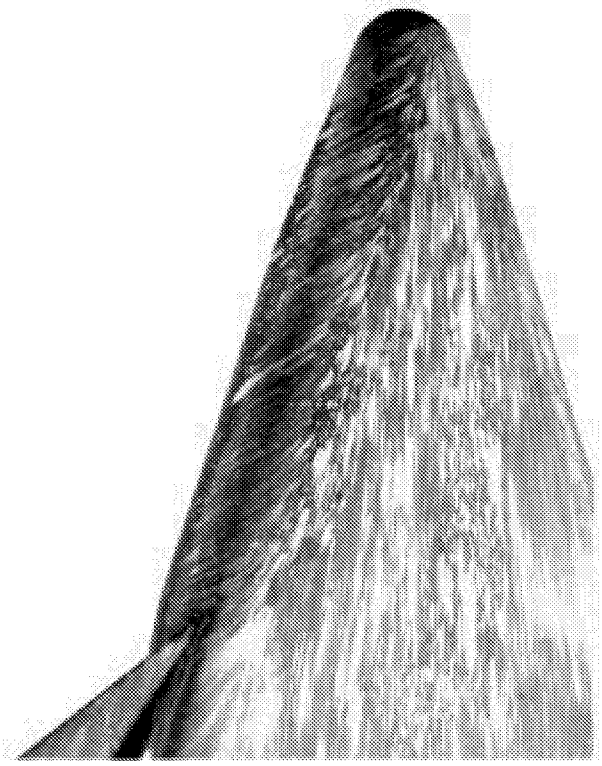

Run 9
α = 40-deg
Re_∞/ft = 2.19 x 10^6
δ_{BF} = 0-deg

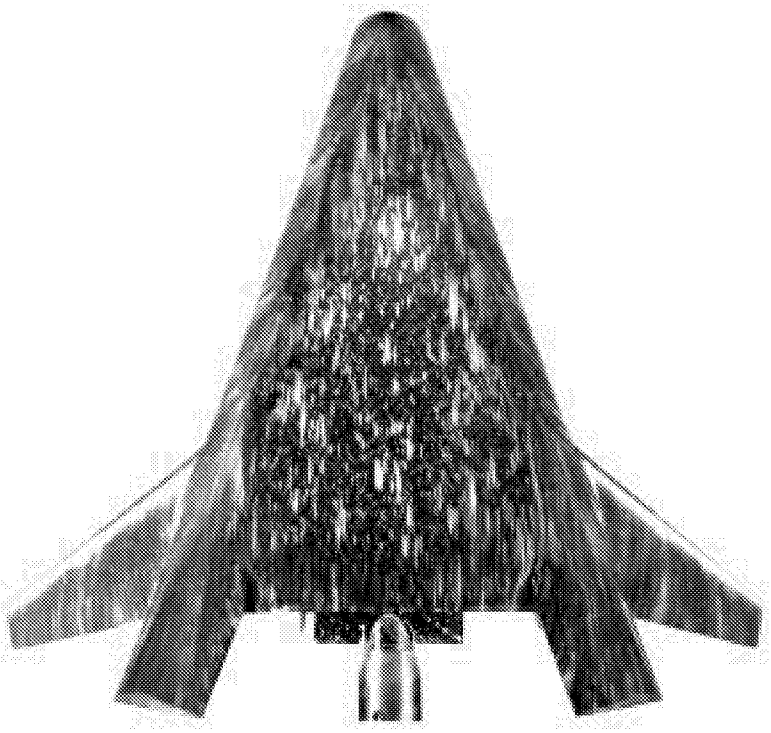

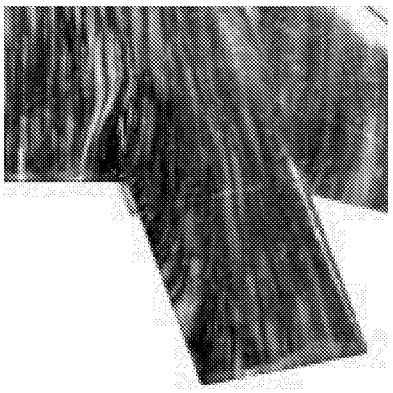

Run 10
α = 30-deg
Re_∞/ft = 2.21 x 10^6
δ_{BF} = 0-deg

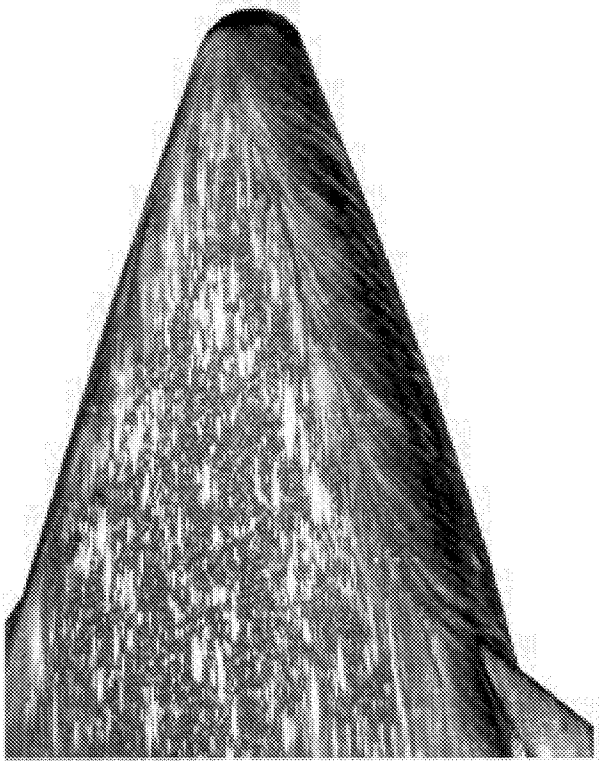

Run 10
α = 30-deg
Re_∞/ft = 2.21 x 10^6
δ_{BF} = 0-deg

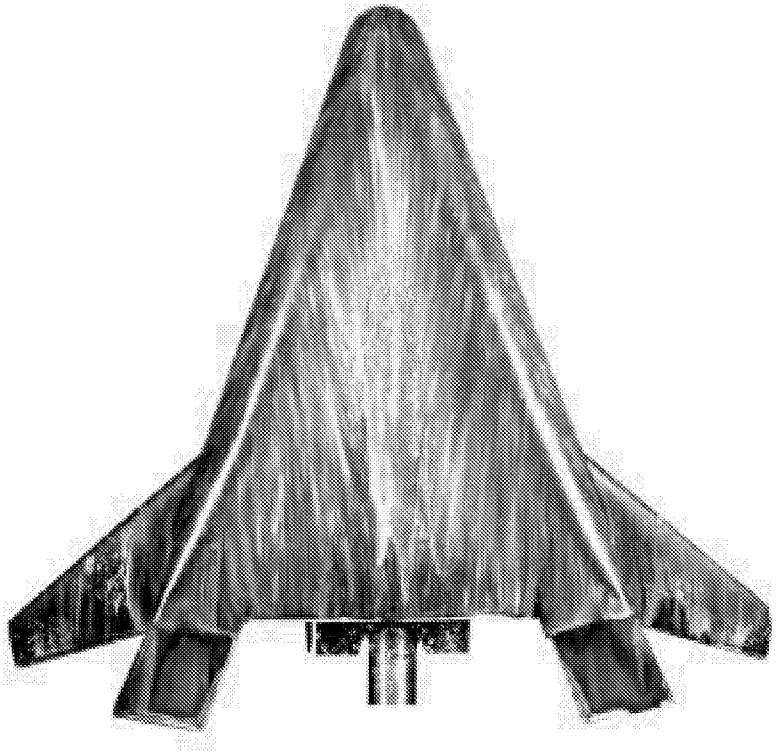

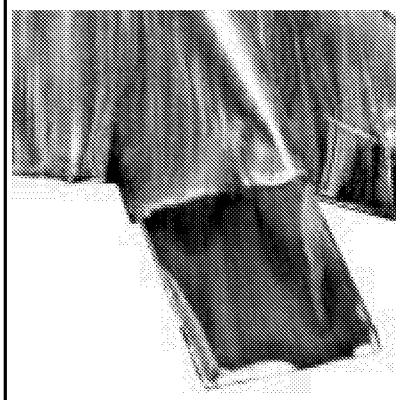

Run 165
α = 20-deg
Re_∞/ft = 4.29 x 10^6
δ_{BF} = 20-deg

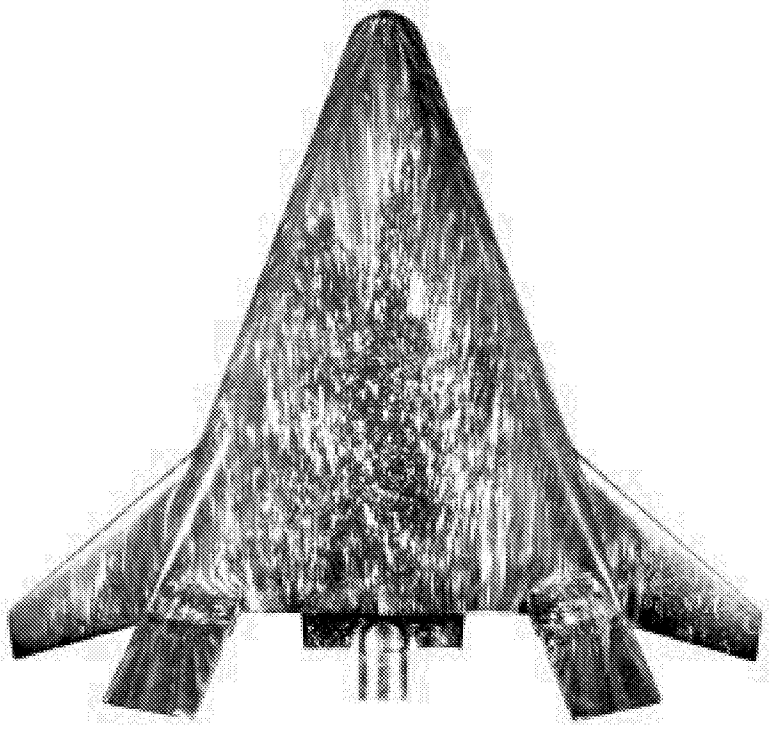

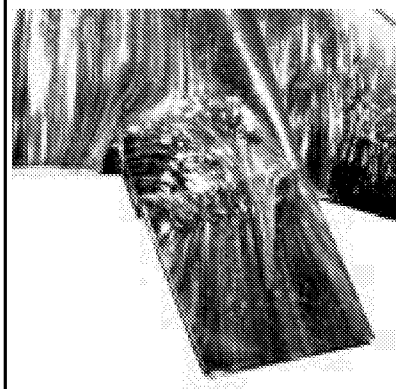

Run 166
α = 20-deg
Re_∞/ft = 1.02 x 10^6
δ_{BF} = 20-deg

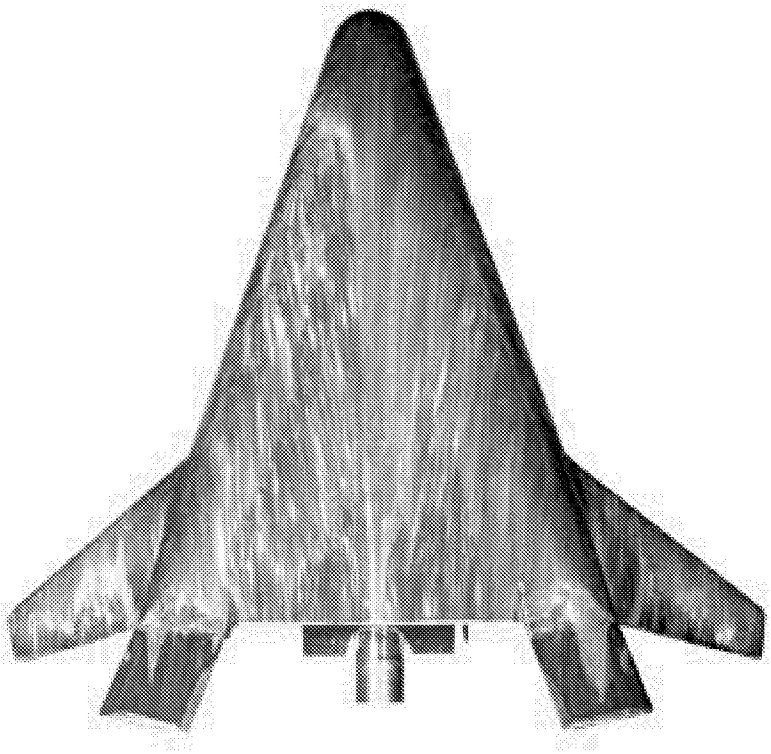

Run 167
α = 20-deg
Re_∞/ft = 2.14 x 10^6
δ_{BF} = 20-deg

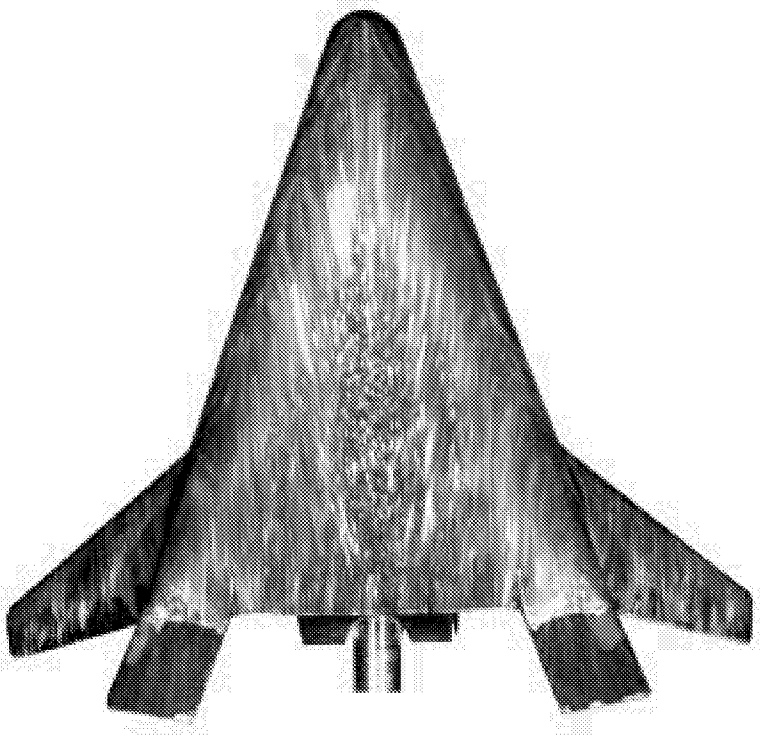

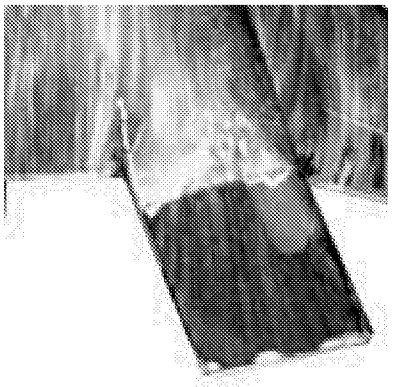

Run 168
α = 20-deg
Re_∞/ft = 3.12 x 10^6
δ_{BF} = 20-deg

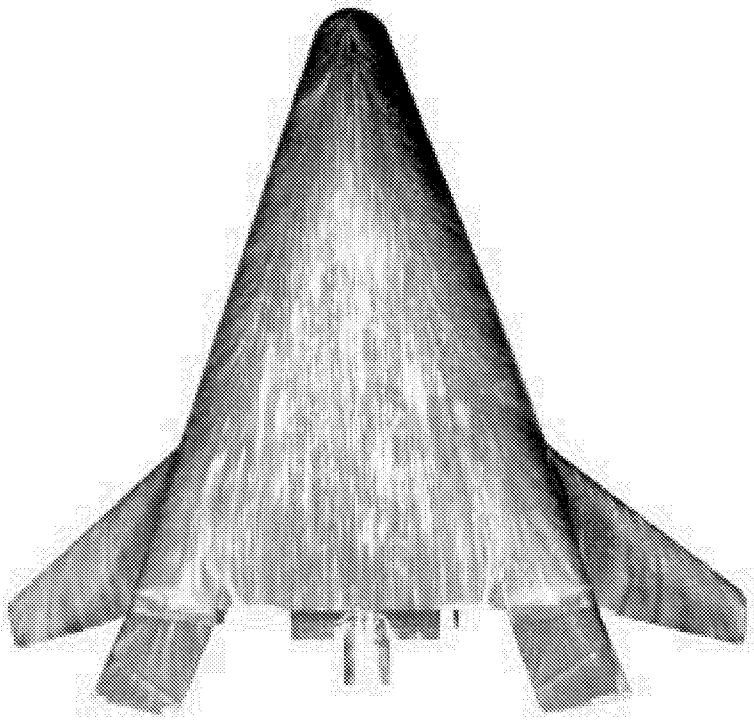

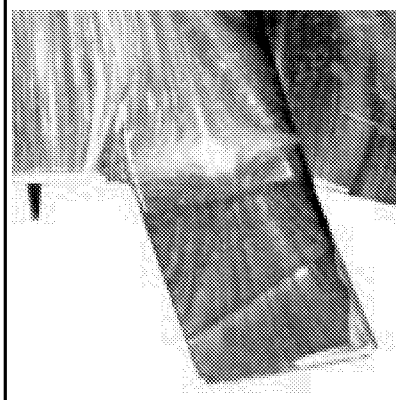

Run 169
α = 40-deg
Re_∞/ft = 2.2 x 10^6
δ_{BF} = 20-deg

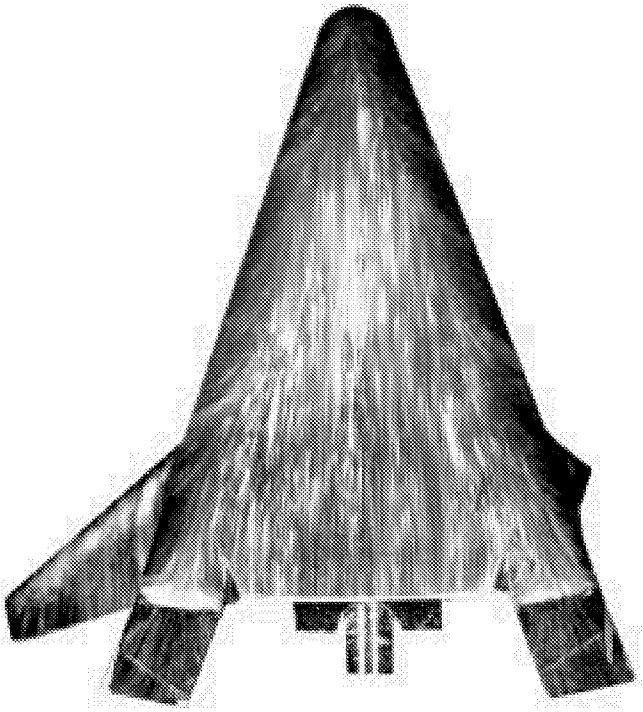

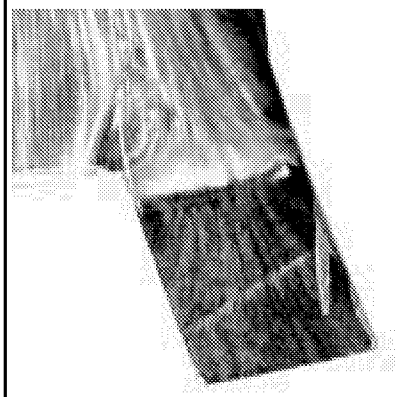

Run 170
α = 40-deg
Re_∞/ft = 4.33 x 10^6
δ_{BF} = 20-deg

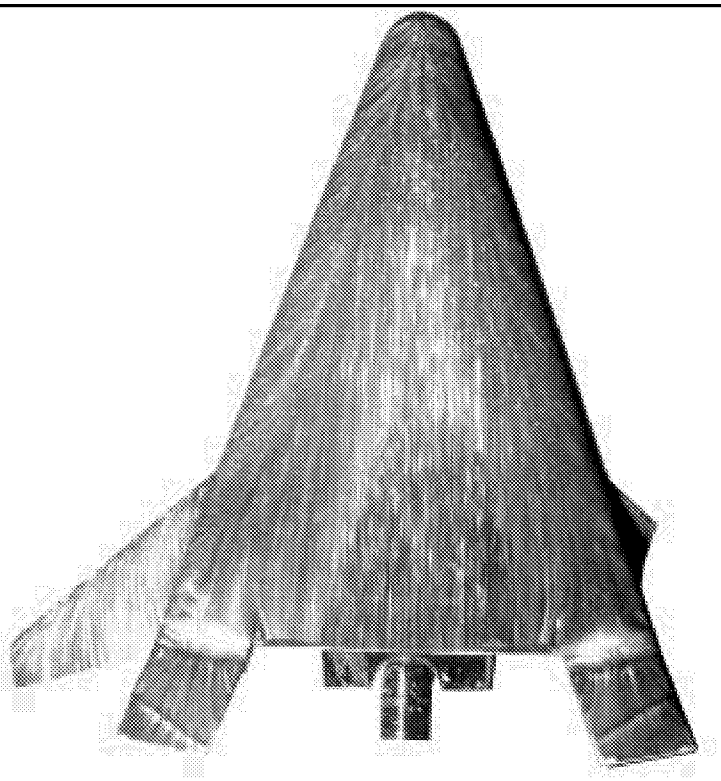

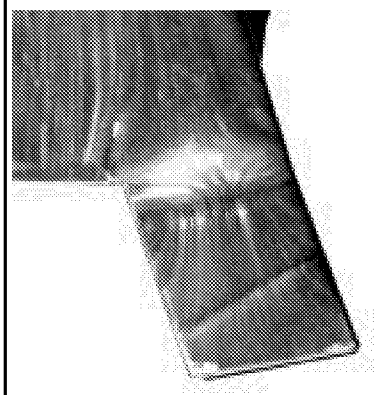

Run 171
α = 40-deg
Re_∞/ft = 1.14 x 10^6
δ_{BF} = 20-deg

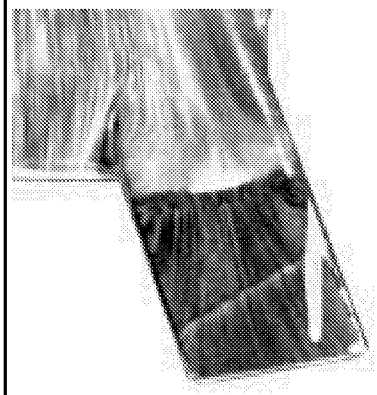

Run 172
α = 40-deg
Re_∞/ft = 3 x 10^6
δ_{BF} = 20-deg

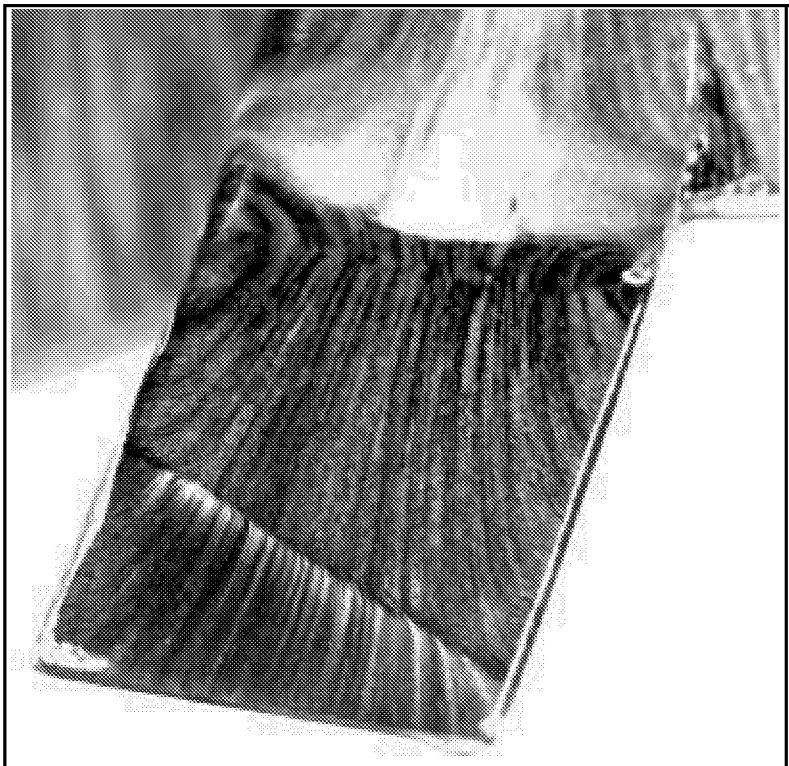

Run 172
α = 40-deg
Re_∞/ft = 3 x 10^6
δ_{BF} = 20-deg

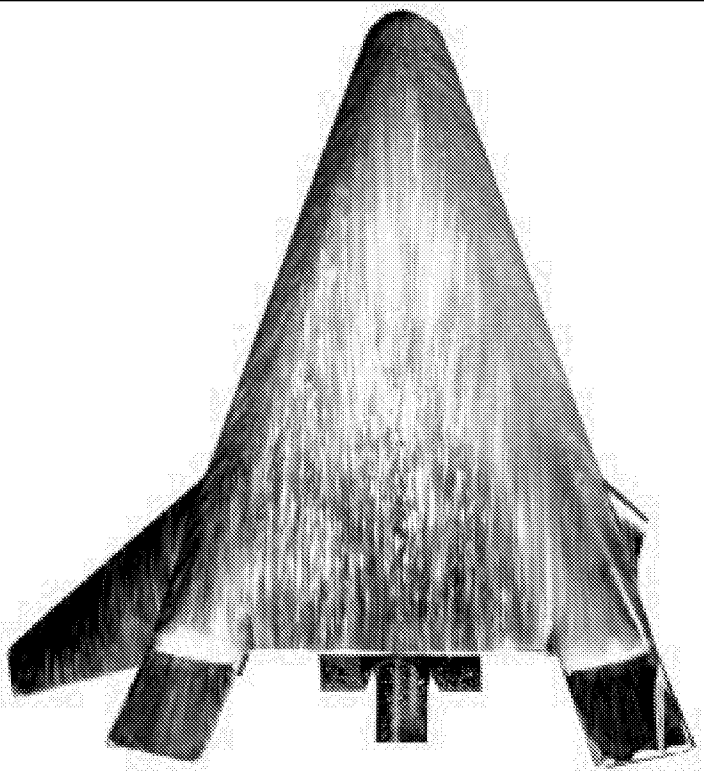

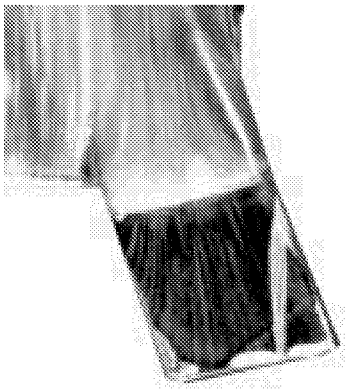

Run 173
α = 30-deg
Re_∞/ft = 2.21 x 10^6
δ_{BF} = 20-deg

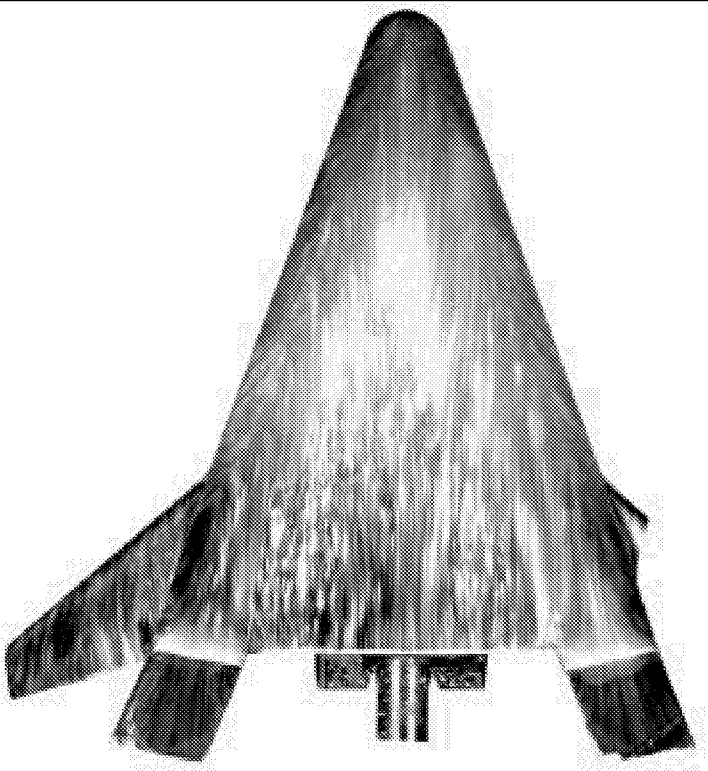

Run 174
α = 30-deg
Re_∞/ft = 3.12 x 10^6
δ_{BF} = 20-deg

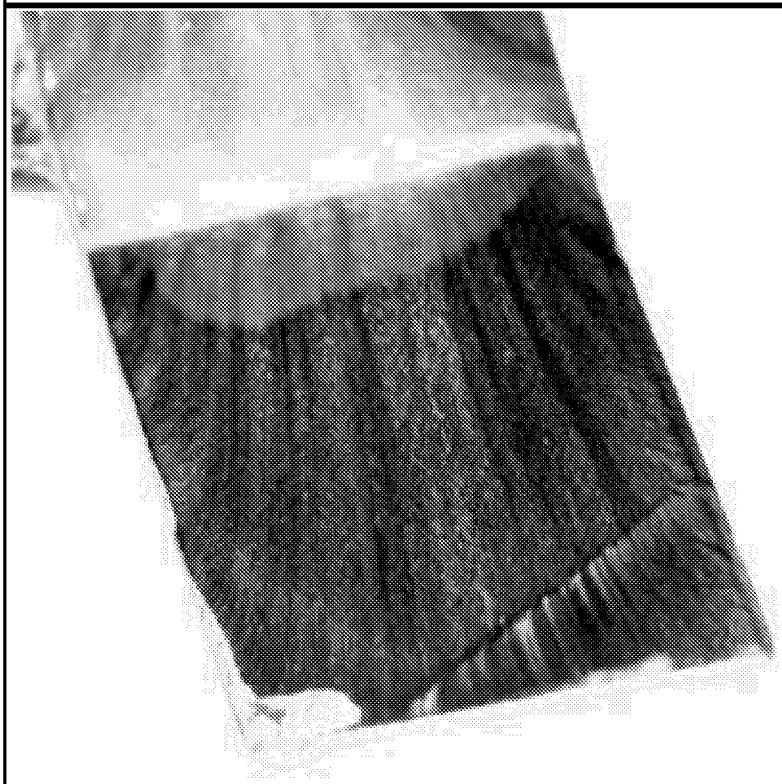

Run 174
α = 30-deg
Re_∞/ft = 3.12 x 10^6
δ_{BF} = 20-deg

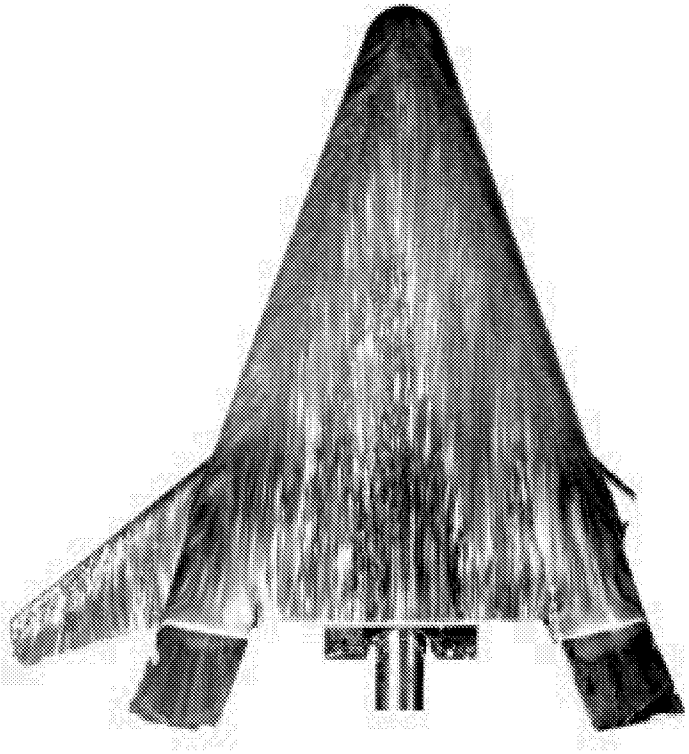

Run 175
α = 30-deg
Re_∞/ft = 4.35 x 10^6
δ_{BF} = 20-deg

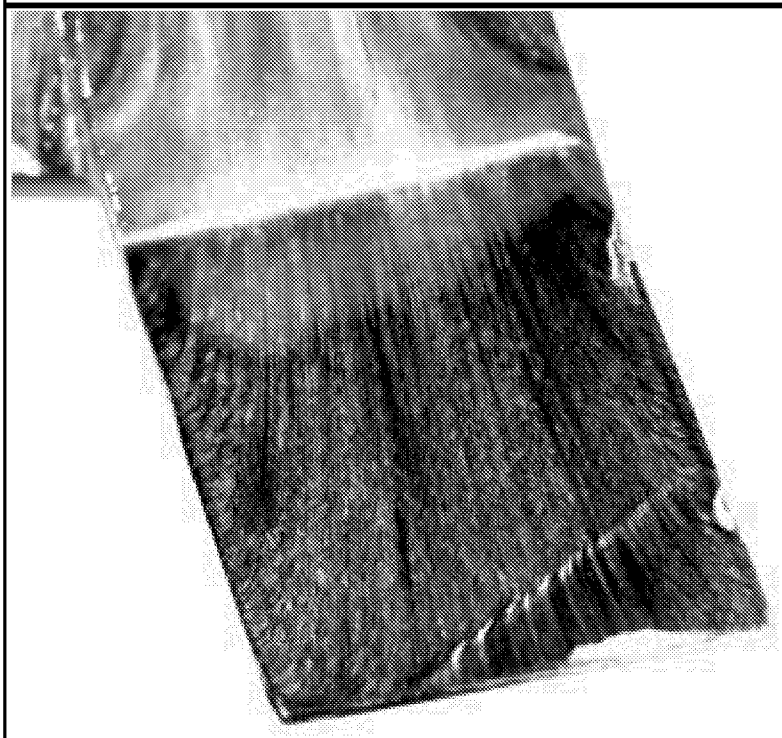

Run 175
α = 30-deg
Re_∞/ft = 4.35 x 10^6
δ_{BF} = 20-deg

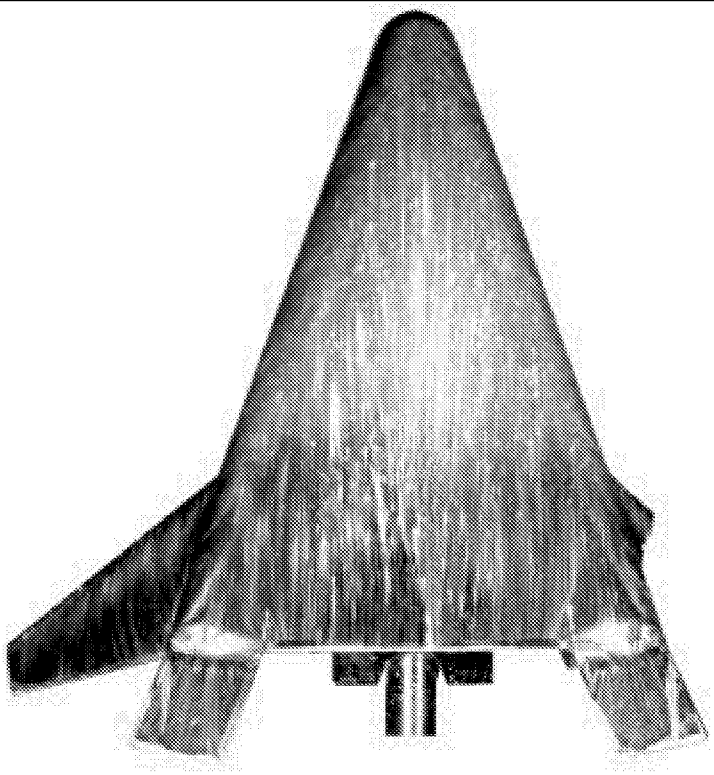

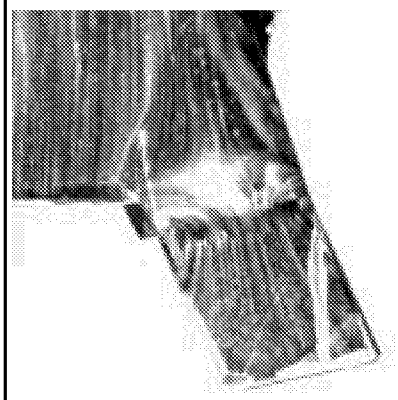

Run 176
α = 30-deg
Re_∞/ft = 1.13 x 10^6
δ_{BF} = 20-deg

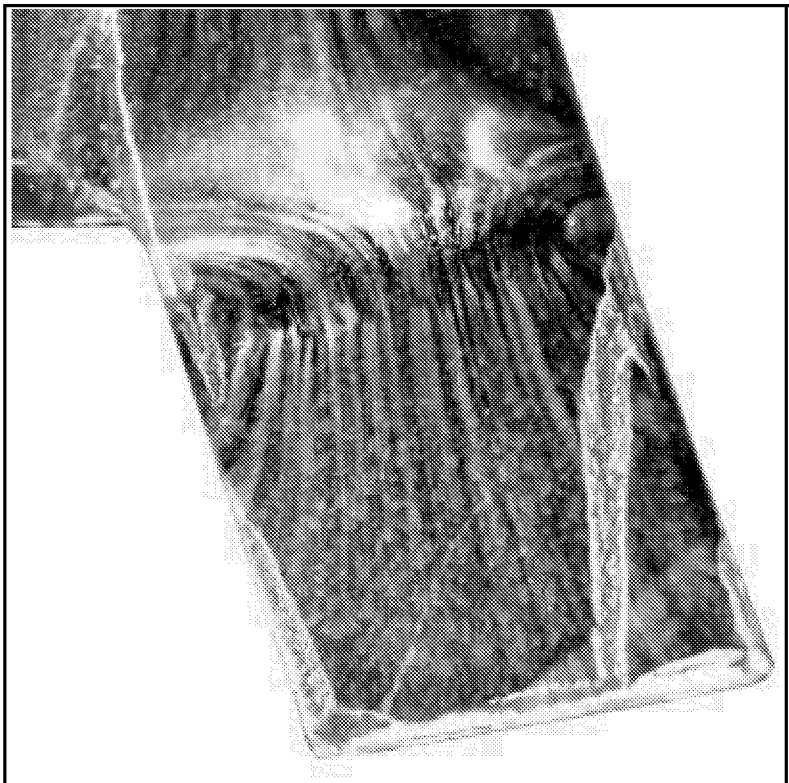

Run 176
α = 30-deg
Re_∞/ft = 1.13 x 10^6
δ_{BF} = 20-deg

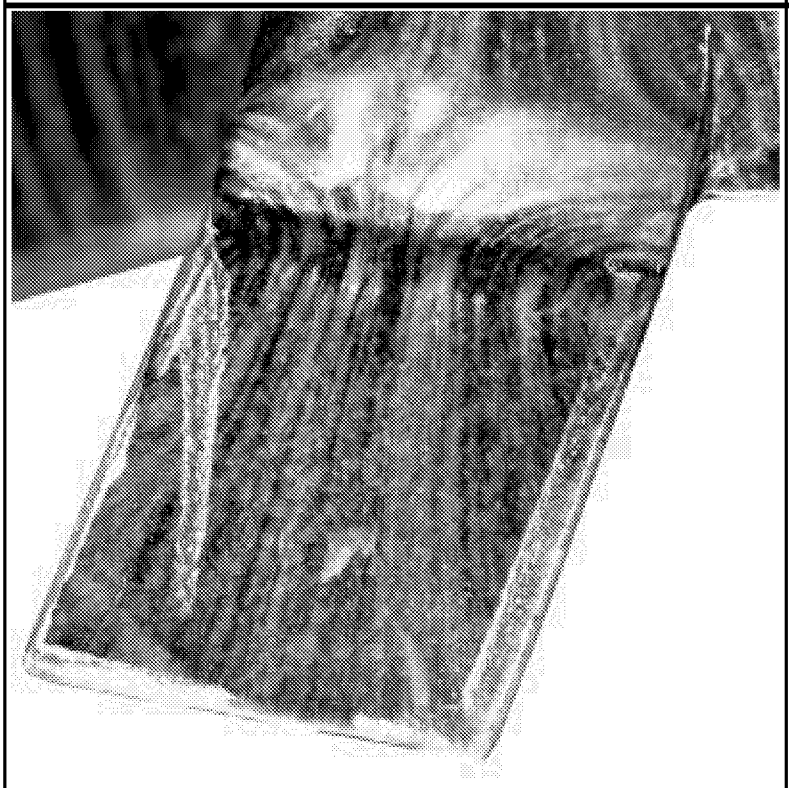

Run 176
α = 30-deg
Re_∞/ft = 1.13 x 10^6
δ_{BF} = 20-deg

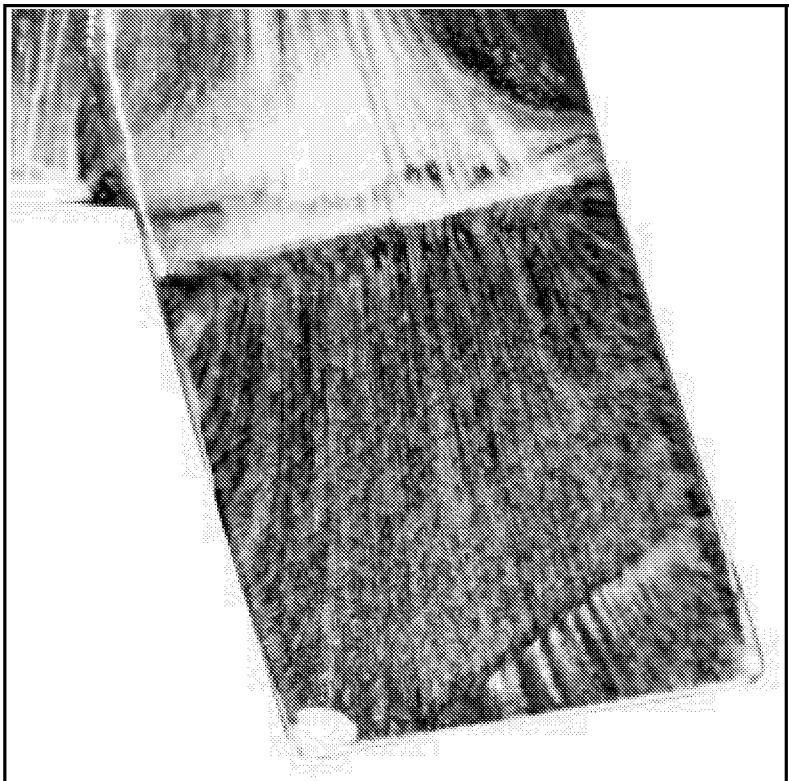

Run 177
α = 30-deg
Re_∞/ft = 2 x 10^6
δ_{BF} = 20-deg

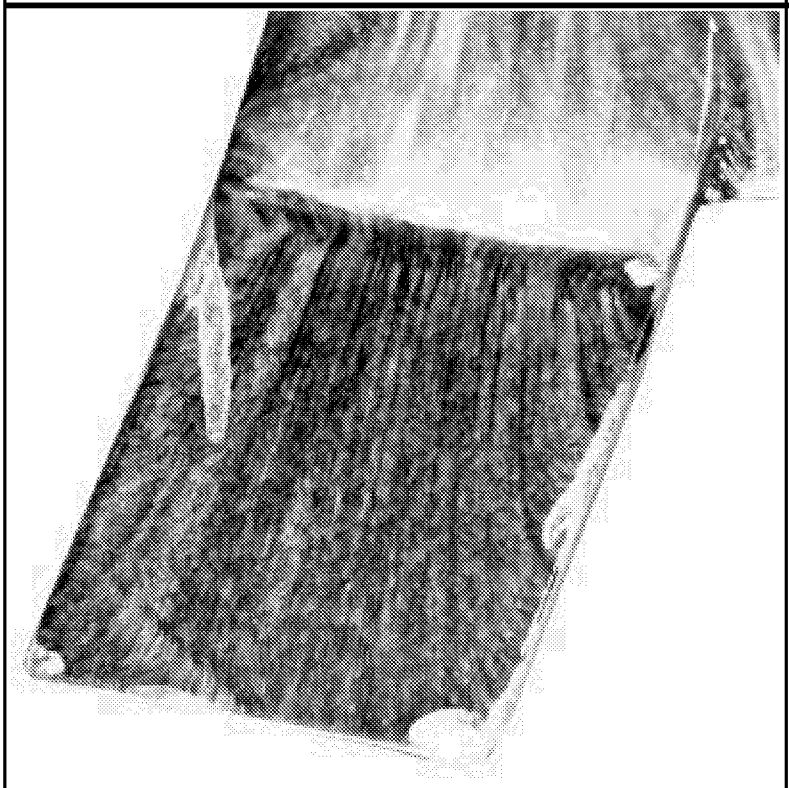

Run 177
α = 30-deg
Re_∞/ft = 2 x 10^6
δ_{BF} = 20-deg

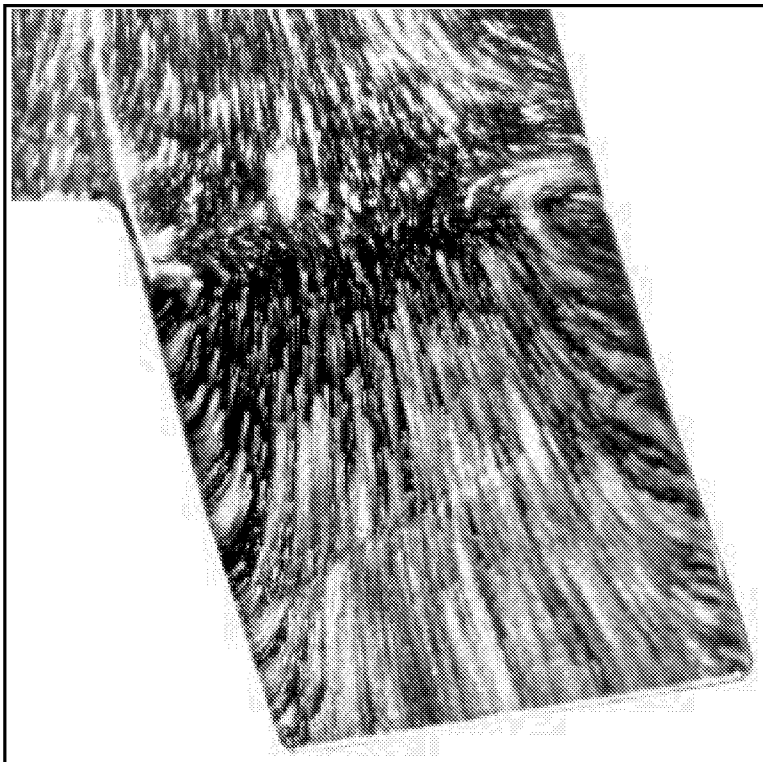

Run 178
α = 40-deg
Re_∞/ft = 2 x 10^6
δ_{BF} = 20-deg

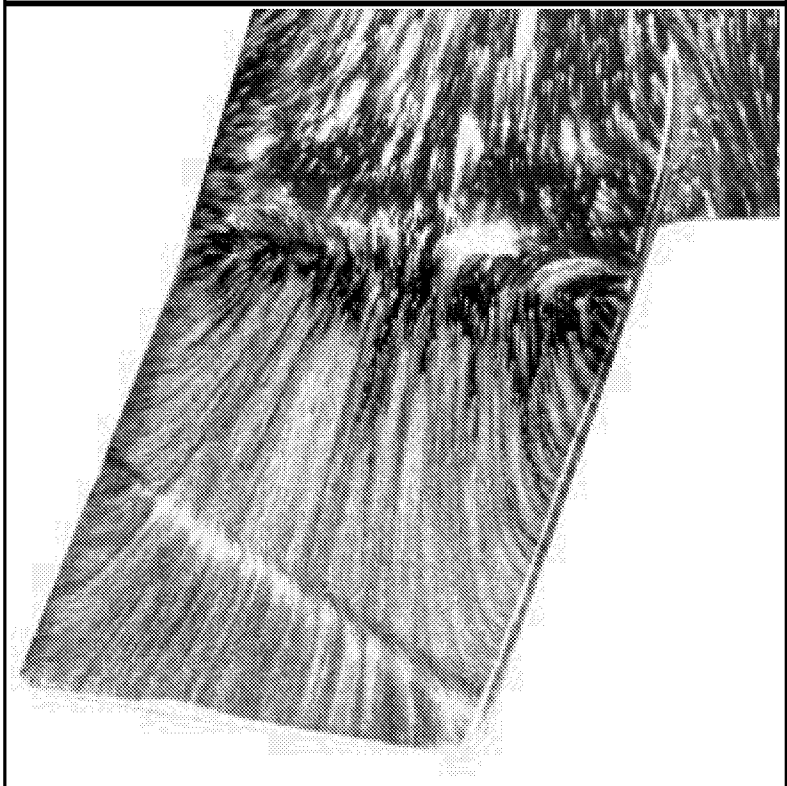

Run 178
α = 40-deg
Re_∞/ft = 2 x 10^6
δ_{BF} = 20-deg

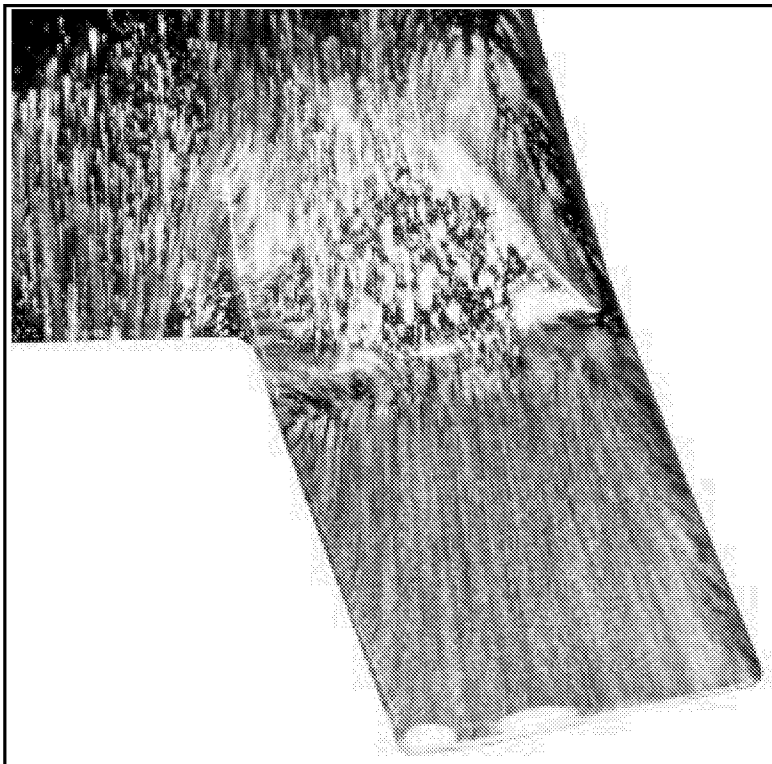

Run 179
α = 20-deg
Re_∞/ft = 2 x 10^6
δ_{BF} = 20-deg

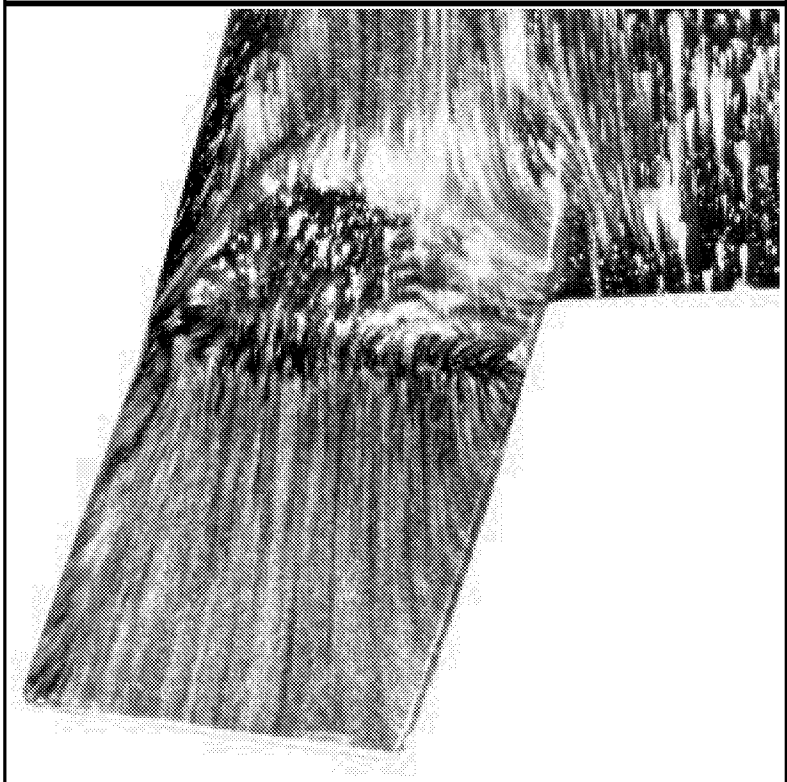

Run 179
α = 20-deg
Re_∞/ft = 2 x 10^6
δ_{BF} = 20-deg

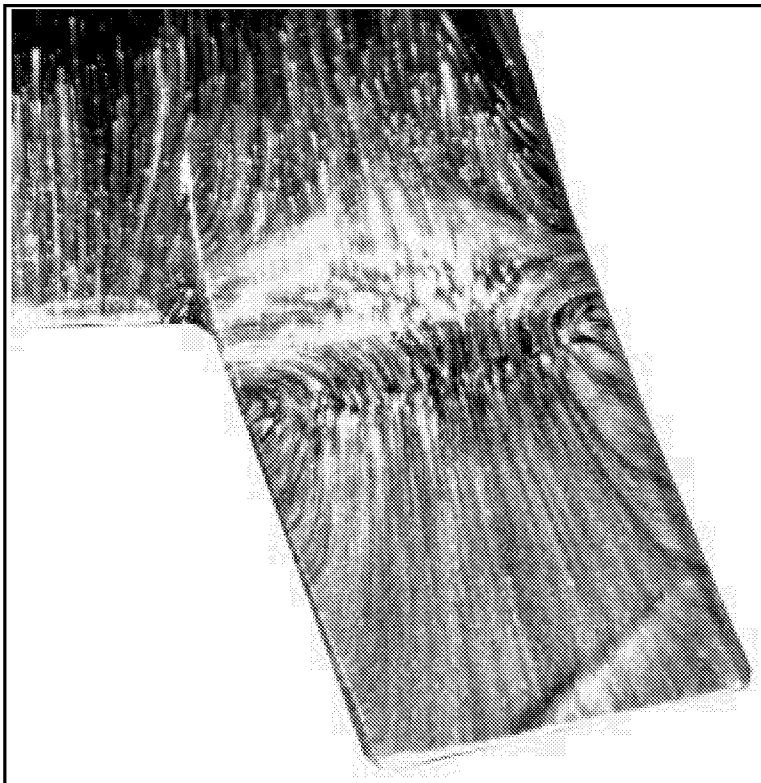

Run 180
α = 30-deg
Re_∞/ft = 1 x 10^6
δ_{BF} = 20-deg

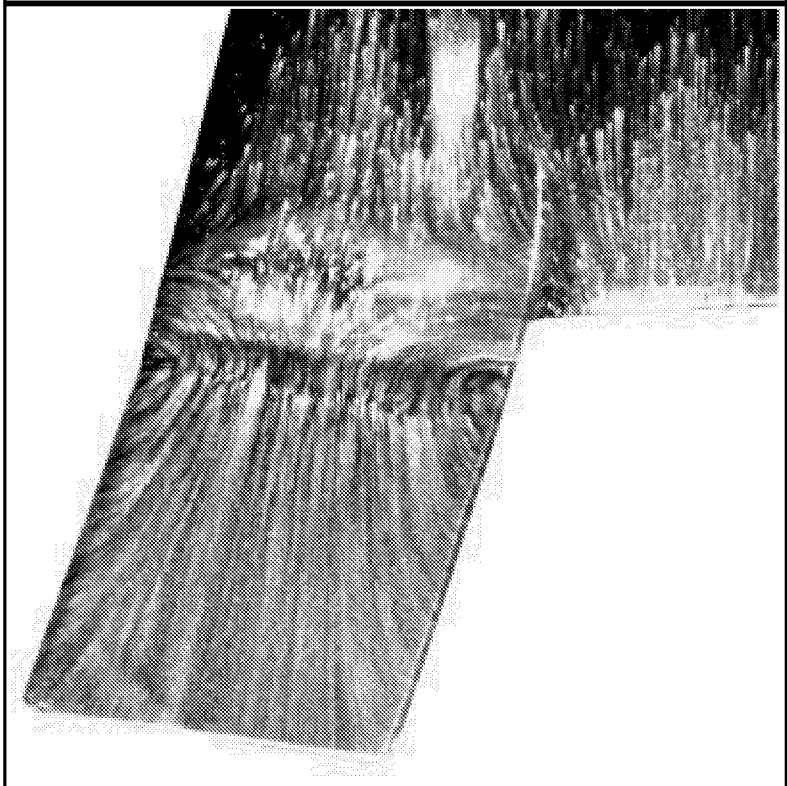

Run 180
α = 30-deg
Re_∞/ft = 1 x 10^6
δ_{BF} = 20-deg

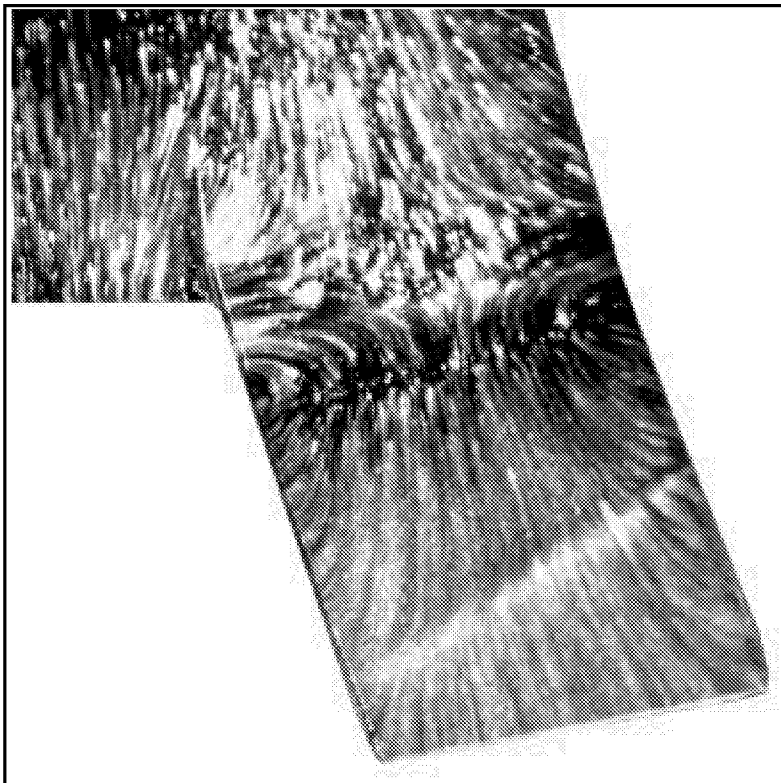

Run 181
α = 40-deg
Re_∞/ft = 1 x 10^6
δ_{BF} = 20-deg

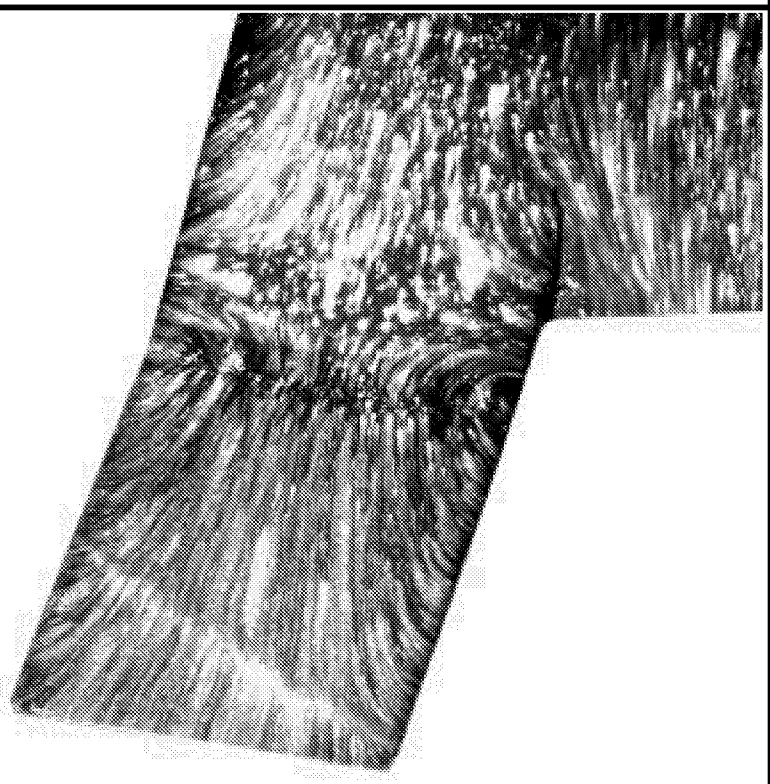

Run 181
α = 40-deg
Re_∞/ft = 1 x 10^6
δ_{BF} = 20-deg

REPORT DOCUMENTATION PAGE

Form Approved
OMB No. 0704-0188

1. AGENCY USE ONLY (Leave blank)	2. REPORT DATE	3. REPORT TYPE AND DATES COVERED
	March 1999	Technical Memorandum

4. TITLE AND SUBTITLE
X-33 (Rev-F) Aeroheating Results of Test 6770 in NASA Langley 20-Inch Mach 6 Air Tunnel

5. FUNDING NUMBERS
242-80-01-01

6. AUTHOR(S)
Scott A. Berry, Thomas J. Horvath, Matthew K. Kowalkowski, and Derek S. Liechty

7. PERFORMING ORGANIZATION NAME(S) AND ADDRESS(ES)
NASA Langley Research Center
Hampton, VA 23681-2199

8. PERFORMING ORGANIZATION REPORT NUMBER
L-17824

9. SPONSORING/MONITORING AGENCY NAME(S) AND ADDRESS(ES)
National Aeronautics and Space Administration
Washington, DC 20546-0001

10. SPONSORING/MONITORING AGENCY REPORT NUMBER
NASA/TM-1999-209122

11. SUPPLEMENTARY NOTES

12a. DISTRIBUTION/AVAILABILITY STATEMENT
Unclassified-Unlimited
Subject Category 34 Distribution: Standard
Availability: NASA CASI (301) 621-0390

12b. DISTRIBUTION CODE

13. ABSTRACT (Maximum 200 words)
Aeroheating characteristics of the X-33 Rev-F configuration have been experimentally examined in the Langley 20-Inch Mach 6 Air Tunnel (Test 6770). Global surface heat transfer distributions, surface streamline patterns, and shock shapes were measured on a 0.013-scale model at Mach 6 in air. Parametric variations include angles-of-attack of 20-deg, 30-deg, and 40-deg; Reynolds numbers based on model length of 0.9 to 4.9 million; and body-flap deflections of 10-deg and 20-deg. The effects of discrete roughness elements on boundary layer transition, which included trip height, size, and location, both on and off the windward centerline, were investigated. This document is intended to serve as a quick release of preliminary data to the X-33 program; analysis is limited to observations of the experimental trends in order to expedite dissemination.

14. SUBJECT TERMS
Hypersonic, aerothermodynamics, boundary layer transition, phosphor thermography

15. NUMBER OF PAGES
99

16. PRICE CODE
A05

17. SECURITY CLASSIFICATION OF REPORT	18. SECURITY CLASSIFICATION OF THIS PAGE	19. SECURITY CLASSIFICATION OF ABSTRACT	20. LIMITATION OF ABSTRACT
Unclassified	Unclassified	Unclassified	UL